REPORT NO. DOT-TSC-OST-73-29, IX

CONCEPT FOR A SATELLITE-BASED ADVANCED AIR TRAFFIC MANAGEMENT SYSTEM

Volume IX. System and Subsystem Performance Models

C. Chen
R.G. Loeliger
F.S. Nakamoto
J.C. Elsey
J.B. King
J.H. Mitzel
J.W. Petway
I.M. Weiss
C.A. Wolfe

FEBRUARY 1974
FINAL REPORT

DOCUMENT IS AVAILABLE TO THE PUBLIC THROUGH THE NATIONAL TECHNICAL INFORMATION SERVICE, SPRINGFIELD, VIRGINIA 22151.

Prepared for
DEPARTMENT OF TRANSPORTATION
OFFICE OF THE SECRETARY
Office of Systems Engineering
Washington DC 20590

Technical Report Documentation Page

1. Report No.	2. Government Accession No.	3. Recipient's Catalog No.
DOT-TSC-OST-73-29, IX		

4. Title and Subtitle	5. Report Date
CONCEPT FOR A SATELLITE-BASED ADVANCED AIR TRAFFIC MANAGEMENT SYSTEM Volume IX. System and Subsystem Performance Models	February 1974
	6. Performing Organization Code
7. Author(s) *C. Chen, R.G. Loeliger, F.S. Nakamoto, J.C. Elsey, J.B. King, J.H. Mitzel, J.W. Petway	8. Performing Organization Report No. DOT-TSC-OST-73-29, IX
9. Performing Organization Name and Address Autonetics 3370 Miraloma Avenue Anaheim, CA 92803	10. Work Unit No. (TRAIS) OS404/R-4509 11. Contract or Grant No. DOT-TSC-508
12. Sponsoring Agency Name and Address Department of Transportation Office of the Secretary Office of Systems Engineering Washington, DC 20590	13. Type of Report and Period Covered Final Report October 1972 through October 1973 14. Sponsoring Agency Code

15. Supplementary Notes 7. *I.M. Weiss, C.A. Wolfe
*Under contract to: Department of Transportation, Transportation Systems Center, Kendall Square, Cambridge, MA 02145

16. Abstract

This volume presents the models used to analyze basic features of the system, establish feasibility of techniques, and evaluate system performance. The models use analytical expressions and computer simulations to represent the relationship between system structure and state variables, system inputs, and system output measures.

This volume presents the following information: (1) Descriptions of the performance models and simulations used in the evaluation of the Satellite-Based Advanced Air Traffic Management System (SAATMS), (2) the simulation used to determine the capacity and delay performance of SAATMS, (3) the language, simulation methods, and basic structure of the simulation, (4) the models used in the evaluation of the SAATMS safety, (5) the criteria used in the selection of the safety model along with its derivation and application, (6) a description of the subsystem performance models used in the analysis of the surveillance detection scheme, (7) the covariance analyses for the satellite tracking, surveillance, and navigation subsystems, and (8) the analysis of the satellite constellation to determine the effect of the constellation on the geometric dilution of precision.

This volume should be used in conjunction with Volume III where subsystem mechanizations are presented and Volume V where system performance is analyzed.

17. Key Words	18. Distribution Statement
Modeling, System Performance, Capacity, Safety, Delay, Satellite Tracking, Satellite Detection, Satellite Constellation, Simulation	DOCUMENT IS AVAILABLE TO THE PUBLIC THROUGH THE NATIONAL TECHNICAL INFORMATION SERVICE, SPRINGFIELD, VIRGINIA 22151.

19. Security Classif. (of this report)	20. Security Classif. (of this page)	21. No. of Pages	22. Price
UNCLASSIFIED	UNCLASSIFIED	140	

Form DOT F 1700.7 (8-72)

☆ U. S. GOVERNMENT PRINTING OFFICE : 1973 725-504/328

CONTENTS

CONTENTS (continued)

ILLUSTRATIONS

ILLUSTRATIONS (continued)

TABLES

GLOSSARY

AATMS	Advanced Air Traffic Management System
ACC	Airport Control Center
ADF	Automatic Direction Finder
ADIZ	Air Defense Identification Zone
AGL	Above Ground Level
AMF	Analog Matched Filter
AOPA	Aircraft Owners and Pilots Association
ARINC	Aeronautical Radio, Inc.
ARTCC	Air Route Traffic Control Center
ARTS	Automated Radar Terminal System
ATC	Air Traffic Control
ATCAC	Air Traffic Control Advisory Committee
ATCRBS	Air Traffic Control Radar Beacon System
ATCS	Air Traffic Control System
ATM	Air Traffic Management
CA	California
CARD	Civil Aviation Research and Development
CAS	Collision Avoidance System
CCC	Continental Control Center
CNI	Communication Navigation Identification
CNMAC	Critical Near Midair Collisions
COMM	Communications
CONUS	Continental United States
CP	Central Processor
CST	Central Standard Time
CW	Continuous Wave

GLOSSARY (continued)

DABS	Discrete Address Beacon System
DOD	Department of Defense
DOT	Department of Transportation
DME	Distance Measuring Equipment
DNSDP	Defense Navigation Satellite Development Program
DNSS	Defense Navigation Satellite System
ERP	Effective Radiated Power
ESRO	European Satellite Reserach Organization
EST	Eastern Standard Time
ETA	Estimated Time of Arrival
FAA	Federal Aviation Administration
F&E	Facilities and Equipment
FL	Florida
FM	Frequency Modulation
FSS	Flight Service Station
GA	General Aviation
GAATMS	Ground-Based Advanced Air Traffic Management System
GDOP	Geometric Dilution of Precision
GFE	Government Furnished Equipment
IAC	Instantaneous Airborne Count
ICAO	International Civil Aviation Organization
ID	Identification
IFR	Instrument Flight Rules
ILS	Instrument Landing System
IMC	Instrument Meteorological Conditions

GLOSSARY (continued)

I/O	Input/Output
IOP	Input Output Processor
IPC	Intermittent Positive Control
IPS	Instructions Per Second
IR	Infrared
JFK	Kennedy International Airport
LA	Los Angeles
LAT	Latitude
LAX	Los Angeles International Airport
LORAN	Long Range Navigation
LOS	Line-of-sight
LRR	Long Range Radar
MIPS	Million Instructions Per Second
MLS	Microwave Landing System
MODEM	Modulator-Demodulator
MSL	Mean Sea Level
MTBF	Mean Time Between Failures
NAFEC	National Aviation Facilities Experimental Center
NAD	North American Datum
NAS	National Airspace System
NASA	National Aeronautics and Space Administration
NAV	Navigation
NDB	Non-Directional Radio Beacon
NEF	Noise Exposure Factor
NFCC	National Flow Control Center

GLOSSARY (continued)

NMAC	Near Midair Collisions
NOTAM	Notice to Airmen
NOZ	Normal Operating Zone
NWS	National Weather Service
O&M	Operations and Maintenance
PCA	Positively Controlled Airspace
PIREPS	Pilot Reports
PN	Pseudo-Noise
PPM	Pulse Position Modulation
PWI	Pilot Warning Indicator
RAM	Random Access Memory
RCAG	Remote Control Air-to-Ground Facility (Present System)
RCAGT	Remote Communication Air-Ground Terminal
RCC	Regional Control Center
R&D	Research and Development
RDT&E	Research, Development, Test, and Evaluation
RF	Radio Frequency
RNAV	Area Navigation
ROM	Read-Only Memory
SAATMS	Satellite-Based Advanced Air Traffic Management System
SAMUS	State Space Analysis of Multisensor System
SID	Standard Instrument Departure
S/N	Signal-to-Noise
SNC	Surveillance, Navigation, Communication
STAR	Standard Arrival Routes
STC	Satellite Tracking Center
STOL	Short Takeoff and Landing

GLOSSARY (continued)

TACAN	Tactical Air Navigation
T&E	Test and Evaluation
TCA	Terminal Controlled Airspace
TOA	Time of Arrival
TRACAB	Terminal Radar Approach/Tower Cab
TRACON	Terminal Radar Approach Control
TRSA	Terminal Radar Service Areas
TRW	Thompson Ramo Wooldridge
TSC	Transportation Systems Center
TX	Texas
VFR	Visual Flight Rules
VHF	Very High Frequency
VMC	Visual Meteorological Conditions
VOR	Very High Frequency Omni-Directional Range
VORTAC	Very High Frequency Omni-Range TACAN
VVOR	Virtual VOR
2D	Two Dimensional
3D	Three Dimensional
4D	Four Dimensional

1. INTRODUCTION

In the study and design of large scale systems, models are used to analyze basic features of the systems, to establish feasibility of techniques, and to determine the ability of the systems to satisfy performance specifications. The models represent the relationships among the structure and the state variables of the systems, the inputs to the systems, and the output measures of the systems through the use of analytical expressions and computer simulations. Models should abstract those factors of the system which have significant influence on input-output and parameter-output relationships. The model must be able to represent closely those relationships which exist in the real system. The models can then be used to evaluate the performance of a hypothetical system or to establish the system requirements to meet a specific level of performance without actually developing the system. The models can also be used to investigate the sensitivity of the system input-output relationships with respect to the system parameters and the system structure.

There has been a great deal of effort devoted to computer simulations of air traffic control systems. Most of the large scale simulations have been developed with specific objectives in mind. As there was no general air traffic control model, nor a special purpose model which was suitable for the study of an Advanced Air Traffic Management System, Autonetics developed a set of air traffic control models to be used for SAATMS evaluation and for development of generic AATMS requirements.

Several modeling approaches were considered during the study; the selection of the approach was based on the ability of the model to evaluate system performance, the programming feasibility, the required computation time, and the flexibility of the program to be extended to study of systems of similar nature.

This report presents the following:

(1) Descriptions of the performance models and simulations used in the evaluation of the Satellite-Based Advanced Air Traffic Management System.

(2) The simulation used to determine the capacity and delay performance of SAATMS.

(3) The language, simulation methods, and basic structure of the simulation.

(4) The models used in the evaluation of the SAATMS safety.

(5) The criteria used in the selection of the safety model along with its derivation and application.

(6) A description of the subsystem performance models used in the analysis of the surveillance detection scheme.

(7) The covariance analyses for the satellite tracking, surveillance, and navigation subsystems.

(8) The analysis of the satellite constellation to determine the effect of the constellation on the geometric dilution of precision.

2. PERFORMANCE MODELS DESCRIPTION

2.1 Analytic Models and Computer Simulations

Analytical models yield mathematical relationships between system variables by applying calculus, probability, queuing theory, and mathematical programming. The usefulness of such relationships depends on the number and type of simplified assumptions made in deriving the expressions. The simplest model measures the capacity of a "single lane" sky highway under the assumption that all aircraft travel in-trail, and separated by a distance exactly equal to Q, and all have the same velocity V. In this case, capacity C is given by

$$C = \frac{V}{Q} \tag{1}$$

An analytic expression has been developed for the case where there are N different classes of aircraft with velocities V_i (i = 1, N) and the required minimum separations between each class may be different. Let Q_{ij} be the minimum separation required between an aircraft of class i followed by an aircraft of class j. Assume that the length of the trail is L, that no overtaking of aircraft is allowed, and that the population for class i is P_i. The index i is chosen in such a way that $V_i > V_j$ if $i > j$. It can be shown that the capacity of the trail is

$$C = \frac{\left(\sum_i P_i\right)^2}{\sum_i \sum_j P_i P_j \left[\frac{Q_{ij}}{V_k} + L\left(\frac{1}{V_i} - \frac{1}{V_j}\right) E_{ij}\right]} \tag{2}$$

where $k = \max(i, j)$

and $E_{ij} = 1$ if $i < j$

$= 0$ if $i > j$

This relationship is more realistic, it is more complicated, and no account is taken of how well aircraft can be controlled to be exactly a distance of Q_{ij} apart.

Another class of analytic model which considers the delay that randomly arriving entities may encounter is M/G/1 delay model. The expected delay of a "customer" in a queuing situation with Poisson arrivals and a general service time distribution is given by

$$Wq = \frac{\lambda \; E \; [t_s^{\,2}]}{2 \; (1 - \lambda \; E \; [t_s])} \tag{3}$$

for $\lambda \cdot E\,[t_s] < 1$ (i.e., unsaturated situation), where λ is the average arrival rate, t_s is the service time and E is the expectation operator.

Most of the analytical expressions are for isolated parts of the air traffic system, under restricted or simplified assumptions. In-trail capacity models discussed above are valid for a single section of an air highway; they can not be readily extended to more general route structures, nor can they be easily augmented to other air traffic models. Similarly, the M/G/1 delay model is valid for a "point facility" and Poisson arrival only. It can not be used to obtain results for interconnected facilities. Though Poisson arrival is found to be an adequate description of a unregulated raw demand, the demand on facilities other than the first stage of the system are outputs of previous stages, and can not be considered as independent variables. Other important factors affecting delay and delay distribution can not be properly adopted in the M/G/1 model.

The complexity of their interrelationships necessitate the use of digital simulation models to describe the behavior of a Satellite-Based Advanced Air Traffic Management System.

2.2 Languages and Simulation Methods

Several general purpose and simulation languages were compared for use in simulating an air traffic control system. Simulation languages such as GPSS, SIMSCRIPT, and the most recently introduced SIMPL/1, are relatively easy to program and debug. However, these languages are not cost effective for large simulations. They are also more difficult to adapt to different special types of constraints. Since the simulation may be used by many different organizations for different studies, it is not desirable to have a program written in a language which few people could understand. The most widely used general purpose language, FORTRAN, is thus preferable and the simulation has been written in this language.

Since the number of variables is large and the dynamics of an AATMS is complex, a great amount of computer time would be required for continuous time simulation. In one portion of the simulation, the track model, discrete time simulation has been used to reduce such computational requirements. The simulation clock advances from one sampling to the next in a single step of varying duration. The main part of the simulation, called the network model, has been programmed in the form of an event simulation. This is also a discrete time simulation, where the simulation clock advances from one event time to the next in a single step. The state of the system is calculated at the event time or sampling time.

2.3 Basic Structure of the Simulation

The basic tasks of the SAATMS study were to evaluate the performance of the SAATMS subsystems, to establish the system requirements to meet the project demand and to study the sensitivities of the system input-output relations to the variation of parameters, constraints and scenarios. The basic performance measures to be considered have been defined as capacity, delay and safety. The most dominant system parameters are: surveillance and navigation accuracies and update rates, system delay time, and blunder acceleration protection. The demand is contained in the scenario description along with other factors such as aircraft characteristics, airspace structures, airport configurations, and the system rules and procedures. The models are required to be capable of establishing input-output relations under the given scenario conditions. The basic configuration of the models is shown in Figure 2.3-1.

2.4 Separation Standard Model

2.4.1 Model Objectives and Basic Assumptions

The Separation Standard Model was developed to establish basic relationships between subsystem parameters (e.g., surveillance accuracy and navigation accuracy) and system level parameters such as separation standard and intervention rate. Separation standard can be considered as the primary intermediate variable which links system performance measures with the basic parameters of the system.

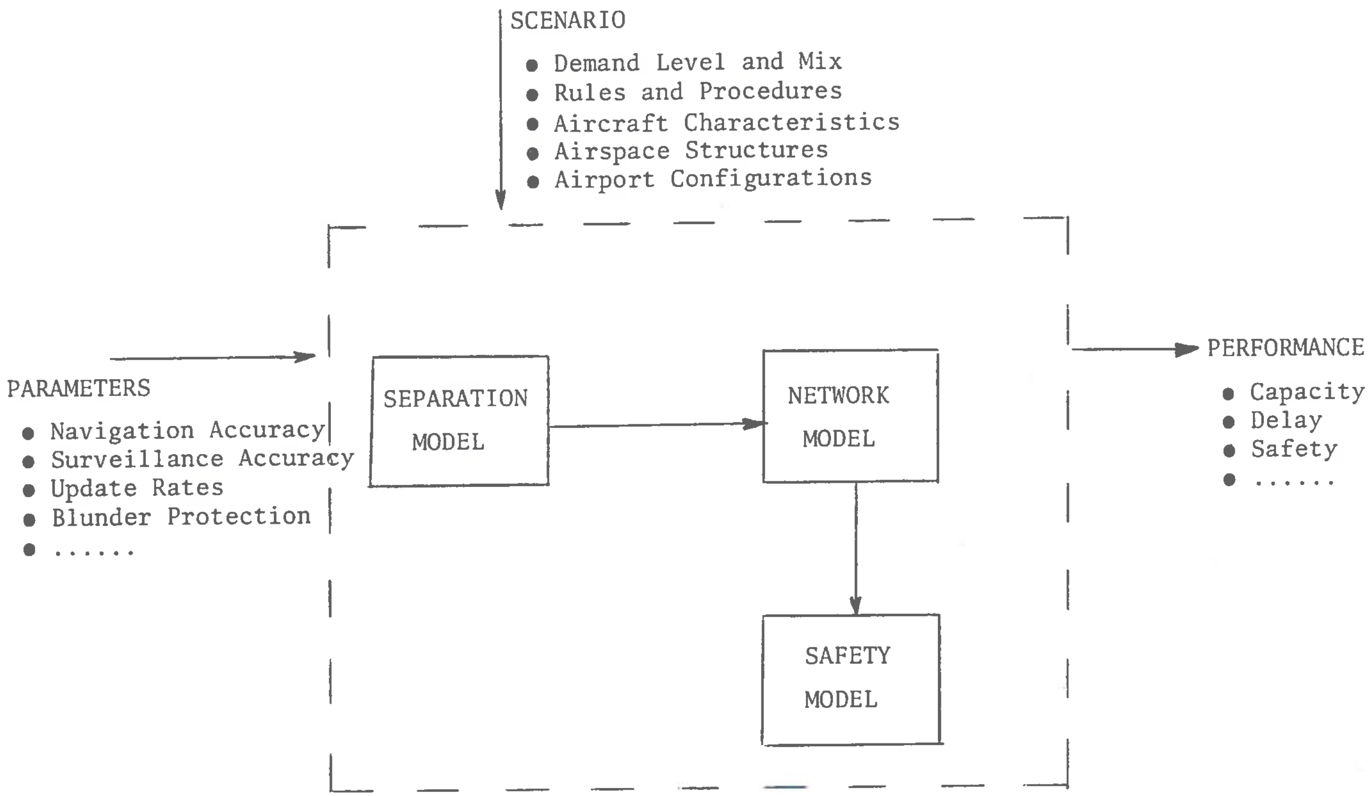

Figure 2.3-1. Basic Model Configuration

A separation standard is established to maintain an adequate level of safety. The probability that two aircraft will be sufficiently far from their expected relative position as to cause a conflict situation is estimated to give a measure of safety. This probability strongly depends on navigation, surveillance, communication and aircraft characteristics. There are other factors which influence separation requirements and yet can not be accurately estimated or measured. Blunder is one of the most important factors which affect safety. However, a blunder acceleration function can take many varieties of forms in time and position space. The frequency of its occurrence is also not known. Correcting manuevers would depend on individual pilot capabilities and the specific situation which are not well defined. Thus, in establishing a separation standard model, certain assumptions are needed.

The separation standard, Q_S, is a function of several distances as shown in Figure 2.4-1. It is given by

$$Q_S = \frac{W_{NF}}{2} + W_{BF} + W_{BL} + \frac{W_{NL}}{2} + W_{T_{LF}} + W_M \qquad (1)$$

$$= W_N + W_B + W_{T_{LF}} + W_M$$

for $W_{NF} = W_{NL} = W_N$ and $W_B = W_{BF} + W_{BL}$

where

W_{NF} = Width of the Normal Operating Zone (NOZ) for the following aircraft

W_{NL} = Width of the NOZ for the leading aircraft

W_{BF} = Width of the buffer zone for the following aircraft

W_{BL} = Width of the buffer zone for the leading aircraft

$W_{T_{LF}}$ = Wake turbulence danger distance (function of the leading and following aircraft)

W_M = Aircraft miss distance for both aircraft experiencing maximum protected blunders.

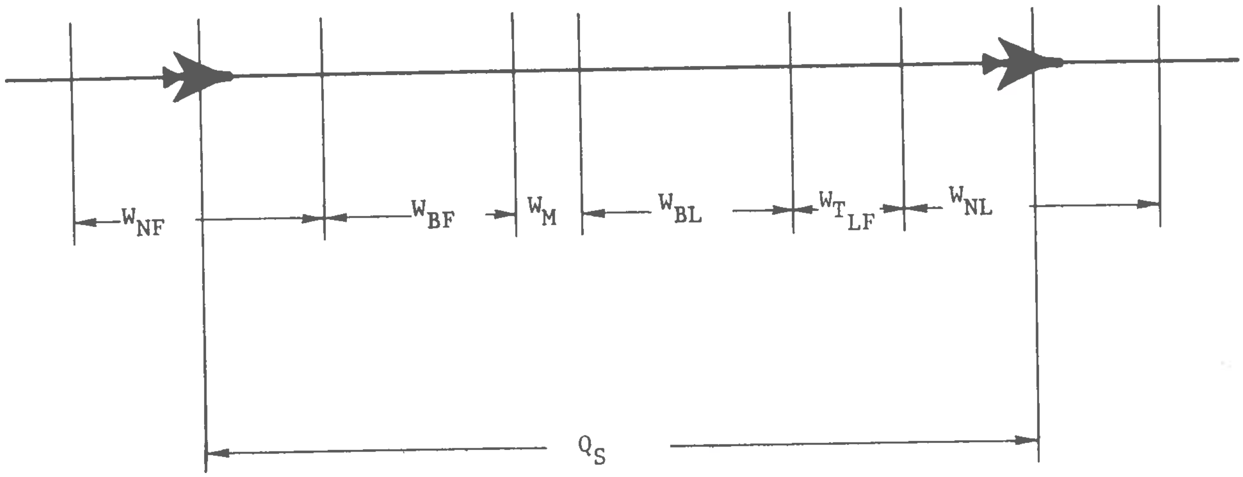

Figure 2.4-1. Separation Standard Distances

Analytic calculations of the buffer zone width are obtained under the assumption of second order aircraft dynamic equations. It is also assumed that the blunder acceleration is a constant acceleration of the maximal value the system is designed to safeguard against, and the correcting acceleration is of constant value.

Analytical calculations are also made, under the same assumption, to obtain the form of the necessary intervention criteria in the relative position-velocity space so that aircraft will not cross a given boundary. This basic form of intervention criterion is used in the track model to establish width of normal operation zone.

2.4.2 Track Model

The diagram of Track Model is shown in Figure 2.4-2. The actual aircraft acceleration is denoted by $\ddot{r}$, actual aircraft velocity by $\dot{r}$, and actual aircraft position by r. Desired aircraft position and velocity, which are assumed to be known, are denoted by r_d and $\dot{r}_d$, respectively. Navigation velocity and position errors are denoted $\Delta\dot{r}_n$ and Δr_n, respectively, while the surveillance velocity and position errors are denoted $\Delta\dot{r}_s$ and Δr_s. The errors are assumed to be independent of state, i.e., $\Delta\dot{r}$ and Δr are not functions of $\dot{r}$ or r. The surveillance and navigation errors are assumed to have Gaussian distribution and are generated in the program using Monte Carlo techniques. Navigation velocity, $\dot{r}_n$, is the sum of the actual aircraft velocity and the navigation error. Navigation position r_n, surveillance velocity $\dot{r}_s$, and surveillance position r_s, are similarly defined. All errors are added to their corresponding actual values at the sampling time. Navigation and surveillance update intervals are τ_n and τ_s, respectively. The pilot initiated correcting command is assumed to be proportional to the difference between the navigation value and the desired value. Velocity and position control loop gains are Ku and Kp, respectively. Deviations of surveillance data from the corresponding desired values are used in issuing ATC commands; no command is issued if the surveillance state lies in the normal operating zone. When an aircraft is detected by the surveillance subsystem to be outside of normal operating zone, a command of magnitude A_c is issued; the sign of this command depends on the direction of deviation. The intervention criteria is based on both position and velocity information. A pure time delay of τ_D accounts for the total amount of time needed in communication and decision making. It is also assumed that when an ATC correcting command is given, no self-correcting command will be applied. Correcting commands act on an aircraft through the aircraft response characteristics which are modeled by a first order loop; feedback gain, K_a, is an aircraft response parameter. A limiter is assumed to limit the commanded acceleration to a maximum value, A_L. In addition to the commanded acceleration, there are two other accelerations considered in the track model. Disturbance acceleration (including blunder acceleration) is denoted by A_d and the acceleration due to aerodynamic drag is assumed to be proportional to the actual velocity $\dot{r}$, with a proportional factor K_d.

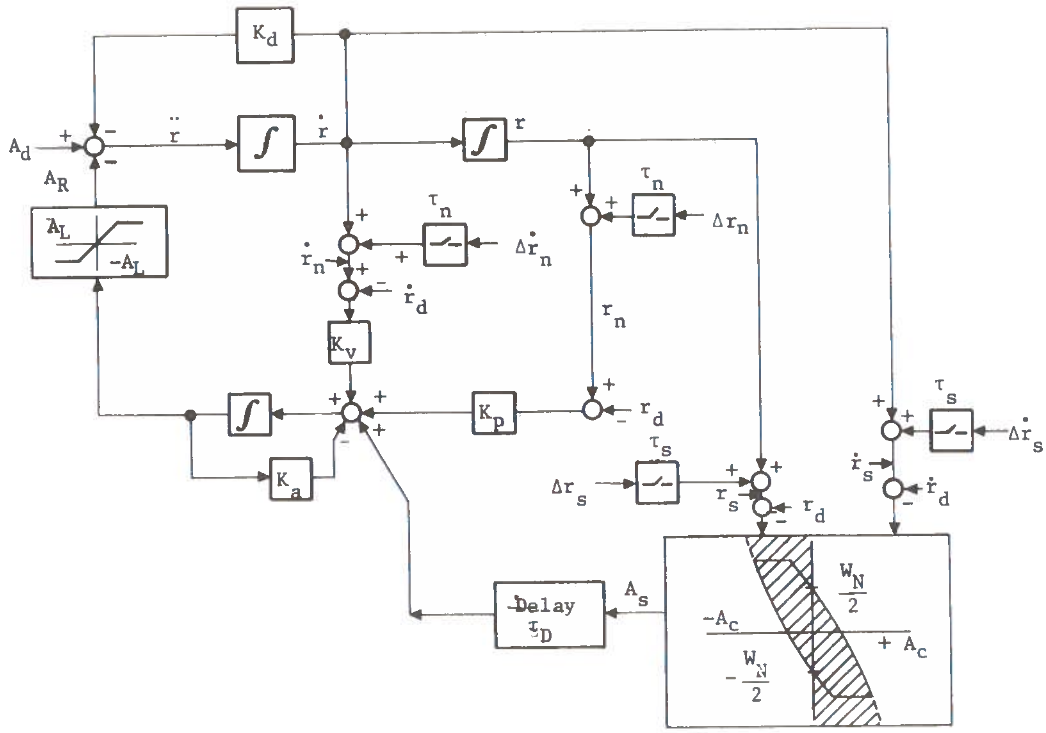

where

A_d	Disturbance acceleration (includes blunder acceleration)
r, $\dot{r}$, $\ddot{r}$	Actual aircraft position, velocity, acceleration
r_d, $\dot{r}_d$	Desired aircraft position, velocity
$\Delta\dot{r}_n$, Δr_n	Navigation velocity and position errors
$\Delta\dot{r}_s$, Δr_s	Surveillance velocity and position errors
τ_n, τ_s	Navigation, surveillance update interval
$\dot{r}_n$, r_n	Navigation velocity and position
$\dot{r}_s$, r_s	Surveillance velocity and position
K_a	Aircraft response parameter
K_v, K_p	Velocity and position control loop gains
K_d	Aerodynamic drag term
A_s	Commanded ATC corrective acceleration, $\pm A_c$ (0 if aircraft in shaded region)
W_N	Width of NOZ
A_L	Limit on commanded acceleration

Figure 2.4-2. Diagram of Track Model

The overall model is highly nonlinear due to the nonlinear elements in the loop and the variable structures of the system. A rectangular integration procedure is used for integration. The model is one dimensional but is applicable to all dimensions through proper choice of parameter values. The intervention rate is an output from the model and is obtained by counting the number of times a non-zero (ATC) acceleration command is generated. Time histories of all the model variables (e.g., an aircraft phase plane trajectory) are available as model outputs. Probability density and distribution functions for r and $\dot{r}$ are also available.

The track model is constructed to study the operation of aircraft in and around its normal operating zone. The model distinguishes between actual states, navigation states and surveillance states to determine the need for system intervention as depicted in Figure 2.4-3. The model can be used to determine the effects of navigation accuracy, surveillance accuracy, update rate, system delay and blunder protection on the operation of aircraft.

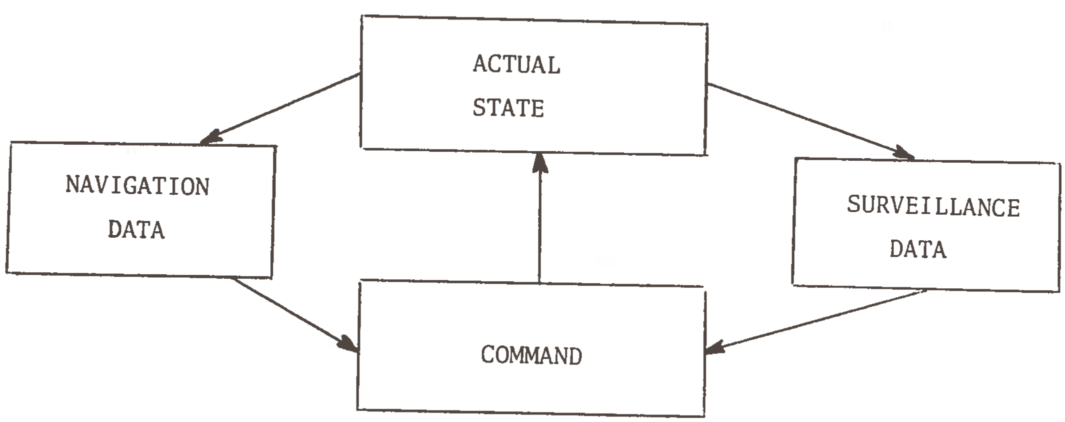

Figure 2.4-3. Interaction of Actual State and Surveillance/Navigation Data

2.5 Capacity and Delay Models

2.5.1 Basic Assumption and Inputs to the Model

The capacity and delay model is also designated as the network model, since a network structure consisting of nodes and connecting branches is used to represent the structure of an air traffic control system. Figure 2.5-1 shows an example of the network structure for a single runway. A network can represent any portion of an air traffic system to varying degrees of desired detail. This digital simulation model is used to run aircraft along the routes in airspace and on the ground. Monte Carlo runs are made to determine system capacity and user delays for each specific scenario, as a function of the system parameters.

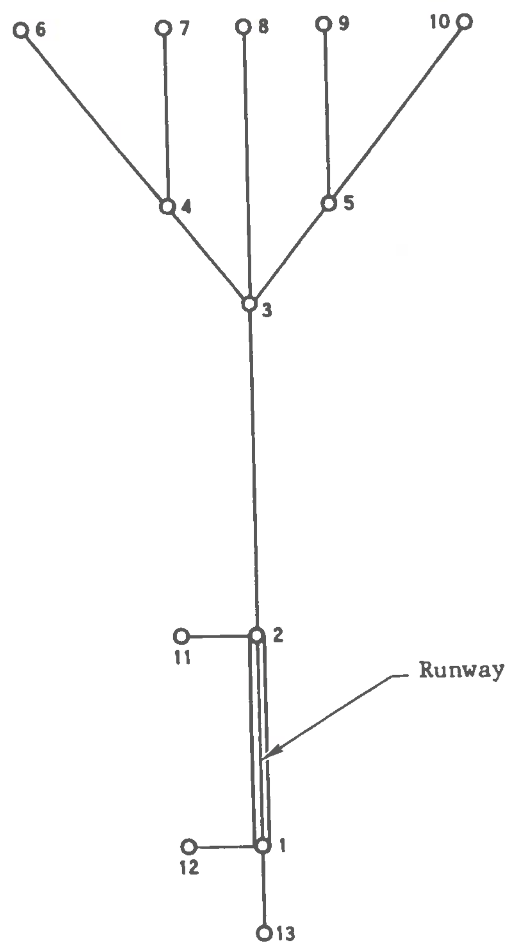

Figure 2.5-1. Example Network Structure for Single Runway

In the model, each significant point of the space is defined as a node. Each node is assigned a node number; its location and other important characteristics which may affect the model operation are also specified. The number and sequence of nodes which describe an aircraft route are also specified. Velocities of each class of aircraft at different nodes are specified for all routes. Dimension statements in the program limit the total number of permissible nodes and routes; size of the computers and the degree of detail desired are dominant factors in defining these dimensions.

Aircraft are classified according to their speeds, runway occupany times and their performances. The maximum number of aircraft classes allowed in each run is 5, however, this can be modified by changing dimension statements as required.

A separation standard is defined for each node in the system and each pair of all possible combinations of aircraft classes. In other words, SEP (i, j, k) gives the necessary separation standard at node i when a class j aircraft follows a class k aircraft. By properly defining nodes and velocities, both spatial separation standards and additional time separation requirements based on arrival/departure rules or departure/departure rules can be properly introduced.

Demand levels for each route, as well as their mix and statistical inter-arrival time distributions must be included as input data. Analysis of current demand data shows that Poisson distributions properly describe most unconstrained, unregulated traffic demand. Other types of demand can be generated by separate programs or subroutines and put into the program demand array. Prescheduled flight plans can also be used to fill the demand array. In the way the demand is generated, the case where demand level is a function of the time of the day can be handled with slight modification. The demand array includes information on arrival times (the desired times for aircraft to enter the system), aircraft routes and aircraft classes. The demand array or on-line generated demand is used to drive the simulation.

The duration of the simulation is also prescribed by input data. Since the flight record is deleted when the flight reaches its destination, there is no limitation on the duration of a run as long as the maximum number of aircraft in the system at any instant of time does not exceed certain array dimensions. Statistical data of the simulation can be gathered from t = 0 or from any other specified time to the desired final time. Thus, the simulation can be used for both transient response and steady state analyses. The admissible number of aircraft any any instant of time is constrained by the length of the recording space reserved for flight plans and by the length of "next event matrix". Length of spaces reserved for recording system status may also be a constraint, if the demand exceeds system capacity and extremely long delays are experienced.

The whole program consists of a main program and three subroutines. Figure 2.5-2 shows the program structure of the model. Main program, ATCSUP, has control concerning what is to be done in a particular run. ATCIN contains most of the input and initialization. ATCFLT is the main event processor; some of the output data is accumulated in this subroutine. ATCED is the output editor which organizes the remainder of the output data.

2.5.2 Model Functional Description

The large number of variables and the complex dynamics of the air traffic management system impose severe requirements in terms of computer size and computation time for continuous time simulation. The network model is an event-oriented discrete simulation. In such a simulation, continuous pictures of the system status are not available. Instead, a whole series of "snapshots" are used to describe the situation of an air traffic system. More specifically, these "snapshots" are taken only at the instants when "events" occur. Furthermore, each "snapshot" focuses on only that portion of the system situation which has major impact on the event. The information handled in the digital simulation has been refined to a degree that the computer can be utilized efficiently without losing the essential features of the system. It is this basic feature of the simulation approach which results in the high degree of efficiency and the flexibility of the network model.

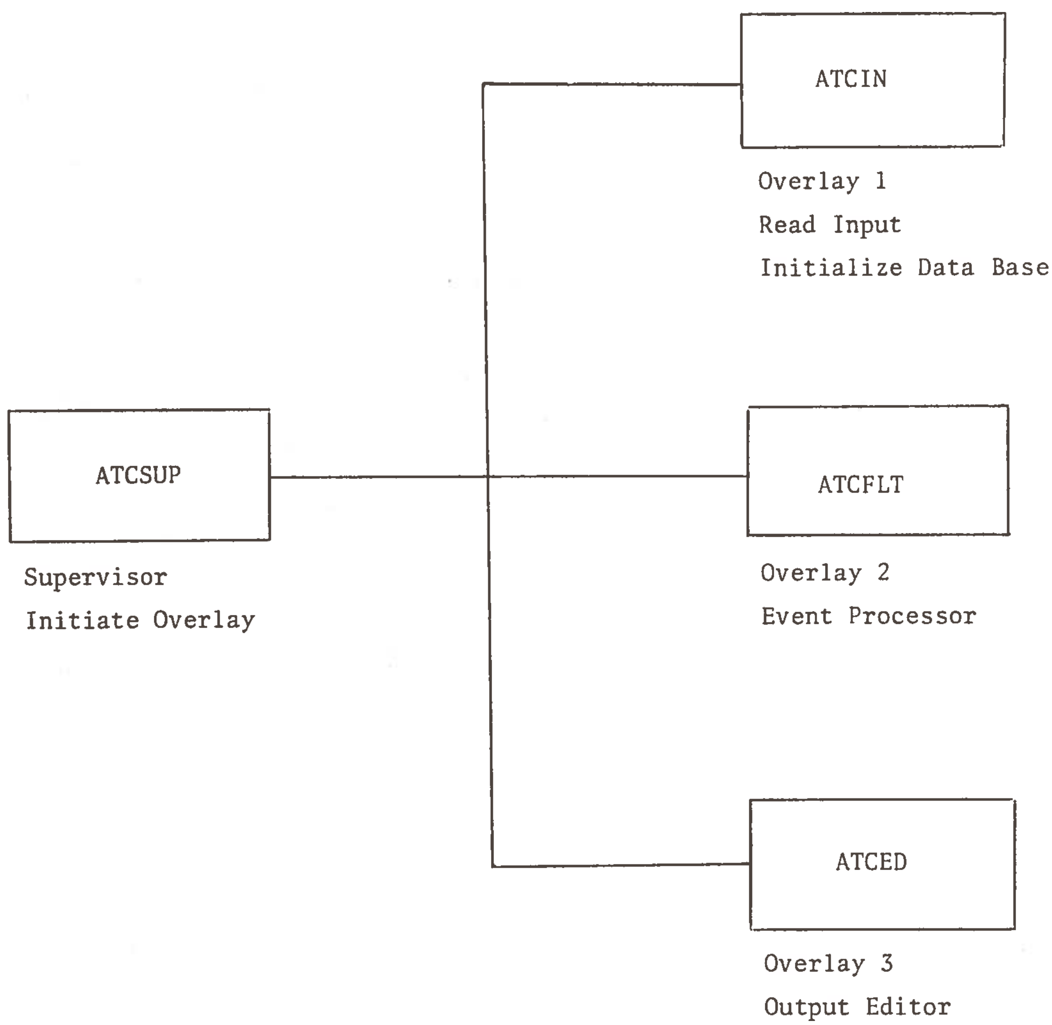

Figure 2.5-2. Program Structure of Network Model

Each aircraft constitutes an entity to the model. The basic event in the model occurs when an aircraft arrives at a new node. As mentioned earlier, significant points of the air space or ground space structure are considered as nodes of the network. Figures 2.5-3 and 2.5-4 present a two dimensional view of a simplified functional diagram. The functional flow chart (as viewed from the simulation system) is shown in Figure 2.5-3, while the basic flow of information as viewed by an aircraft is shown in Figure 2.5-4.

Demand data, including routes, aircraft classes, and desired times to enter the system are either generated on-line in the program or stored in the demand array in the initial phase of a run. Initially, only the first flight along each route is entered into the system.

When an aircraft enters the system, a flight plan is created and stored in the program. The computer stores the desired time the aircraft takes to go from one node to the next along its route and the aircraft's nominal velocity along each specified branch of the network that constitutes its route. This flight plan data is based on the aircraft's desired route, time of entry into the network structure, the aircraft class, and the specified velocity of the aircraft in each phase of flight.

Aircraft are considered as new aircraft when they first enter the system. Their first events are the first "next events" for the flights. These "next events" together with next events of all the flights which are already in the system form the listing"next event matrix". Consequently, the length of this listing is the number of active aircraft in the system.

To determine what event to treat next, a search is made in "next event matrix" to identify time and flight number of the earliest "next event" in the matrix. Since the listing may be very long when the number of active aircraft in the system is large, a special way of organizing these data has been used in the program. Elements in next event matrix are classified into a number of classes according to the remoteness of the desired event times. The search is done only in the class of imminent events.

If the earliest "next event" is the first event of a new aircraft, the next flight along the same route is entered into the system as a new aircraft and its flight plan is constructed and added to the flight plan block. The first desired event of this new flight is also added to next event matrix.

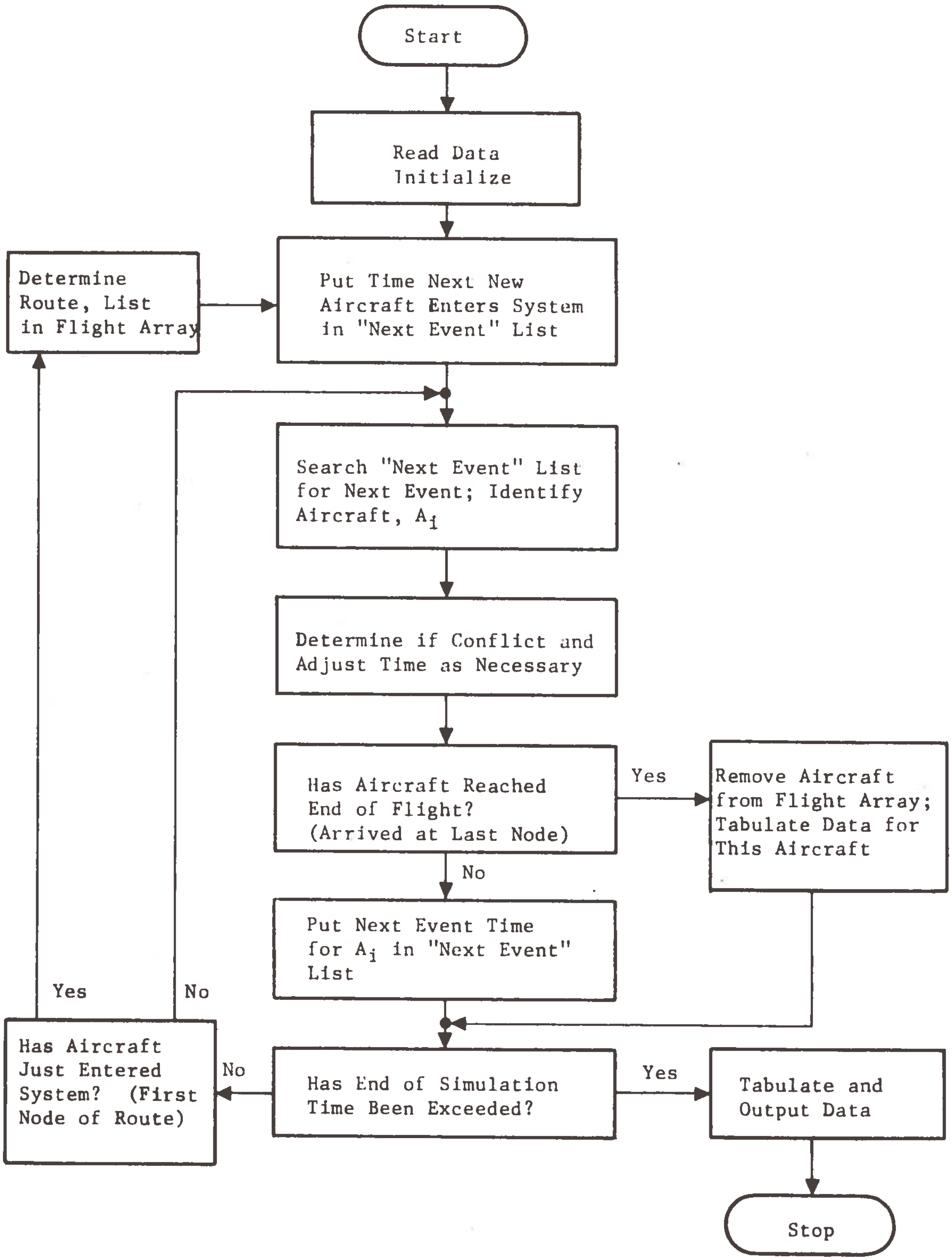

Figure 2.5-3. Simplified Flow Diagram of Network Event Step Computer Simulation Program

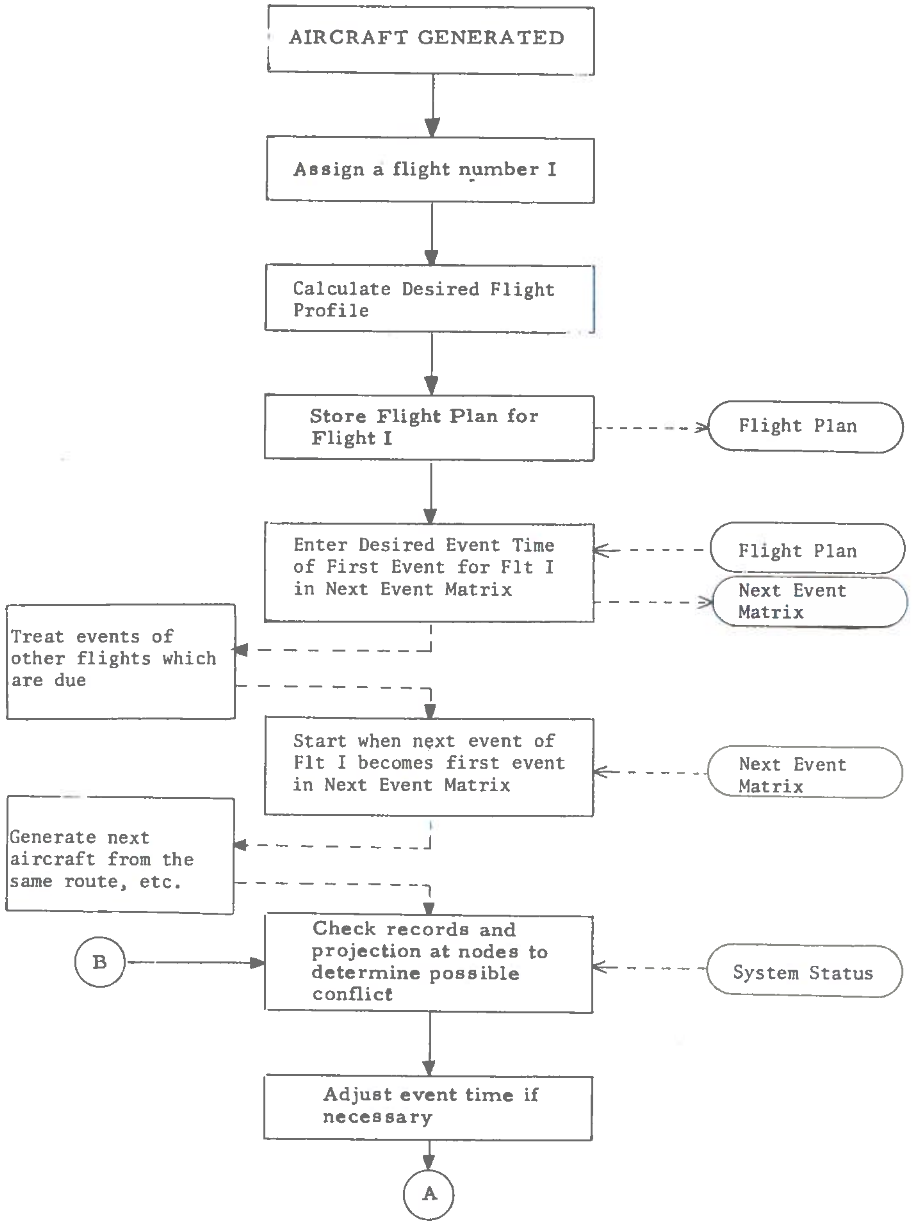

Figure 2.5-4. Simplified Flow Diagram of Network Model as Viewed from an Entity

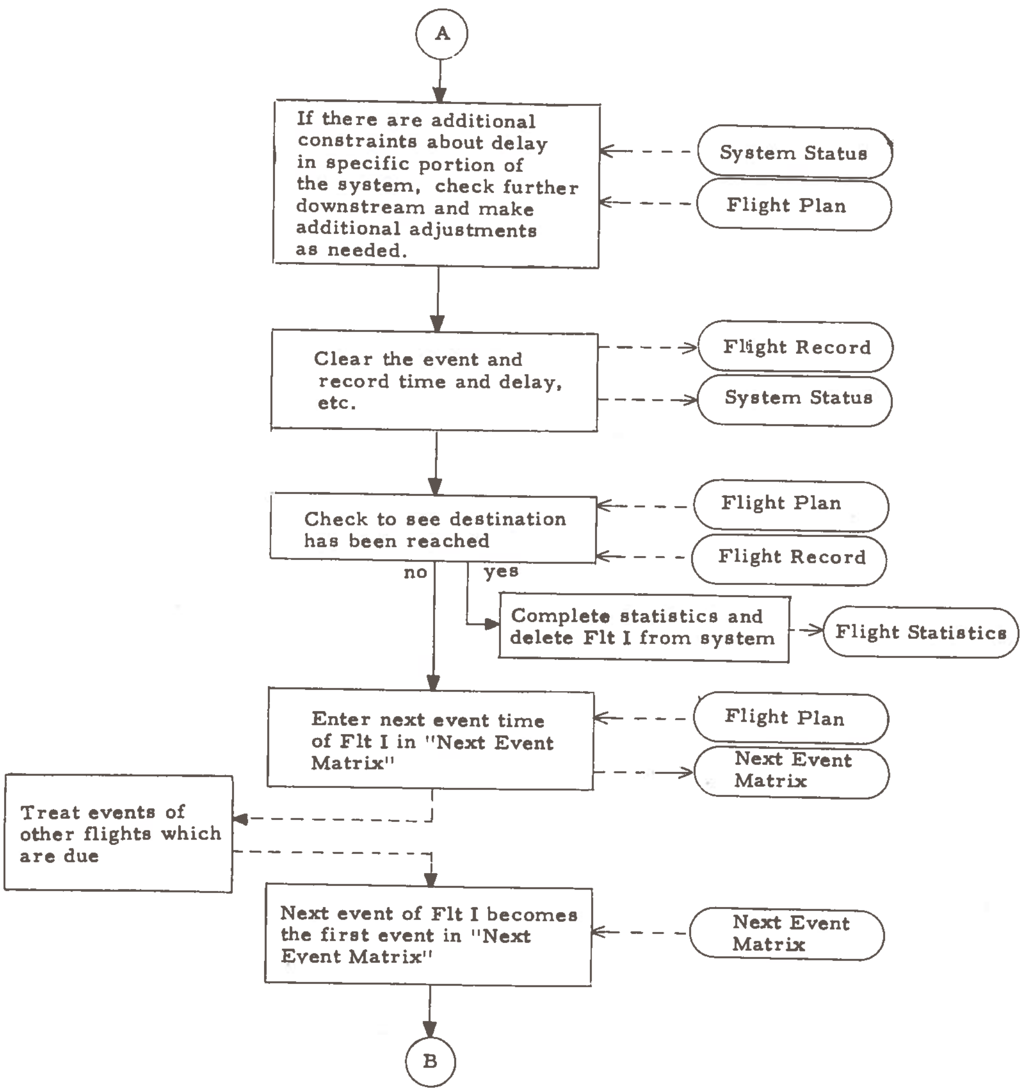

Figure 2.5-4. (Continued)

Once the earliest event in the "next event matrix" is singled out, the flight number and the node number of that event is identified. Based on the node under consideration, class of current aircraft, system situation, separation standard and other constraints, the desired event time is examined to verify the availability of the node. In this step, separation standard matrix and system status are used. System status consists of two groups of records. One portion, the node event matrix, has the record of latest event occured or scheduled for all nodes. Another portion keeps track of all reservations at the nodes to allow late comers to use available slack time. An adjustment of an event time is made, if necessary, to avoid conflicts. If there are additional constraints about delay in a specific portion of the space, it is necessary to check further down stream nodes and to make additional adjustments in the event time at the current node, so that these constraints will not be violated when the flight reaches there. The event is then cleared and scheduled to take place. The information is recorded in the flight record used to update information on system situation. The node and the projected desired time of the new next event for that flight is then derived from current status of the flight and the flight plan. The new next event is put into "next event matrix" unless the flight has reached its destination. A new search in "next event matrix" for the earliest subsequent next event is initiated at this time. The simulation clock also advances from the desired event time of the previous event to desired time of this event in one single step. The process continues in this manner until the simulation clock time exceeds specified final time.

A sequential flight record is also maintained as an aircraft proceeds along its route. This record contains the time of the day that the flight passes each node and the amount of delay encountered between each pair of nodes. When a flight reaches its destination, information on how much delay it has experienced and where it has occurred are available. Of course, the total delay of a flight can be obtained by adding all delays. Statistics of delay and capacity efficiency are derived by using the delay information of all flights. Saturation capacity is the value of capacity efficiency achieved when the average delay is infinite. The information on where delays occurred can be used to determine congestions and bottlenecks.

Both the flight plan and flight "record of a flight are available as outputs, however, they are presently destroyed when the flight is complete. Some event records may be retained until the time the flight has no further influence on the system. For example, in a simulation of a single runway for dedicated takeoff operation, a flight may be considered as completed when it has left the end of the runway. However, the event records of the flight must be kept for at least 60 seconds if IFR operation is considered, when a constraint of 60 seconds minimum time separation between departures is imposed.

As the information (flight plan/record, system situation record) retained in the program are those of active aircraft and essential system situations only, the memory requirements posed on computer are kept at minimum. By recycling memory spaces for different flights, the program can run for any duration of time with any total number of flights as long as the length of each information group does not exceed its corresponding reserved memory space at any instant of time. Because of this efficient use of memory, the simulation is capable of handling larger systems and/or more detailed simulations.

It is to be noted that this simulation does not model on optimal flow control planning function since no information of future inputs is used. It is possible to have new inputs generated randomly as the simulation is operated. All flights and events are presently treated on a first-come first-served basis. Since the program considers the system status in the vicinity of simulation clock time only, it is not necessary to readjust the whole sequence of event times when an event is treated.

In summary, the network model is a fast-time event simulation. The computation time and memory requirement has been minimized by processing event by event and using information in the vicinity (both in time and space) of the event. The capacity and delay of the system are obtainable through the operation of the model.

2.6 Safety Models

2.6.1 Choice of Safety Performance Model

Two measures of a SAATMS safety performance have been developed in the literature. The first measure defines safety in terms of the blunder protection afforded to each individual aircraft in the system at any instant of time. The probability of a conflict given that a blunder has occurred is treated in the separation and intermittent positive control studies (References 1 through 5). Statistics on the frequency and magnitude of blunders, however, are not available. Moreover, safety estimates for an ATM system must consider not only blundering airplanes but representations of all aircraft in the system and the corresponding expected number of conflicts between aircraft over a specific period of time.

The second measure is the conflict risk, which is used to determine the total system safety rather than individual aircraft safety. The conflict risk is defined to be the probability that the conflict volume of one aircraft overlaps the conflict volume of a second aircraft. The conflict volume of an aircraft has boundaries which roughly coincide with the physical dimensions of the aircraft, a specified miss distance, and can be extended to include the wake vortex region associated with the aircraft.

Table 2.6-1 contains a comparison of several techniques which can be used to determine the probability of a conflict between airplanes in a system. The techniques are characterized by:

1. The aircraft encounter geometries treated.
2. The assumptions made on statistical quantities, e.g., distribution shapes, and interaction parameters, e.g., relative velocity.
3. Whether they are a sub-class of one of the other reference works
4. The computational ease of utilization, which is a subjective judgement on the difficulty of setting up the model and obtaining support data for the calculations
5. The generality of the model.

TABLE 2.6-1. CONFLICT RISK TECHNIQUES

	A) Encounter Geometry	i) Parallel Track	ii) Intersecting Path	iii) Following	iv) Curved Path	v) Random Flight	B) Assumptions	i) Gaussian Distribution	ii) Distribution Tails	iii) Independence r, ṙ	iv) Independence, x, y, z	v) Spherical Conflict Volume	vi) Rectangular Conflict Vol.	vii) Relative Velocity	viii) Proximity Time	C) Derivation Hierarchy[1]	D) Computation Ease[2]	E) Applicability[3]
1) Bellantoni [(6)]																		
a) Equation 1		X	X	X	X												5	1
b) Equation 2		X	X		X					X				X		1a	4	2
c) Equation 4		X		X						X				X		1a	4	3
d) Equation 5		X	X	X	X					X		X				1a	4	2
2) Koenke [(7)]																		
a) Equation 3A (same as 1a)		X	X	X	X												5	1
b) Example III-1		X	X	X	X			X		X		X				2a	4	2
c) Example III-1, Case 1				X				X		X		X		X		2a	4	3
d) Example III-1, Case 2					X			X		X		X		X		2a	4	5
e) Equation 3·11 (Statistical 2a)		X	X	X	X											2a	3	1
3) Bellantoni [(8)]																		
a) Crossing Conflict Risk		X	X						X	X				X		1b	1	3
b) Following conflict Risk				X					X	X				X		1b	1	5
4) Reich [(9)], Hershkowitz [(10)]		X							X	X	X		X		X	1a	1	3
5) Steinberg [(11)]		X						X		X	X		X	X		4*	1	5
6) Taylor [(12)]		X						X			X		X		X	4	1	3
7) Koetsch [(13)]		X						X			X		X	X	X	6	1	3
8) Graham[(14)], Willis[(15)], Alexander [(16)]						X								X		1**	1	5

1. Reference from which this result can be derived using simplifying assumptions, numbers refer to entries in the chart.

2. Computational ease - number 1 being easiest and 5 being hardest - this is an opinion on the computer mechanization, time, and support data difficulties.

3. Applicability - generality of method with number 1 being the most general and 5 being the least general.

* This technique determines a probability model without the relative velocity considerations of Reference 4.

** A general random gas model can be obtained from 1 above.

Depending on the assumptions used in the crossing frequency model (References 6 and 7), one can obtain the parallel track model (References 9 through 11) or versions of the random gas model (References 14 through 16). The gas model is limited in its simplicity, cannot handle fixed encounter geometries, and obtains extremely pessimistic estimates (Reference 7). The parallel track model is limited in its lack of geometric flexibility. The position probability models of References 12 and 13 are earlier, simpler treatments of the problem. Because of these deficiencies, the crossing frequency model was chosen as the model. For conflict risk calculations, the conflict risk equations (Reference 8) were chosen for the analysis, since they are compatible with the format of the demand data projected for the 1995 time frame and are computationally easy to use. Bellantoni modified Equation 2 (Reference 6) in order to obtain the conflict risk equations of the AATMS requirements specification document (Reference 8).*

2.6.2 Safety Performance Model Derivation

The conflict risk equations (Reference 7)were used in the safety analysis of the Advanced Air Traffic Management System (Reference 2). This section presents Bellantoni's derivation of the crossing conflict risk equation. The average probability of a conflict, assuming large relative velocity between aircraft, is given by

$$P_c = \int_{\tilde{\bar{r}}(t_0)}^{\tilde{\bar{r}}(t_1)} d\,\tilde{\bar{r}} \cdot \overline{\Delta S_c}\, W_r\, (\overline{0},\, t) \tag{1}$$

*A similar derivation would result using Equation 5 of Reference 6, which assumes spherical collision volumes.

where

P_c = The average probability of a conflict

$\tilde{\bar{r}}(t_0)$, $\tilde{\bar{r}}(t_1)$ = Relative position vector between two aircraft at times t_0 and t_1, respectively.

$\overline{\Delta S_c}$ = Conflict cross-section vector with respect to the relative velocity vector; if the conflict cross-section volume, S_c, has no concavities then $\overline{\Delta S_c}$ is the area A_c of the orthogonal projection of the cross-section volume onto a plane perpendicular to the relative velocity vector.

S_c = The conflict cross-section volume is the volume obtained by convoluting the conflict volumes of the two vehicles

W_r $(\bar{0}, t)$ = Probability density distribution of the vehicles relative position at time t, i.e., the probability that two vehicles have $\bar{0}$ vector separation when the nominal vehicle separation is $\tilde{\bar{r}}(t)$.

In this formula, P_c may be visualized as the volume swept out through the position distribution W_r, by the collision surface S_c, in going from $\tilde{\bar{r}}(t_0)$ to $\tilde{\bar{r}}(t_1)$ (Reference 6). A cross-section of spherical probability density distribution is represented in Figure 2.6-1.

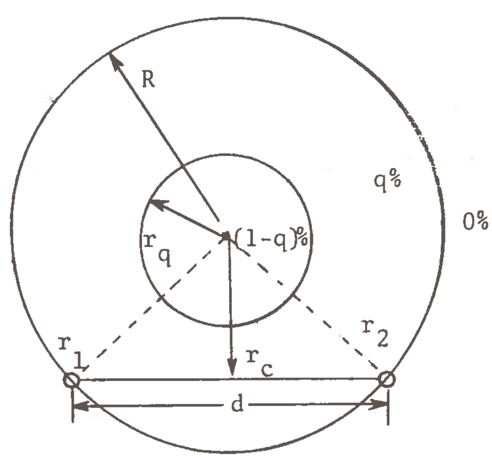

Figure 2.6-1. Cross Section of Spherical Probability Density Distribution of Relative Position

For Figure 2.6-1, (1-q)% of W_r $(\overline{0}, t)$ is contained in a sphere of radius r_q and q% of the distribution is contained between spheres of radius r_q and R. Therefore,

$$W_r(\xi, t) = \begin{cases} \dfrac{1-q}{4/3\pi\, r_q^{3}} & \text{For } \xi \le r_q \\[2ex] \dfrac{q}{4/3\pi\,(R^3 - r_q^{3})} & \text{For } r_q \le \xi \le R \end{cases} \qquad (2)$$

This level tails model of the probability density distribution used in the derivation is a pessimistic model (Reference 9 and 10). The closest approach between the vehicles r_c, Figure 2.6-1, is obtained while the relative position of the vehicles changes from r_1 to r_2. Note that zero contribution to the value of P_c in Equation 1 will result outside of the sphere of radius R. Equation 1 can now be represented as follows:

$$P_c = \frac{q\, A_c}{4/3\pi\,(R^3 - r_q^{3})} \cdot 2\sqrt{R^2 - r_c^{2}} \qquad (3)$$

with

$$d = 2\sqrt{R^2 - r_c^{2}}$$

Now choose R such that P_c will be maximized (a conservative assumption). Differentiating P_c with respect to R and setting the resulting equation equal to zero, leads to:

$$R^3 - r_q^{3} = 3R^3 - 3Rr_c^{2}$$

Assuming $r_q \simeq 0$ (another conservative assumption) and solving for R results in

$$R^3 = (3/2)^{3/2}\, r_c^{3}$$

and subsequently substituting this value in Equation 3, one obtains,

$$P_c = \frac{3q\, A_c\, r_c}{2\sqrt{2}\pi(\sqrt{27/8}\, r_c^{3} - r_q^{3})} \qquad (4)$$

The effects of the conservative simplifying assumptions utilized in the derivation were reduced by calibrating the conflict risk equation to past system safety data. In order to transform the spherical probability distribution version of the problem as configured in Figure 2.6-1 and presented in Eq. (1) to the more general ellipsoid case, a normalized version of Eq. (4) is contained in Reference 8 and presented in the next section.

2.6.3 Application of Safety Model

The number of conflicts expected for a SAATMS over a period of time was chosen as a measure of total system safety. The conflict equations chosen for use in the study are compatible with the format of the demand data projected for the 1995 time frame and they are computationally easy to use. The equations are also compatible with past data concerning collisions and critical near mid-air collisions (CNMAC). The conflict equations can be calibrated to past data (1968 data were available) [Reference 17], thereby reducing the effects of conservative simplying assumptions utilized in this derivation. A conflict or a critical near mid-air collision is defined as a near miss of 150 feet or less.

The number of conflicts model was used to compute the expected number of conflicts in the enroute airspace in 1995. The values computed were based on the projected demand data supplied by TSC, which provided the number of flight path crossings and aircraft passages in the enroute airspace for 1995. The expected number of conflicts for the SAATMS, the Ground-Based Advanced Air Traffic Management System (GAATMS), and the present system were computed.

The number of crossing and passage* conflicts for the year 1995 are given by (Reference 8)

$$N_C\ 1995 = \frac{3 \cdot q \cdot K}{2\sqrt{2}\,\pi} \sum_h \frac{A_{cn}(h)\, r_{cn}(h)}{\sqrt{\frac{27}{8} r_{cn}^3(h) - r_{qn}^3}}\, N_P\ 1995\ (h) \qquad (5)$$

where

K = Normalization factor obtained from the 1968 CNMAC data (Reference 17)

q = Fraction of the relative position error distribution, E, that lies outside the ellipsoid given by the semi-axes x_q, y_q, z_q (chosen components of a vector $\bar{r}_q$)

$$r_{qn} = \left[\left(\frac{x_q}{\sigma_x}\right)^2 + \left(\frac{y_q}{\sigma_y}\right)^2 + \left(\frac{z_q}{\sigma_z}\right)^2\right]^{1/2} = \text{Normalized magnitude of } \bar{r}_q$$

N_P 1995(h)= Number of encounters per year in an altitude band, h, derived from the demand level data and the airspace structure

σ_x, σ_y, σ_z= Standard deviations of the relative position error distribution, E, of aircraft pairs along ellipsoid semi-axes.

A_c (h) = Conflict cross-sectional area determined for 150 feet conflict and the aircraft mix at altitude band, h, normalized with respect to σ_x, σ_y, σ_z.

r_{cn} (h) = Minimum normalized nominal passage distance

$$\left[\left(\frac{x\ (h)}{\sigma_x}\right)^2 + \left(\frac{y\ (h)}{\sigma_y}\right)^2 + \left(\frac{z\ (h)}{\sigma_z}\right)^2\right]^{1/2}$$

where x (h), y (h), z (h) are the relative closest approach coordinates of two vehicles along axes of σ_x, σ_y, σ_z in an altitude band h.

---

*Two aircraft on crossing paths which come within some prescribed distance of each other constitute a crossing. The same condition for two aircraft on the same path constitute a passage (overtake).

Equation 5 was calibrated to the 1968 base year using the 1968 CNMAC data. The calibration factor was obtained by solving for K from Equation 5 using the 1968 CNMAC data as the number of conflicts and by using parameters applicable to the 1968 system. The calibration equation is

$$K = \frac{4\ \mathrm{CNMAC}_{1968}}{\left(\frac{3q'}{2\sqrt{2}\ \pi}\right) \sum_h \frac{A_c'(h)\ r_{cn}'(h)}{\left(\sqrt{\frac{27}{8}\ r_{cn}^3(h)' - r_{qn}'^3}\right)} \cdot N_{P1968}(h)} \qquad (6)$$

where the primed values imply the use of 1968 parameters and 4 CNMAC_{1968} = N_{C1968}. The factor of four is predicated on an estimate that only 25 percent of the CNMAC are reported.

To compute the number of conflicts expected in 1995, resulting from use of the present system, the GAATMS, and the SAATMS, estimates of their relative position error statistics were derived. The relative position errors (σ_x, σ_y, σ_z) were treated as independent errors in the horizontal and vertical dimensions (σ_H, σ_z). These values were estimated from the surveillance error statistics. The navigation and surveillance data were not combined statistically to obtain a composite relative position error estimate. This is a reasonable method for estimation in that the surveillance data are used to provide aircraft separation, while the navigation data are used to determine the normal operating zones which result in acceptable intervention rates. The horizontal accuracy values estimated for the present system and GAATMS assume that the aircraft are uniformly distributed within the radar range and that the angle of the position vector to the radar line of sight is uniformly distributed (see Section 2.6.4).

The average value of the closest approach distance for crossing and passage is estimated from the airspace structure and is normalized to obtain

$$r_{cn}(h) = \left[\left(\frac{x_H(h)}{\sigma_H}\right)^2 + \left(\frac{z(h)}{\sigma_z}\right)^2\right]^{1/2} \qquad (7)$$

where

x_H (h) = Nominal horizontal passage separation distance for altitude band h

z (h) = Nominal altitude separation distance in altitude band h

An IFR/IFR enroute example of x_H (h) is the specified 10 min separation for crossing aircraft and an assumed 7 nmi separation for passing aircraft. The 10 min separation corresponds to different average separation distances for each altitude band due to differing aircraft velocities in each altitude band.

The average collision cross-section, A_c (h), is determined by the aircraft dimensions, wake turbulence, and the specified 150 ft miss distance. The average collision cross-section is dependent on the mix of aircraft in each altitude band. The average collision cross-section is normalized by the position keeping accuracy and is given by

$$A_c\ (h) = \frac{\ell}{\sigma_H} \cdot \frac{S}{\sigma_z} \tag{8}$$

where

ℓ = Diameter of the collision cross-section cylinder

S = Height of the collision cross-section cylinder

The magnitude of q is related to the chosen ellipsoid semi-axes x_q, y_q, z_q; q is the probability that the relative position error, E, exceeds x_q, y_q or z_q. Equivalent probability distribution axes were chosen for the horizontal and vertical dimension, $r_{x,y}$ and z_q, respectively (components of $\bar{r}_q$). The horizontal and vertical values chosen were kept constant in the evaluation of the three systems. The normalized vector, $\bar{r}_{qn}$, is given by

$$r_{qn} = \left[\left(\frac{r_{x,y}}{\sigma_H}\right)^2 + \left(\frac{z_q}{\sigma_z}\right)^2\right]^{1/2} \tag{9}$$

where

σ_H = Horizontal position keeping accuracy

σ_z = Vertical position keeping accuracy

For fixed values of $r_{x,y}$ and z_q, if σ_H and σ_z become smaller (i.e., the position keeping accuracy improves), the value of q will become smaller. The magnitude of q thus reflects the relative system surveillance accuracies. Conservative estimates of q were obtained through the use of the Tchebycheff inequality. These estimates are independent of the actual shape of the tails of the relative position error distribution. The tacit assumption involved in the use of the Tchebycheff inequality is that the actual shape of the relative position error distribution remains constant from system to system. The concept implicit in the assumption of a constant distribution is that the probability of a blunder occurrence is proportional to system accuracy.

The values for the number of conflicts for the three systems are obtained by Equations 5 through 9, along with estimates of q based on the statistics of the systems and the projected 1995 demand data. The number of conflicts computed were for the crossing and passage of IFR/IFR enroute aircraft. The crossing and passage conflicts for VFR/VFR and VFR/IFR aircraft under surveillance by the system can also be determined by the same equations if the demand data are properly defined.

Several other models were (Reference 2) used in the safety analysis for the SAATMS. The enroute demand model was used to obtain the number of IFR/IFR, VFR/IFR, and VFR/VFR crossings and passages, N_{P1995} (h), for use in Equation 5. The number of enroute VFR/VFR and VFR/IFR conflicts for unsurveilled airspace in the year 1995 were determined. The probability of a passage being within X ft. was needed in conjunction with the enroute demand data to obtain the results.

2.6.4 Auxiliary Models

2.6.4.1 Relative Horizontal Surveillance Accuracy, σ_H, for Radar System

A radar system is used to measure the relative position between aircraft for the present system and the Ground-Based Advanced Air Traffic Management System. The azimuth measurement error is linearly related to the range of the measured aircraft from the radar site, whereas the range error is a constant over the radar range. The relative horizontal surveillance accuracy in the direction of the vector distance between measured aircraft is required for the conflict risk equations. An average relative horizontal surveillance accuracy is calculated over the possible relative position vector angles with the radar line of sight. The position of the airplanes being measured are assumed distributed uniformly within the radar range coverage and the relative position vector angle with the radar line of sight is assumed to be uniformly distributed. The azimuth error is modeled as

$$\sigma_\theta = \overbrace{[2(6076) \sin\tfrac{\theta}{2}]}^{K_1} \sigma_r \tag{10}$$

where

K_1 = A constant which is calculated from the radar angular uncertainty.

r = The range of the airplane from the radar site.

θ = Radar angular measurement uncertainty

σ_r = The range measurement uncertainty.

The azimuth and range uncertainties for each airplane are assumed independent; therefore, the relative azimuth and range errors are as follows:

$$\begin{aligned} \sigma_{\bar{r}} &= \sqrt{2}\,\sigma_r \\ \sigma_{\bar{\theta}} &= \sqrt{2}\,\sigma_\theta \end{aligned} \tag{11}$$

The sum square variance of the relative surveillance position error $\sigma_H{}^2$ in the direction of the relative position, as shown in Figure 2.6-2 is:

$$\sigma_H{}^2 = \sigma_{\bar{\theta}}{}^2 \cos^2\alpha + \sigma_{\bar{r}}{}^2 \sin^2\alpha \tag{12}$$

where α = Angle between the perpendicular to the radar line of sight and the relative position vector.

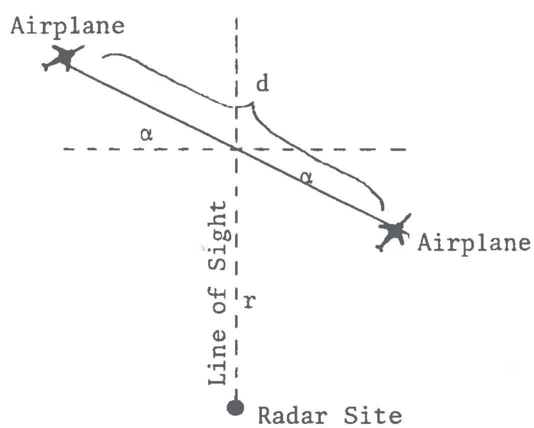

Figure 2.6-2. Relative Radar Surveillance Geometry

The average variance of the relative surveillance position error, $\overline{\sigma_H}^2$, is as follows:

$$\overline{\sigma_H^2} = \frac{1}{\pi/2} \cdot \frac{1}{R} \int_0^R \int_0^{\pi/2} 2\, K_1^2\, r^2 \cos^2\alpha + \sigma_{\overline{r}}^2 \sin^2\alpha \;\; d\alpha\, dr \qquad (13)$$

where α and r are assumed uniformly distributed

$$0 \leq r \leq R$$
$$0 \leq \alpha \leq 90°$$

Substituting the identities

$$\cos^2\alpha = 1/2\ (1 + \cos 2\alpha)$$
$$\sin^2\alpha = 1/2\ (1 - \cos 2\alpha)$$

and carrying out the required integration leads to:

$$\overline{\sigma_H} = \sqrt{\frac{\sigma_{\overline{r}}^2}{2} + \frac{\sigma_{\overline{\theta}max}^2}{6}} \qquad (14)$$

where

$\sigma_{\theta max}$ = the $\sigma_{\overline{\theta}}$ at a range of R nmi.

This equation is used to calculate the horizontal surveillance accuracy (Reference 2).

2.6.4.2 Random Probability That Two Aircraft are at Close Proximity During an Overtake

The random probability of an overtaking aircraft being in close proximity to the aircraft being passed can be calculated assuming a uniform position distribution for each of the interacting aircraft, a_1 and a_2, over the VOR route width 2D [see Figure 2.6-3(A)].

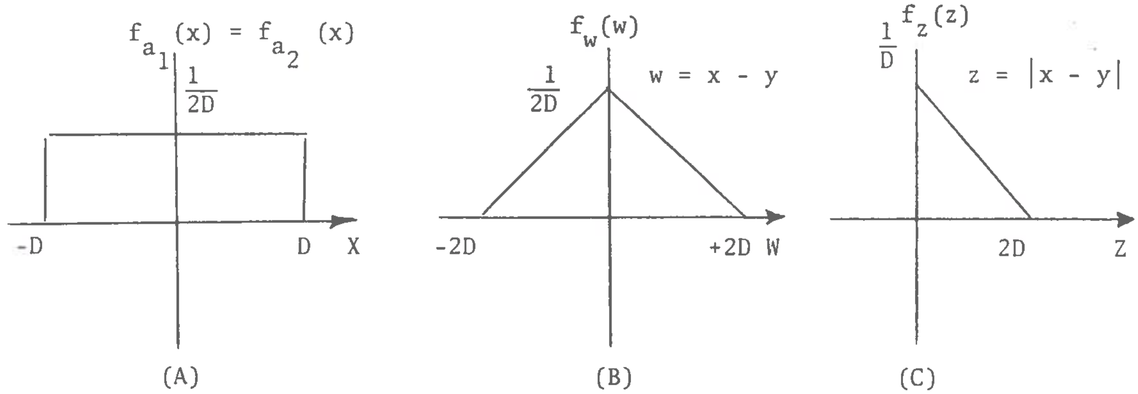

Figure 2.6-3. Probability Distributions

The random probability distribution for the distance between the two aircraft is shown in Figure 2.6-3(B) (Reference 18) and the probability that the two aircraft are an absolute distance Z apart is shown in Figure 2.6-3(C).

The probability, P, that the two aircraft are within a distance d of each other is indicated as the shaded portion in Figure 2.6-4

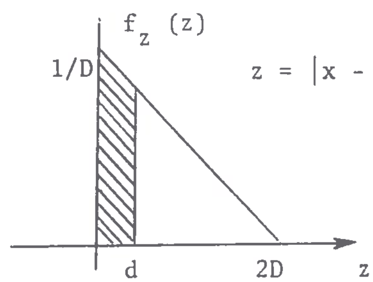

Figure 2.6-4. Probability of Passing Aircraft Within a Specified Distance

The probability, P, is given by

$$P = 1 - \frac{1}{2} \frac{(2D-d)^2}{2D^2} \tag{15}$$

For a VOR route of 2D = 5 nmi and a miss distance of d = 150' (Reference 21), P = 0.0098.

This probability can then be multiplied by the number of passages occurring on each route to obtain the expected number of VFR/VFR and VFR/IFR conflicts that will occur over any desired period of time.

3. SATELLITE SURVEILLANCE DETECTION ANALYSIS

3.1 The Detection Scheme

The surveillance identification scheme employed assures that aircraft throughout CONUS can be tracked with extremely high probability regardless of location or bank angle. In this subsection the philosophy of the detection scheme and the waveform chosen are discussed.

In the proposed scheme each aircraft periodically transmits a unique ID that is relayed by several satellites and detected on the ground. The aircraft position is computed using the times-of-arrival (TOA) from the various satellites. A minimum of four TOAs is needed for a 3-D position estimate. With the 15 satellite constellation discussed in Volume II, the number of visible satellites from any point in CONUS at any time is 8 to 11. Each aircraft-satellite channel has error-detecting capability that allows all reliable data during a particular update to be used in the position computation.

An extremely important property of the adopted scheme is that a given aircraft-satellite RF link is not indispensible at any time. Since each link has error-detecting capability, only links which provide error-free detections are used during a given update period. This dispensible-link property is extremely important because the reliability of any aircraft-satellite RF link varies with time. For example, either or both of the following might happen during a particular update period:

1. The jth satellite is in a very disadvantaged portion of an aircraft's antenna pattern because of a combination of location and bank angle. This causes decreased signal energy to reach the satellite and increases the probability of missed detection.

2. An excessive amount of multi-access noise occurs in the jth satellite during the given update period. This increases the probability of false alarm. Multi-access noise refers to the interference between simultaneous users that exists in all random access schemes. Since a large number of aircraft use the single wide-bandwidth channel with no time synchronization between aircraft each transmission serves as noise to all others.

If a given link was indispensible, detection thresholds would have to be chosen on the basis of the worst possible aircraft-satellite orientation. Such a worst-case scheme seems non-feasible (reference 20). With the dispensible link scheme proposed here, severely disadvantaged links are simply not used when they are unreliable. A given aircraft-satellite link is used only during those times when it provides error-free information.

An aircraft ID consists of three psuedo-noise (PN) pulses as shown in Figure 3.1-1. Each pulse is 40 μsec long consisting of 400 chips of 100 nsec duration. The phase coding of the individual pulses and the spacing between pulses are varied to yield 10^6 unique IDs. For each aircraft-satellite-ground link there is a receiver that detects individual pulses, combines the pulses to form IDs, and associates a TOA with each ID.

The surveillance function has both a tracking and acquisition mode. In the track mode a receiver looks for the kth ID only during a certain time interval called a reporting window. The center of the window is the time that the ID is expected to arrive. The expected time is available because of the periodicity of the surveillance updates. The width of the window is based on the uncertainty in the TOA estimate.

During a particular reporting period of the kth aircraft one of three events can occur in the jth channel:

1. The ID is detected once in the reporting window (unambiguous detection)

2. The ID is detected more than once in the window (ambiguous detection)

3. The ID is not detected in the window (missed detection)

If unambiguous detection occurs, the TOA is used as one of the inputs to the position estimate. If either ambiguous detection or missed detection occurs, the jth satellite does not contribute to the position estimate for that period.

Ambiguous or missed detection causes the window width to increase by the nominal width, δ. Unambiguous detection always reduces the window to its nominal width. If the window width is 3 δ, ambiguous detection causes no change in the window and missed detection causes loss-of-lock. Loss-of-lock means that the kth aircraft must be reacquired in the jth satellite channel.

In order to be tracked, an aircraft must first be acquired. The acquirer looks for all possible IDs minus those that are currently being tracked. The jth satellite channel has a potential acquisition of the kth aircraft if it detects the kth ID three times and the TOAs differ in time by $T_k \pm \delta$. Once TOAs for the kth aircraft are received from at least four satellites, track is initiated.

3.2 Summary of Detection Analysis Results

A mathematical model of the satellite surveillance scheme was derived. This model was used to guide the selection of the various system parameters, to evaluate the system performance, and to indicate the sensitivity and relative importance of the different parameters.

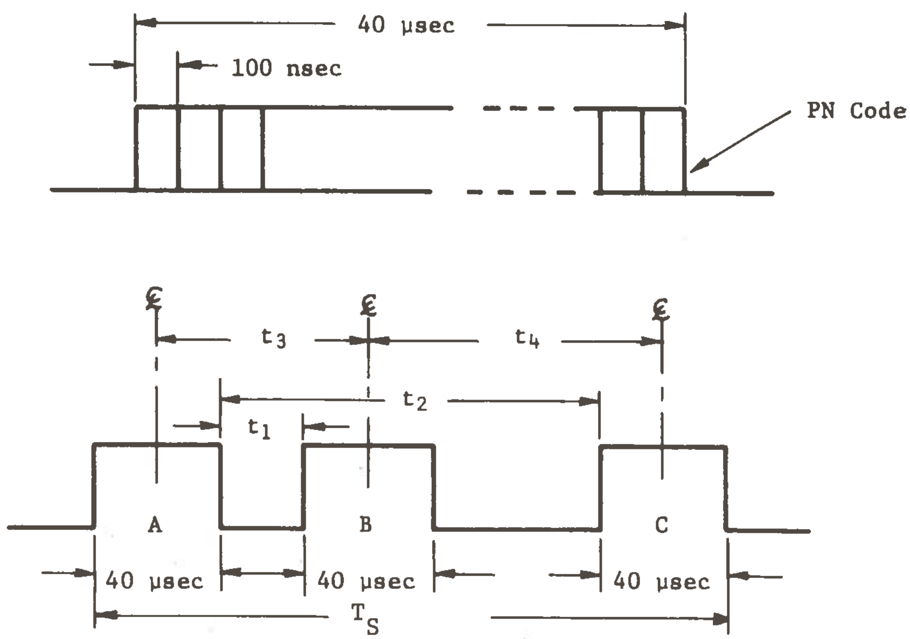

$0.3 \leq t_1 \leq 1.8$ μsec

$45.0 \leq t_2 \leq 46.5$ μsec

$40.3 \leq t_3 \leq 41.8$ μsec

$44.7 \leq t_4 \leq 46.2$ μsec

$125.0 \leq T_s \leq 126.5$ μsec

Figure 3.1-1. Aircraft Surveillance

See Table 3.2-1 for a list of parameters and their definitions.

Decisions concerning the presence or absence of aircraft IDs are made in each satellite channel. The probability of unambiguous detection (i.e., detection with no false alarms) of the kth ID in the jth satellite channel during any update is a fundmental statistic. A lower bound to the probability as a function of signal-to-noise ratio (SNR) is plotted in Figure 3.2-1. Notice that the error-free detection probability is greater than .998 with 13 db SNR.

Several other statistics were parametrically studied. For example, the probability of unambiguous detection from at least 4 out of 5 satellites is greater than .99996 if each satellite has 13 db SNR. Thus, with 13 db SNR, the probability of not obtaining at least 4 unambiguous detections during any update is extremely small. Recall that there are normally 8 to 11 satellite channels with at least 13 db SNR.

The analysis results indicate that 13 db SNR yields excellent system performance using a three-pulse ID scheme. The SNR in a link budget for a geostationary satellite channel is shown in Table 3.2-2. Notice that the available SNR is 22.8 db, leaving a margin of 9.8 db.

The sensitivities of the various system parameters were determined. Only the effect of varying the number of pulses per ID (n) and the number of codes per pulse (C_N) will be discussed here.

The total effect of varying n is shown in Table 3.2-3, where the assumption was made that all other parameter values remain constant. On an SNR basis, n=3 is a logical choice if the number of active aircraft is between 35,000 and 100,000.

The performance sensitivity of the model to C_N was extremely small. Thus, small values of C_N can be planned for. This eases the problem of finding codes with good auto-correlation and cross-correlation properties. The correlation properties of the codes actually used is expected to have large impact on the actual performance attained.

3.3 Detection Model Assumptions

Several assumptions were made to develop the detection model. These assumptions are noted in the following paragraphs.

Each aircraft has a unique ID consisting of a particular sequence of n pulses. Each pulse is one of C_N pseudo-noise codes. It was assumed that noncoherent (i.e., no absolute phase reference) matched filters are used to detect the individual pseudo-noise pulses that combine to form IDs. For $n > 1$, individual pulses are detected instead of whole IDs because of frequency and phase instabilities of long IDs.

The multi-access noise to any given matched filter was assumed to be bandlimited, Gaussian white noise. The assumption was made in order to obtain a relationship between the multi-access noise and the pulse detection

Table 3.2-1. Parameter Definitions

Parameter	Definition
C_N	Number of codes per pulse; i.e., number of distinct matched filters.
n	Number of PN pulses per ID.
N_A	Number of instantaneous active aircraft.
N_T	Total number of unique aircraft ID's.
N_{acq}	Necessary number of consecutive cycles without missed detection in order to have acquisition.
T_K	Reporting repetition interval of kth aircraft (sec).
T_c	Time resolution (sec).
T_{ave}	Average reporting repetition interval of all active aircraft (sec). $\frac{1}{N_A} \cdot \sum_{k=1}^{N_A} T_k$
T_A	Time accuracy which an aircraft can maintain in one reporting interval (sec).
V_m	Maximum uncertainty of the rate of change in aircraft-to-satellite distance (m/sec).
T_P	Pulse width of a single PN pulse.
SNR	Signal-to-noise ratio per pulse .
P_d	Single pulse probability of detection.
P_f	Single pulse probability of false alarm due to noise.
P_s	Single pulse probability of false alarm due to phantom pulse.
P_{fs}	Total single pulse probability of false alarm.
N_W	Single satellite reporting interval window; i.e., "periodically" window (time slots).
N_G	Multi-satellite window due to geometric structure of satellite constellation (time slots).

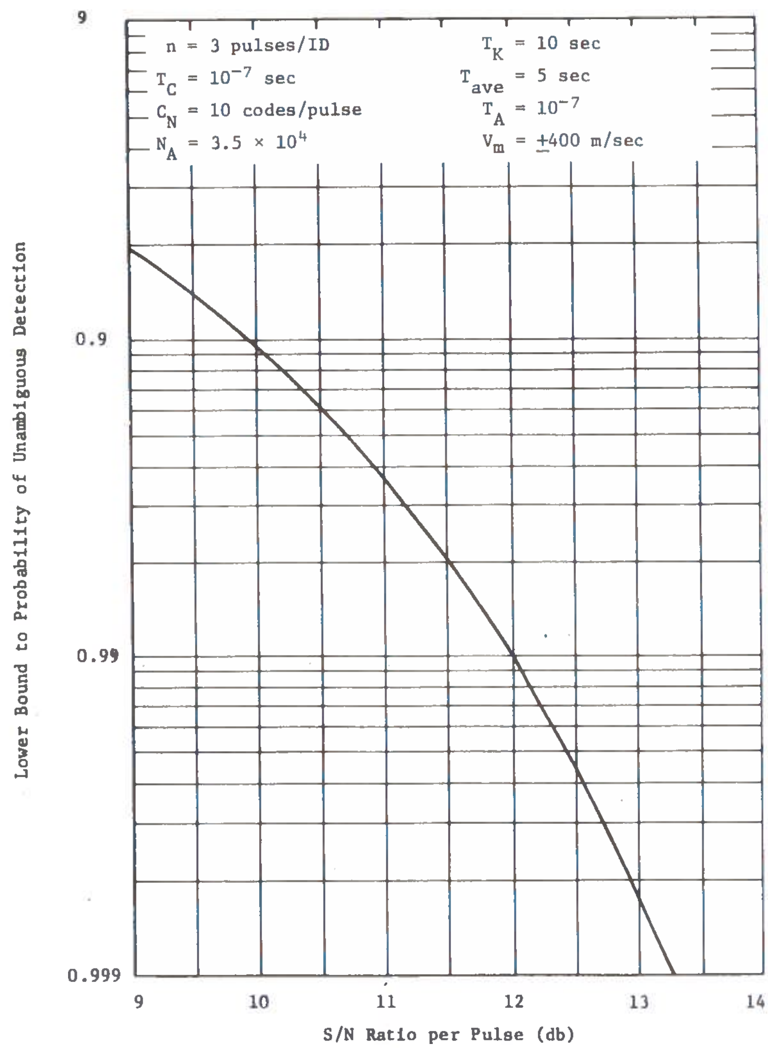

Figure 3.2-1. Probability of Unambiguous Detection

Table 3.2-1. Parameter Definitions

Parameter	Definition
C_N	Number of codes per pulse; i.e., number of distinct matched filters.
n	Number of PN pulses per ID.
N_A	Number of instantaneous active aircraft.
N_T	Total number of unique aircraft ID's.
N_{acq}	Necessary number of consecutive cycles without missed detection in order to have acquisition.
T_K	Reporting repetition interval of kth aircraft (sec).
T_c	Time resolution (sec).
T_{ave}	Average reporting repetition interval of all active aircraft (sec). $\frac{1}{N_A} \sum_{k=1}^{N_A} T_k$
T_A	Time accuracy which an aircraft can maintain in one reporting interval (sec).
V_m	Maximum uncertainty of the rate of change in aircraft-to-satellite distance (m/sec).
T_p	Pulse width of a single PN pulse.
SNR	Signal-to-noise ratio per pulse .
P_d	Single pulse probability of detection.
P_f	Single pulse probability of false alarm due to noise.
P_s	Single pulse probability of false alarm due to phantom pulse.
P_{fs}	Total single pulse probability of false alarm.
N_W	Single satellite reporting interval window; i.e., "periodically" window (time slots).
N_G	Multi-satellite window due to geometric structure of satellite constellation (time slots).

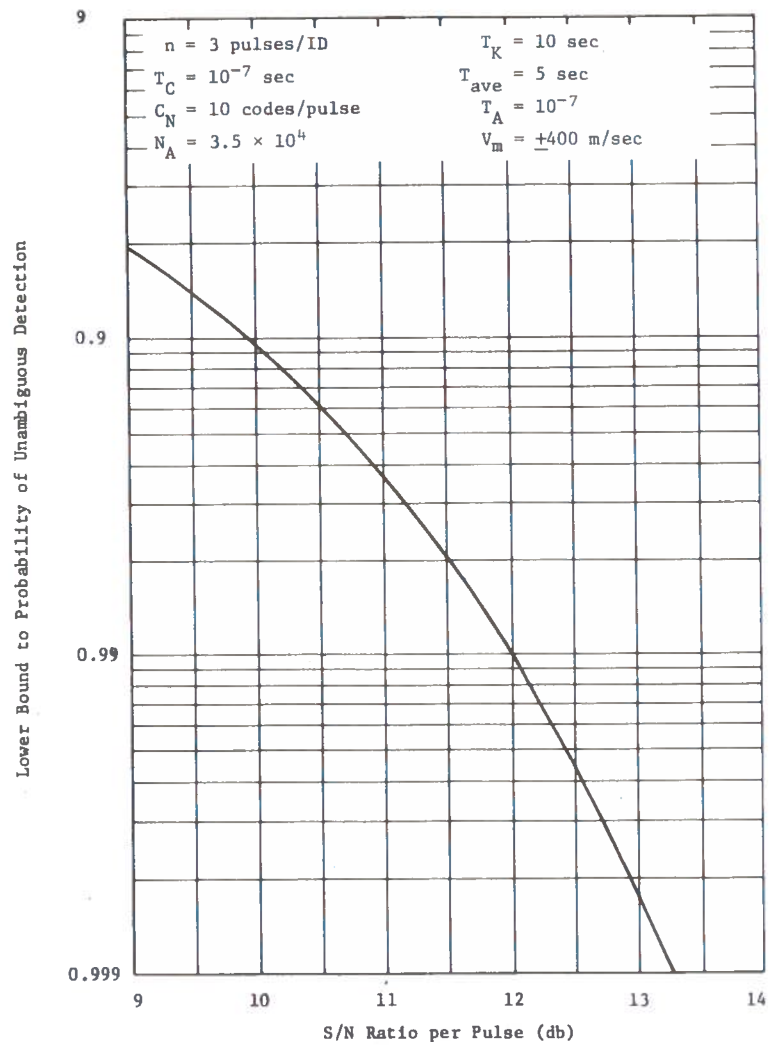

Figure 3.2-1. Probability of Unambiguous Detection

Table 3.2-2. Power Budget for Geostationary Satellite Channel

Transmitted Energy Per Pulse (2 KW for 40 usec)	- 11.0 dbJ
A/C Antenna Gain	4.0 db
Satellite Antenna Gain (10° Beam-70% Efficiency)	24.6 db
Pointing Losses	1.0 db
Miscellaneous Losses (Plumbing = 1 db, Attenuation = 1 db)	2.0 db
Path Loss (f = 1.6 GHz, d = 26,000 mi)	189.0 db
Received Signal Energy Per Pulse	- 174.4 dbJ
Effective Multi-Access Noise Power Density	- 204.2 dbW/Hz
($N_A = 3.5 \times 10^4$ aircraft, $\frac{n}{T} = \frac{3 \text{ pulses}}{5 \text{ sec}}$, BW = 20 MHz)	
Receiver Noise Density	- 201.0 dbW/Hz
Total Background Noise	- 199.3 dbW/Hz
Downlink Degradation (100 w. Xmitted pwr, 15' grd. ant.)	0.1 db
Detection Loss (Limiter & Decorrelation)	2.0 db
SNR Per Pulse	22.8 db
Required SNR	13.0 db
Margin	9.8 db

TABLE 3.2-3. EFFECT OF VARYING THE NUMBER OF PULSES PER ID (N)

n	Effective Multi-Access Noise (dbw/Hz)		Total Background Noise (dbw/Hz)		SNR per Pulse (db)		Required SNR	Margin	
	(a)	(b)	(a)	(b)	(a)	(b)		(a)	(b)
2	-206.0	-202.4	-199.8	-198.6	23.3	22.1	14	9.3	8.1
3	-204.2	-200.6	-199.3	-197.8	22.8	21.3	13	9.8	8.3
4	-203.0	-198.4	-198.9	-196.5	22.3	20.0	12.5	9.8	7.5
5	-202.0	-197.4	-198.5	-195.8	22.0	19.3	12.2	9.8	7.1

(a) $N_A = 3.5 \times 10^4$ active aircraft

(b) $N_A = 10^5$ active aircraft

statistics. The power density was determined by the total number of active aircraft (N_A), the average ID repetition interval (T_{ave}), the number of pulses per ID (n), the bandwidth of the system, and the average received signal energy per pulse. The multi-access noise was assumed independent of the omnipresent thermal noise, and both noise terms were combined to give a total background noise. The background noise and the received signal energy determine a family of (P_d, P_f) pairs for a single pulse.

There will always be ID false alarms because of noise. For $n > 1$, another source of ID false alarms exists that would be present even in a noise-free environment. This second type of false alarm, called phantom IDs, can occur when two or more IDs interleave and yield apparent receptions of additional (phantom) IDs. Figure 3.3-1 shows an example of two IDs correctly received for a two pulse per ID scheme. In the example, the IDs C_1 C_4 and C_8 C_9 were transmitted. Depending on the time spacings involved, the combinations C_1 C_8, C_1 C_9, C_8 C_4, and C_4 C_9 could correspond to possible IDs although these IDs were, in fact, not transmitted.

In order to account for phantom IDs, the assumption was made that for each of the C_N types of pulses there are $\frac{nN_A}{C_N}$ pulses uniformly distributed within any T_{ave} time interval. It was also assumed that detection decisions are made every T_c seconds. T_c is the time resolution of the system; that is, there are T_{ave}/T_c distinct time slots in a T_{ave} second interval. In any given time slot a phantom pulse that could be part of the kth ID has probability

$$P_s = \frac{nN_A \, T_c}{C_N \, T_{ave}} P_d \quad \text{(for } n > 1\text{)}$$

of occurring. If $n = 1$, $P_s = 0$ because all pulses must then be distinct (i.e., $C_N = N_T$ - total number of IDs). The single pulse statistics are thus characterized by the pairs (P_d, P_{fs}) where

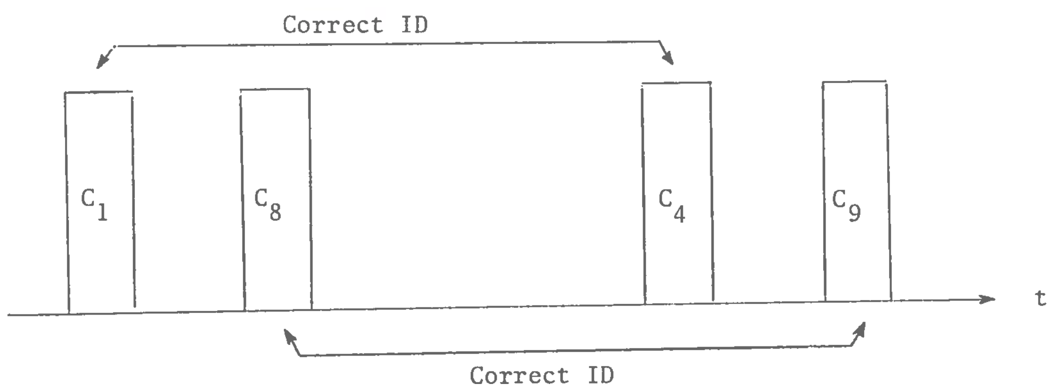

Figure 3.3-1. Possible Phantom IDs

P_d = single pulse probability of detection

P_{fs} = single pulse probability of false alarm

$= P_f + P_s - P_f P_s$

3.4 Probability of Unambiguous Detection in a Single Satellite Channel

Decisions concerning the presence or absence of aircraft IDs are made in each satellite channel. The purpose of this section is to characterize the detection performance of a single satellite channel.

Recall that during a particular reporting period of the kth aircraft one of three events can occur in the jth satellite channel:

1. The ID is detected once in the reporting window (unambiguous detection)

2. The ID is detected more than once in the window (ambiguous detection)

3. The ID is not detected in the window (missed detection)

The window structure gives the system automatic error-detecting capability. Unless unambiguous detection occurs in a given reporting window, it is known that some sort of error has occurred. Since a large number of satellites are available to each aircraft, a logical algorithm is to use only those satellite channels that yield unambiguous detection during a given reporting period. This dispensible-link property eliminates the problem of an aircraft severely disadvantaged in a particular satellite channel.

In the following, unambiguous detection does not include the case of missed detection coupled with exactly one false alarm in the window. Thus, unambiguous detection refers to a correct, positive identification. The important statistic we desire is:

P_1 = probability of unambiguous detection of the kth aircraft in the jth satellite channel during a given reporting period

It is easy to obtain that

$$\underline{P_1} \leq P_1 \leq \overline{P_1} \qquad (1)$$

where

$\underline{P_1}$ = probability of unambiguous detection given that the reporting window has the maximum width of $3N_w$ time slots

$$= P^3(0)\, P_d^{\,n} \qquad (2)$$

$\overline{P_1}$ = probability of unambiguous detection given that the reporting window has the minimum width of N_w time slots

$$= P(0)\ P_d^{\ n} \tag{3}$$

P(0)=probability that no false alarms occur in a reporting window of width N_w time slots

$$= (1-P_{fs}^{\ n})^{N_w} \tag{4}$$

n = number of pulses per ID

N_w = number of time slots in the reporting window

$$= 2\ [V_m T_k/_c + T_A]/T_c$$

Figure 3.2-1 shows the lower bound $\underline{P_1}$ as a function of SNR for the following conditions:

n = 3 pulses/ID

N_A = 10^5 active aircraft

T_c = 10^{-7} seconds

T_k = 10 seconds

T_{ave} = 5 seconds

C_N = 10 codes/pulse

V_m = 400 m/sec

T_A = 10^{-7} seconds

3.5 Model with only Four Available Satellites

In order to obtain the worst-case system performance, we assume only 4 available satellites in this section.

3.5.1 Performance Equations

3.5.1.1 Tracking Mode Perfect Detection Probability

Define perfect detection of the kth aircraft ID during a particular reporting period as unambiguous detection in each of the four available satellite channels.

Let P_D equal the probability of perfect detection. Clearly,

$$P_D = P_1^{\,4} \qquad (1)$$

and

$$\underline{P}_D \leq P_D \leq \overline{P}_D \qquad (2)$$

where

$$\underline{P}_D = \underline{P}_1^{\,4} \qquad (3)$$

$$\overline{P}_D = \overline{P}_1^{\,4} \qquad (4)$$

P_1 and its upper and lower bounds are defined in Section 3.4.

3.5.1.2 Tracking Mode Loss-of-Lock Probability - In any tracking scheme there is a certain probability that track will be lost. We now derive a measure of this event.

Let a cycle be one reporting period and let B represent the following event:

$$B = \left\{ \begin{array}{l} \text{Following a cycle of perfect detection, loss-} \\ \text{of-lock occurs before another cycle of perfect} \\ \text{detection.} \end{array} \right\}$$

Then,

$$\underline{P_{LOSS}} \leq P(B) \leq \overline{P_{LOSS}} \qquad (5)$$

where

$\overline{P_{LOSS}}$ = Probability that perfect detection does not occur in any of three consecutive cycles following a cycle of perfect detection

$$\leq (1 - \overline{P}_D)\ \{1 - \overline{P}_D\ P^4(0)\ [1 + P^4(0) - \overline{P}_D\ P^8(0)]\} \qquad (6)$$

$\underline{P_{LOSS}}$ = Probability that, following a cycle of perfect detection, loss occurs in exactly three cycles

$$= 1 - (1 - P_L)^4 \qquad (7)$$

P_L = Probability that following a cycle of unambiguous detection a triple window occurs in a given satellite channel followed by a cycle of missed detection

$$= (1 - Q_1)\ (1 - Q_2)\ (1 - P_d^{\,n})\ P^3(0) \qquad (8)$$

Q_j = Probability of obtaining an ID only once in a window of size jN_w.

$$= P_d^{\,n}\, P^j(0) + \frac{jN_w\, P_{fs}^{\,n}}{1 - P_{fs}^{\,n}} (1 - P_d^{\,n})\, P^j(0) \qquad (9)$$

For the derivation of Eq. (6), let

$P_D(\leq 3)$ = Probability that perfect detection occurs within 3 cycles following a cycle of perfect detection.

$$= P_D(1) + P_D(2) + P_D(3)$$

where

$P_D(k)$ = Probability that perfect detection occurs exactly k cycles following a cycle of perfect detection.

Notice that $P_D(1)$ is merely $\overline{P}_D$ • $P_D(2)$ and $P_D(3)$ can be lower bounded by

$$P_D(2) \geq \underline{P_D(2)} = (1 - \overline{P}_D)\, P_d^{\,4n} P^8(0) = \overline{P}_D(1 - \overline{P}_D)\, P^4(0)$$

$$P_D(3) \geq \underline{P_D(3)} = [1 - \overline{P}_D - P_D(2)]\, P_d^{\,4n} P^{12}(0) = \overline{P}_D\, P^8(0)[1 - \overline{P}_D - P_D(2)]$$

Thus,

$$P_D(3) = \overline{P}_D + P_D(2) + P_D(3)$$

$$\geq \overline{P}_D + P_D(2) + \underline{P_D(3)} = \overline{P}_D + P_D(2) + \overline{P}_D P^8(0)[1 - \overline{P}_D - P_D(2)]$$

$$\geq \overline{P}_D\, [1 + (1 - \overline{P}_D)\, P^8(0)] + \underline{P_D(2)}\, [1 - \overline{P}_D\, P^8(0)]$$

$$= \overline{P}_D\, \{1 + (1 - \overline{P}_D)\, P^4(0)\, [1 + P^4(0) - \overline{P}_D\, P^8(0)]\}$$

Using $\overline{P_{LOSS}} = 1 - P_D(3)$ yields Eq. (6)

The derivations of Eq. (7), (8), and (9) are fairly straightforward. The first term of the right side of Eq. (9) is the probability of correctly detecting the ID and having no false alarms in the window. The other term is the probability of missed detection and exactly one false alarm.

The probability of obtaining a triple window in two cycles following a cycle of unambiguous detection is simply $(1 - Q_1)(1 - Q_2)$. The probability of missed detection and no false alarms in a triple window is $(1 - P_d^{\,n}) P^3(0)$. Thus, Eq. (8) is derived. Equation (7) follows because loss of signal in any of the four satellites can cause loss-of-lock.

3.5.1.3 Expected Number of False Acquisitions - Let

EF_k = Expected number of false acquisitions of the kth ID during a T_k time interval

Then,

$$EF_k \leq 8 \frac{T_k}{T_c} N_G^{\,3} N_w^{\,4} (N_{acq} - 1) P_{fs}^{\,4nN_{acq}} \tag{10}$$

where

N_{acq} = Minimum number of reporting periods required for acquisition. An aircraft is considered acquired only after N_{acq} consecutive periods of perfect detection.

T_k = Reporting repetition period (sec)

T_c = Time resolution (sec)

N_G = Geometric window (time slots)

N_w = Reporting interval window (time slots)

P_{fs} = Single pulse probability of false alarm

$= P_f + P_s - P_f P_s$

Assuming N_T total ID's

EF_T = Expected number of false acquisitions in time T_k while searching for N_T ID's.

$$= N_T (EF_k) \tag{11}$$

In Eq. (10) and (11) the expected values do not include those cases involving active aircraft where correct detections are mixed with false alarms to yield acquisitions with incorrectly placed windows. Such acquisitions are very likely to be "good" acquisitions, particularly if the aircraft is not moving very rapidly.

3.5.1.4 Probability of Rapid Acquisition - Let N be a random variable representing the number of periods required for the acquisition of an aircraft. The probability that an aircraft is acquired in the minimum time is

$P_A\ (N = N_{acq})$ = Probability that a given aircraft is acquired in N_{acq} reporting periods

$$= P_d^{4nN_{acq}} \tag{12}$$

Equation (12) is merely the probability of successfully detecting each of $4nN_{acq}$ pulses; given that each pulse has probability P_d of being detected. The equation ignores the possibility that an aircraft can be acquired although missed detections occur in m of the $4N_{acq}$ trials, provided that false alarms also happen to occur in each of the m reporting windows. If none of the false detections are in the last reporting period (i.e., the last four-tuple of reception times is perfect) then the acquisition is perfect. If one or more of the false detections occur in the last period, the acquisition is made with imperfect placement of one or more of the reporting windows.

The probability of acquisition within 2 N_{acq} periods is

$P_A\ (N \leq 2\ N_{acq})$ = Probability that a given aircraft is acquired in 2 N_{acq} periods or less

$$= P_d^{4nN_{acq}} [1 + N_{acq}\ (1 - P_d^{4n})] \tag{13}$$

The comments following Eq. (12) also apply to Eq. (13).

3.5.2 Parametric Curves

Unless otherwise indicated, the following parameter values have been assumed for all calculations shown in this section.

N_A = 10^5 active aircraft

N_T = 10^6 unique ID's

T_c = 10^{-7} seconds

T_{ave} = 5 seconds

V_m = $\pm$ 400 m/sec

N_{acq} = 2 periods

C_N = 10 codes/pulse

T_k = 10 sec

n = 3 pulses/ID

T_A = 10^{-7} seconds

N_G = 2.4×10^5

For each value of SNR the (P_d, P_f) combination was chosen to minimize $\overline{P_{LOSS}}$. The value chosen for V_m assumes that the known bias due to satellite velocity is removed.

The effect of varying n on system performance is shown in Figure 3.5-1 thru 3.5-4. As n increases, the SNR required to obtain a given level of performance decreases by approximately $\sqrt{n}$. This is not too surprising since the surveillance scheme is analogous to a radar system using post-detection integration. (Recall that individual pulses are detected.) However, increasing the number of pulses does not necessarily increase system performance. Increasing n reduces the available SNR since the multi-access noise is also increased.

The effect of varying T_k on probability of detection is shown in Figure 3.5-5. Aircraft with low update rates (i.e., large T_k) require higher SNRs than high update users. This is because large T_k imply large reporting windows.

Figure 3.5-6 illustrates the tightness of the bounds for P_D and P_{LOSS}. The requirements imposed on the P_{LOSS} probability require some discussion. Assume a typical flight of 4 hours duration, and a total of 2550 aircraft updates. (3 hrs. at T_k = 8 sec and 1 hr. at T_k = 3 sec.) If in each of the 2550 trials there is a probability of 2.5×10^{-7} of becoming "lost", the probability that the aircraft is lost at least once during its flight in $1 - (1 - 2.5 \times 10^{-7})$ 2550 = 6×10^{-4}. Alternatively, if each of 10^5 CONUS aircraft has probability 2.5×10^{-7} of becoming lost during any given period, an average of .025 aircraft will be lost per cycle. Assuming T_{ave} = 5 sec, about 18 aircraft per hour would have to be reacquired.

The loss-of-lock probability can be lowered by simply allowing for one more coast. That is, the system could expand to quadruple windows instead of stopping with triple windows. Alternatively, track could continue with triple windows until two successive missed detections occurred (instead of one). The cost is a delay in reacquisition.

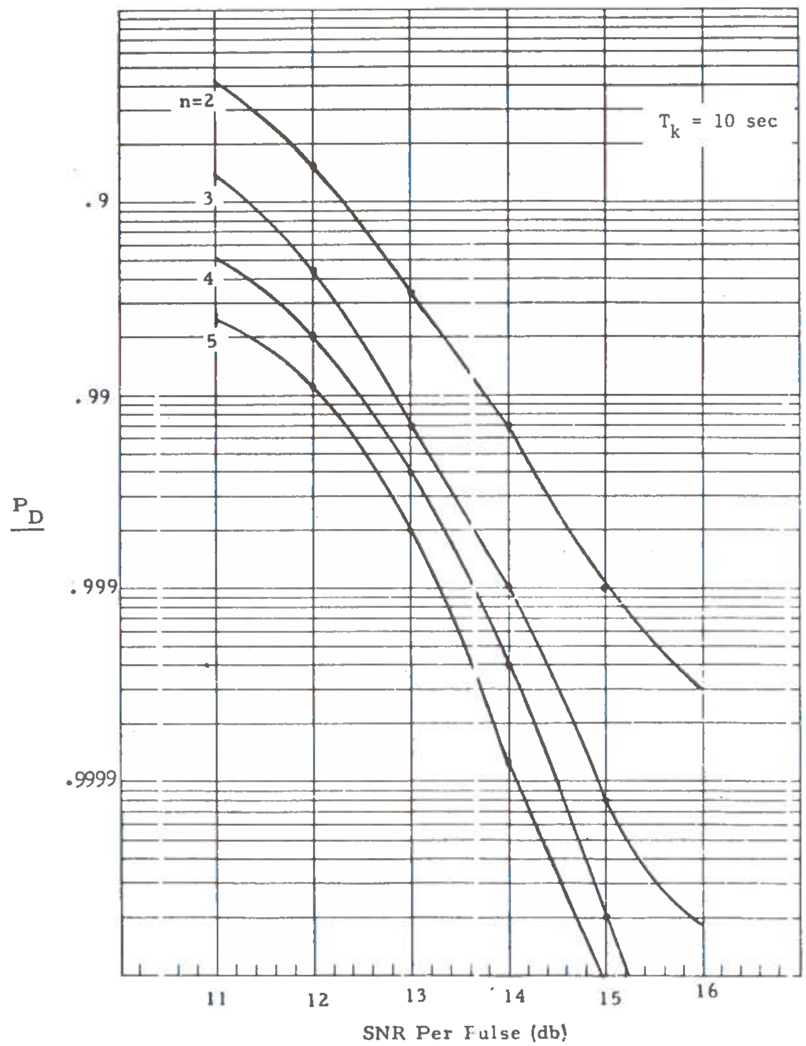

Figure 3.5-1. Lower Bound of Perfect Detection Probability

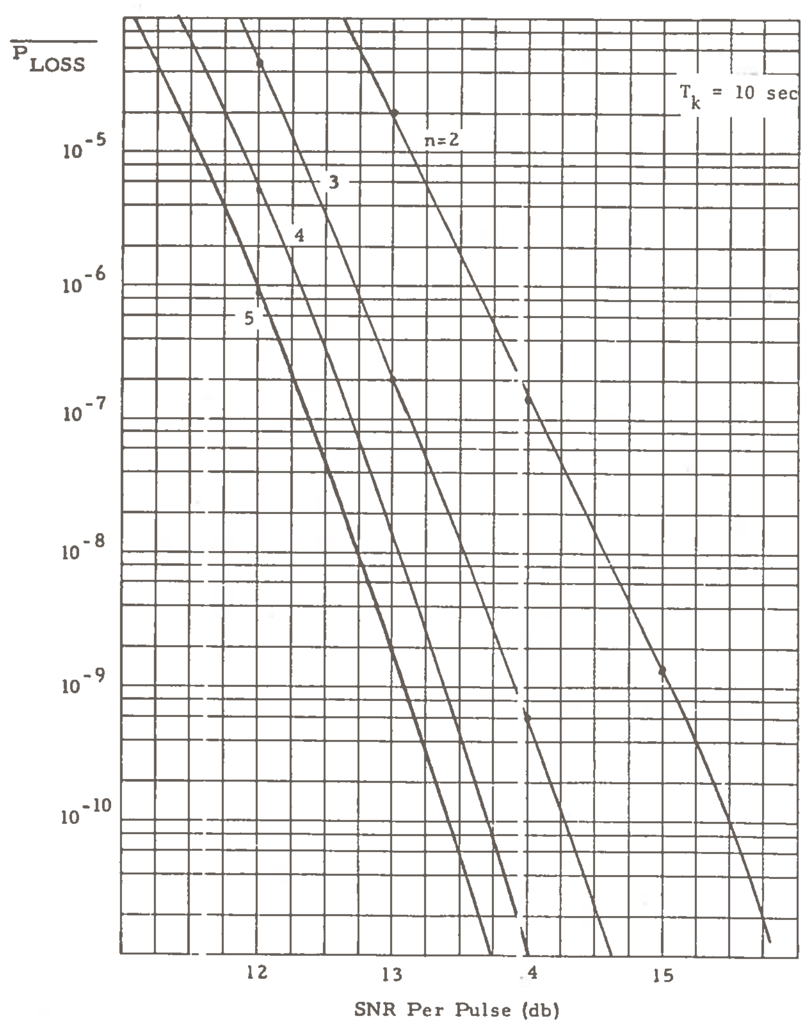

Figure 3.5-2. Upper Bound of Loss-of-Lock Probability

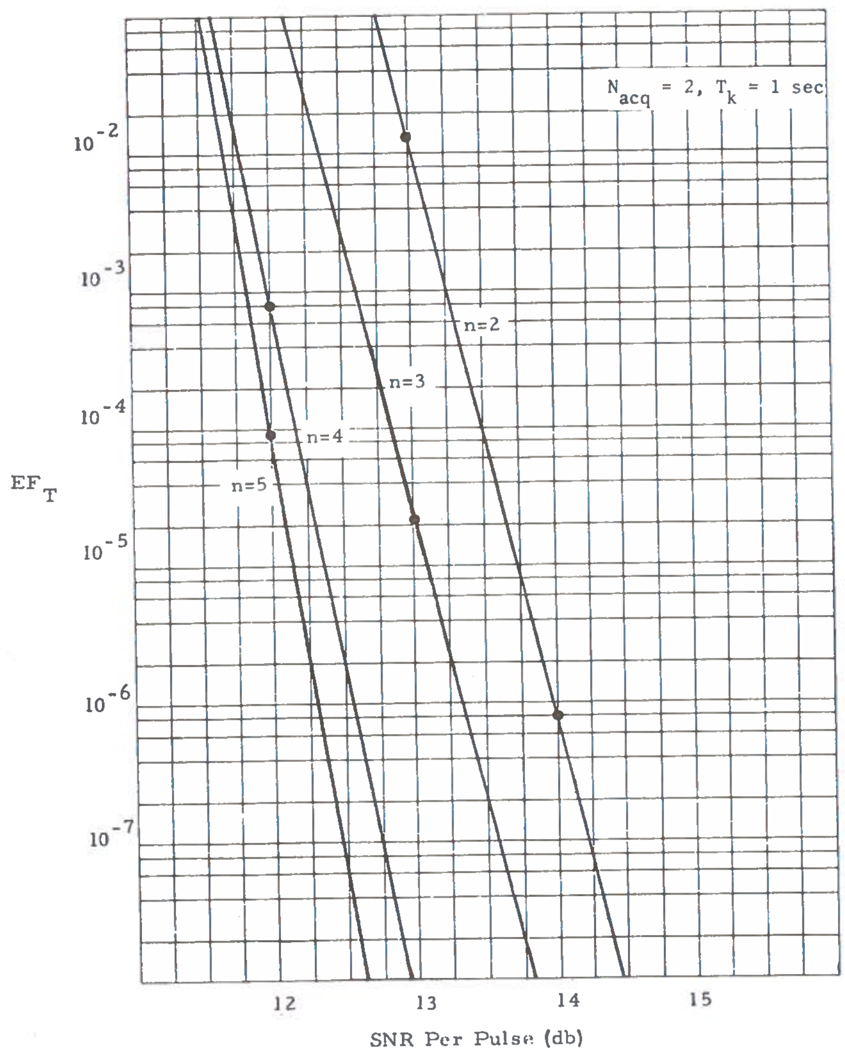

Figure 3.5-3. Expected Number of False Acquisitions Per Reporting Period

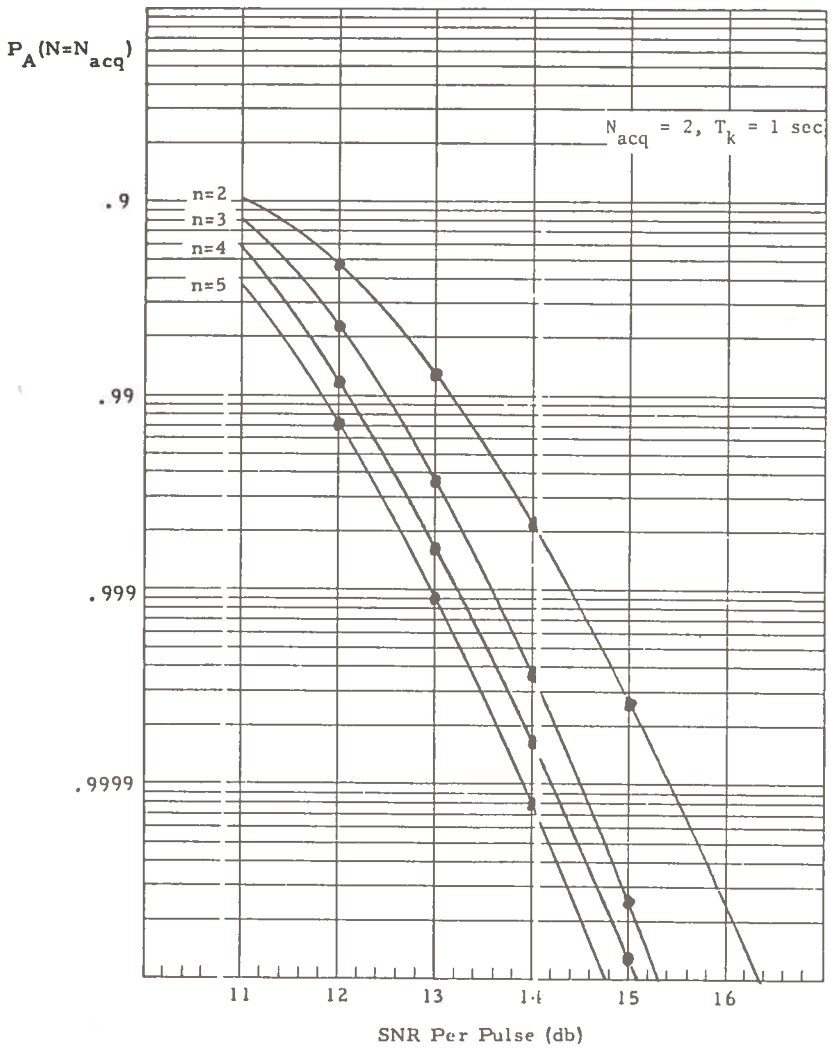

Figure 3.5-4. Probability of Minimum Time Acquisition

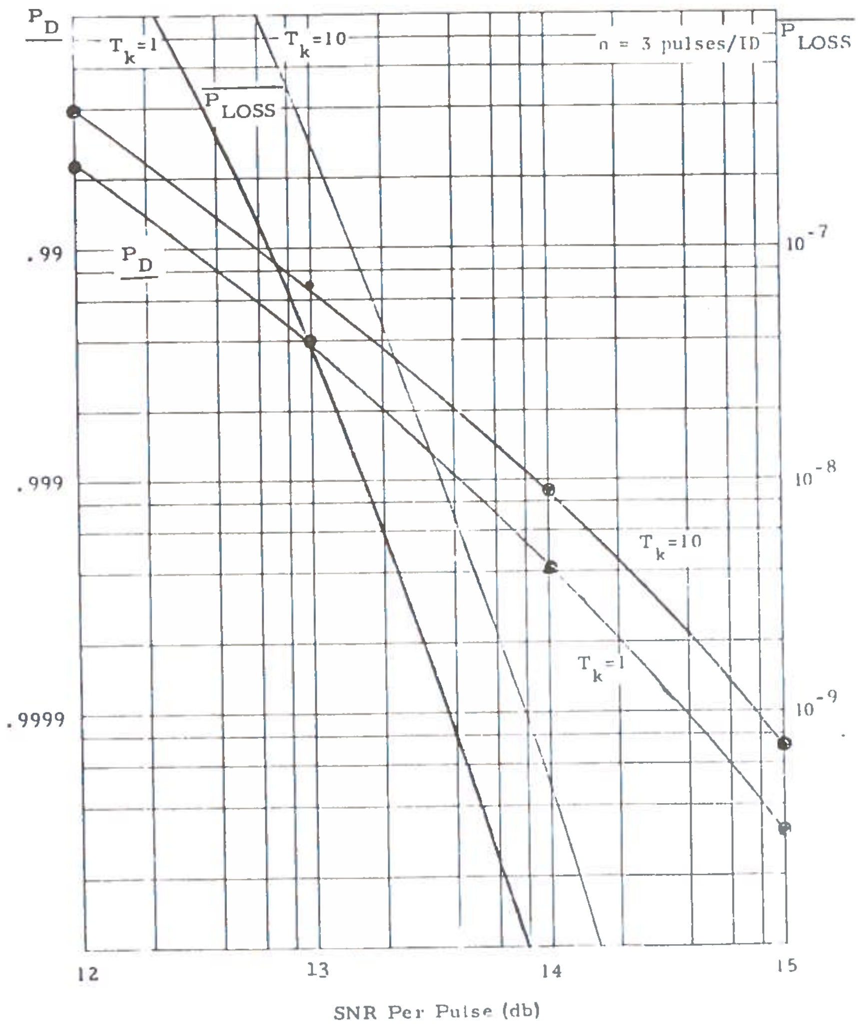

Figure 3.5-5. Sensitivity to Reporting Repetition Interval

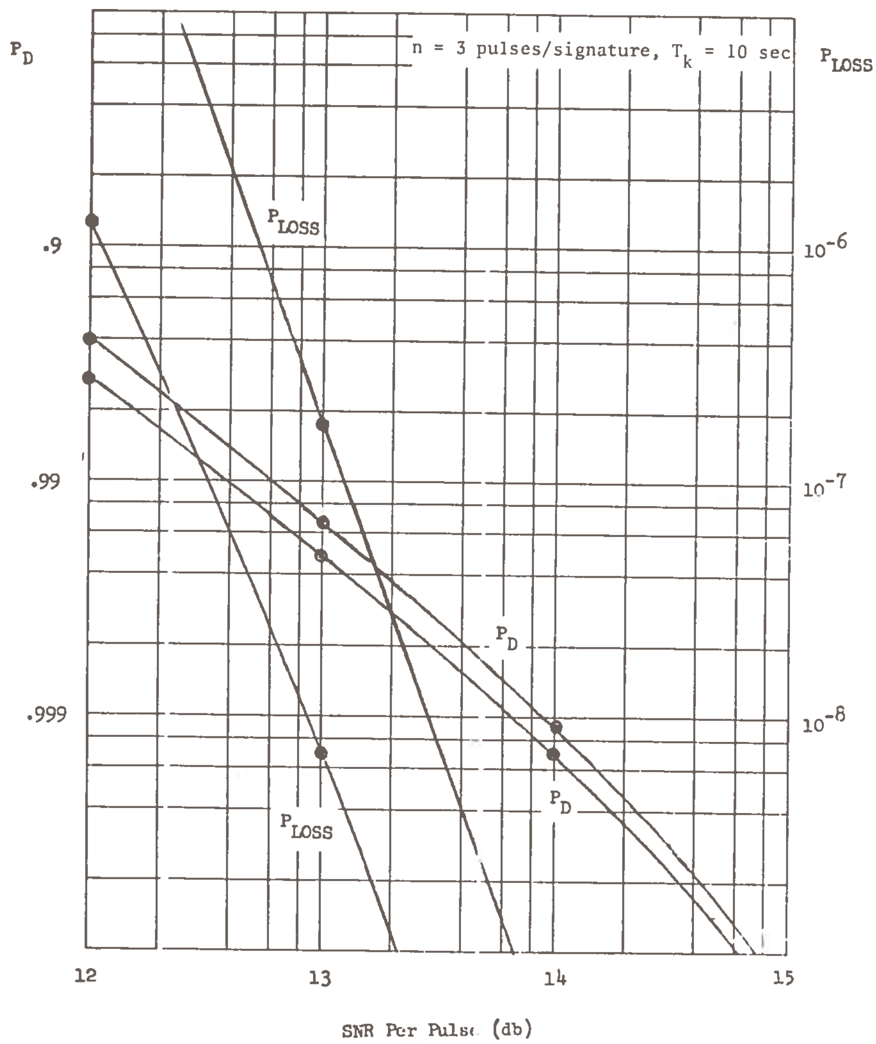

Figure 3.5-6. Upper and Lower Bounds of P_D and P_{Loss}

If the following values are used to define acceptable performance,

$$\left.\begin{aligned} \overline{P_{LOSS}} &\simeq 2 \times 10^{-7} \\ \underline{P_D} &\simeq .99 \end{aligned}\right\} \text{with } T_k = 10$$

$$\left.\begin{aligned} EF_T &\simeq 2 \times 10^{-5} \\ P_A \ (\text{Nacq} = 2) &\simeq .99 \end{aligned}\right\} \text{with } T_k = 1$$

then the required SNRs are:

$n = 2$ SNR $\simeq$ 14

$n = 3$ SNR $\simeq$ 13

$n = 4$ SNR $\simeq$ 12.5

$n = 5$ SNR $\simeq$ 12.2

3.6 RF Link Budget

The available SNR was kept as a parameter in Section 3.5. In this section we demonstrate typical parameter values necessary to obtain the required SNR.

An aircraft-to-geostationary satellite power budget is shown in Table 3.6-1 In the power budget, it is assumed that n = 3 pulses/ID and $N_A = 3.5 \times 10^4$ active aircraft.

Antenna Gains - The value for the aircraft antenna gain was obtained from Reference 21. The value is the result of emperical data from a curved turnstile operating at 1.55 GHz mounted on a Cessna 172 type of aircraft. The antenna beamwidth is approximately 150°.

The satellite antenna gain is for a uniformly illuminated standing wave, circular fed, square array with crossed dipole radiating elements. Seventy (70) percent efficiency is assumed based on the following loss estimate.

Hybrid and balancer losses	.5 db
Transformer (coax-to-hybrid)	.5 db
Coax losses	.5 db

Both the aircraft and satellite antennas are assumed circularly polarized.

TABLE 3.6-1. POWER BUDGET FOR GEOSTATIONARY SATELLITE CHANNEL

Transmitted Energy per Pulse (2 KW for 40 usec)	- 11.0 dbJ
A/C Antenna Gain	4.0 db
Satellite Antenna Gain (10° Beam - 70% Efficiency)	24.6 db
Pointing Losses	1.0 db
Miscellaneous Losses (Plumbing = 1 db, Attenuation = 1 db)	2.0 db
Path Loss (f = 1.6 GHZ, d = 26,000 mi)	189.0 db
Received Signal Energy per Pulse	- 174.4 dbJ
Effective Multi-Access Noise Power Density	- 204.2 dbW/Hz
(N_A - 3.5 x 10^4 aircraft, $\frac{n}{T} = \frac{3 \text{ pulses}}{5 \text{ sec}}$, BW = 20 MHz)	
Receiver Noise Density	- 201.0 dbW/Hz
Total Background Noise	- 199.3 dbW/Hz
Downlink Degradation (100 w. Xmitted pwr, 10' grd. ant.)	0.1 db
Detection Loss (Limiter & Decorrelation)	2.0 db
SNR Per Pulse	22.8 db
Required SNR	13.0 db
Margin	9.8 db

Path Losses - The path loss is based on the range to the geostationary satellite. For those satellites with elliptical orbits, the path loss varies with time. With an eccentricity of .25, the worst case path loss is 190.9 db which occurs at the apogee. If the value of 190.9 db is used in Table 3.6-1 the following changes occur:

Path Loss	-190.9 db
Received Signal Energy Per Pulse	-176.3 dbJ
Effective Multi-Access Noise	-206.1 dbW/Hz
Total Background Noise	-199.8 dbW/Hz
SNR Per Pulse	22.3 db
Margin	9.3 db

Detection Losses - There will be a loss of effective signal power because of frequency instabilities. The loss is approximately

$$\text{Loss} = \left(\frac{\sin \Pi\ \tau\ \Delta f}{\Pi \tau\ \Delta f}\right)^2$$

Where τ is the pulse-width and Δf is the frequency off-set. For τ = 40 usec,

Δf (kHz)	Loss (db)
2	.1
4	.4
6	.8
8	1.5
10	2.4

There are two basic sources for frequency errors. The first is due to doppler shifts caused by the aircraft and satellite relative velocities. Each 100 m/sec of velocity causes about 1 kHz of doppler shift at 1.6 GHz. The second source is due to oscillator instability. Each part per million (ppm) of frequency instability causes 1.6 kHz of frequency shift at 1.6 GHz.

Assuming that the satellite velocity is biased out, 1.5 kHz of doppler shift due to velocity is a reasonable average value. Assuming 2 ppm of oscillator instability yields about 3.2 kHz of frequency off-set. A frequency off-set of 4.7 kHz results in approximately .5 db of loss.

An average limiter loss of 1.5 db is assumed in Table 3.6-1.

3.7 System Parameter Sensitivities and Design Values

Several conclusions concerning the choice of parameter values can be made.

1. n = number of pulses per ID

   The total effect of varying n is shown in Table 3.7-1 where the assumption has been made that all other parameter values remain constant. On an SNR basis, n=3 is a reasonable choice if the number of active aircraft is between 35,000 and 100,000.

   For n = 3 pulses/ID, 10^6 unique IDs can be obtained in several ways. One possible combination is C_N = 16 codes/pulse and 16 possible spacings between each pulse pair. Another combination is C_N = 10 codes/pulse and 32 possible spacings between pulses. The actual combination chosen should be based on the number of good codes that can be found and on implementation considerations. With the analysis model assumed, the detection performance is very insensitive to the actual combination chosen.

2. C_N = number of codes per pulse

   For values between 10 and 100 the performance sensitivity to C_N is very small. Thus, small values of C_N can be planned for. This eases the problem of finding codes with good auto-correlation and cross-correlation properties.

3. Nacq = number of reporting periods required for acquisition

   With Nacq = 2, the expected number of false acquisitions is very small. Thus, for the scheme assumed, Nacq = 2 is sufficient. Larger values of Nacq will further reduce the number of false acquisitions, but will also increase the acquisition complexity and the time required for acquisition.

4. N_A = number of action aircraft

   T_{ave} = average update repetition period

   Two parameters which have a compound effect on the system performance are T_{ave} and N_A. Either increasing T_{ave} or reducing N_A will have the following effects:

   a) Increase the available SNR by decreasing the multi-access noise

   b) Reduce the phantom ID probability

   The first effect is by far the more significant.

TABLE 3.7-1. EFFECT OF VARYING THE NUMBER OF PULSES PER ID (N)

N	Effective Multi-Access Noise (dbw/Hz)		Total Background Noise (dbw/Hz)		SNR per Pulse (db)		Required SNR	Margin	
	(a)	(b)	(a)	(b)	(a)	(b)		(a)	(b)
2	-206.0	-202.4	-199.8	-198.6	23.3	22.1	14	9.3	8.1
3	-204.2	-200.6	-199.3	-197.8	22.8	21.3	13	9.8	8.3
4	-203.0	-198.4	-198.9	-196.5	22.3	20.0	12.5	9.8	7.5
5	-202.0	-197.4	-198.5	-195.8	22.0	19.3	12.2	9.8	7.1

(a) $N_A = 3.5 \times 10^4$ active aircraft

(b) $N_A = 10^5$ active aircraft

N_A can always be reduced by increasing the number of channels used for surveillance. Three possible techniques are:

a) Increasing the frequency bandwidth allocation so that more than one frequency channel is available.

b) Increasing the satellite gains and using more satellites or more than one antenna per satellite.

c) Having ground-based surveillance in certain regions.

The second alternative is probably the most effective.

5. T_k = reporting repetition period of the kth aircraft

It has been shown that the detection is somewhat insensitive to changes in a single aircraft's repetition period. (See Fig.3.5-5) If the PRF for all aircraft is kept equal (i.e., $T_k = T_{ave}$ for all k) then relatively large T_k would be desirable for detection purposes. For example, increasing T_k from 1 to 10 increases the required SNR by about .3 db but decreases the multi-access noise by 10 db.

6. Transmitted Peak Power and Pulse-Width

The primary effect of varying the transmitted power and the pulse-width is the variation in signal energy. The multi-access noise and the decorrelation loss are also effected.

As an example, suppose the pulse-width is reduced from 40 usec to 25 usec. The received signal energy and the multi-access noise are each reduced 2 db, the total background noise is reduced 0.9 db, and the decorrelation loss is reduced 0.4 db. The net result is a decrease of 0.7 db in SNR per pulse. The net loss in SNR can be eliminated by simultaneously increasing the transmitted peak power from 2.0 kw to 2.6 kw.

3.8 Increasing the Number of Satellites

The previous computations were based on a model having only 4 available satellites. As already mentioned, a fundamental property of the adopted scheme is that no single aircraft-satellite link is indispensible at any time. Furthermore, the error-detecting capability of the scheme allows use of all links that provide error-free data. The probability of obtaining at least 4 unambiguous TOA's when more than 4 satellites are available is discussed in this section.

Let <u>perfect detection</u> be defined as unambiguous detection in at least 4 satellite channels. Then,

$P_D(x)$ = probability that at least 4 out of x satellite channels have unambiguous detections

$$= \sum_{k=o}^{x-4} \binom{x}{x-k} P_1^{\,x-k} (1 - P_1)^k \qquad (1)$$

Equation (1) assumes that each of the x satellite channels are independent with probability P_1 of unambiguous detection. Clearly,

$$\underline{P_D}(x) \leq P_D(x) \leq \overline{P_D(x)}$$

where $\underline{P_D(x)}$ and $\overline{P_D(x)}$ are computed from Eq. (1) with P_1 replaced by $\underline{P_1}$ and $\overline{P_1}$ respectively. Figure 3.8-1 shows $\underline{P_D\ (4)}$ and $\underline{P_D\ (5)}$ for the set of parameter values shown.

For a measure of the loss-of-lock probability, let

$P_{LOSS}(x)$ = probability that perfect detection does not occur for three consecutive periods given that x satellites are available.

Clearly, an upper bound to $P_{LOSS}(x)$ is

$$P_{LOSS}(x) \leq [1 - \underline{P_D}(x)]^3 = \overline{P_{LOSS}(x)}$$

Figure 3.8-1 shows $\overline{P_{LOSS}(5)}$ and $\overline{P_{LOSS}}$

With an extra satellite available, about 2 db less SNR is required for the same performance.

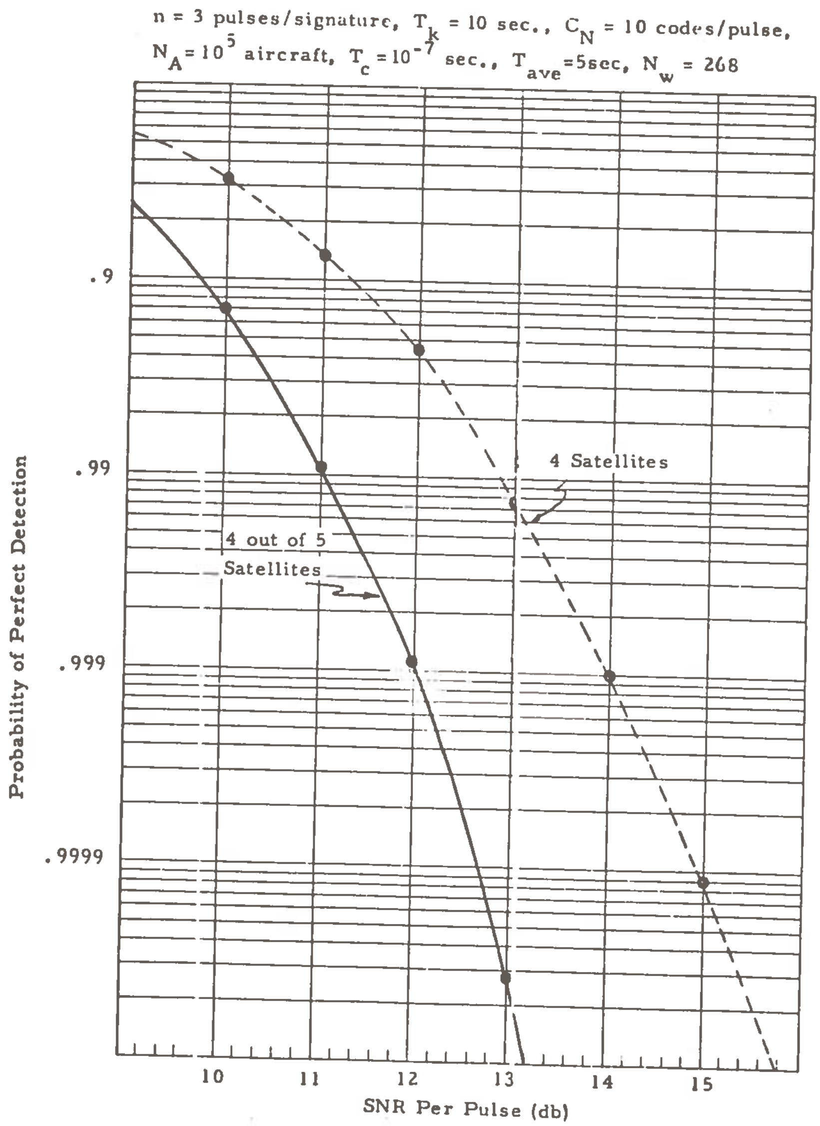

Figure 3.8-1. Lower Bound of Perfect Detection Probability, a Comparison with Four and Five Available Satellites

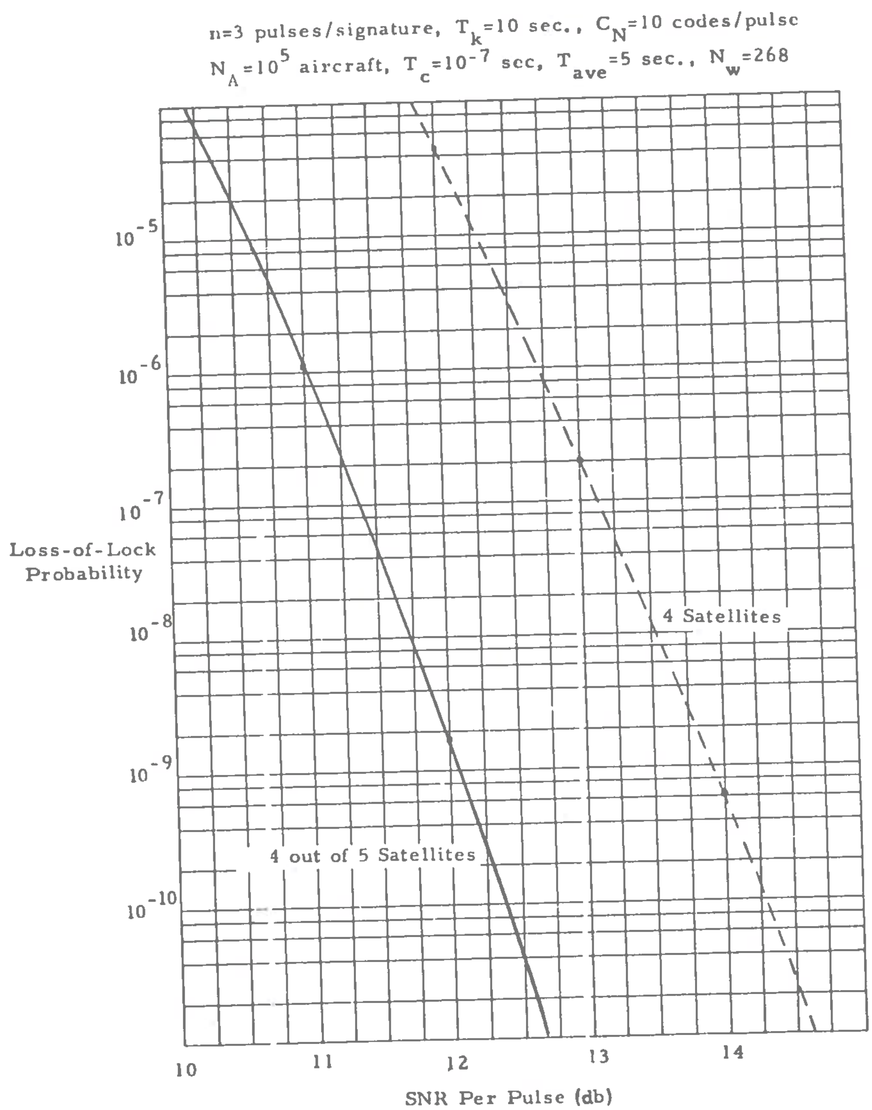

Figure 3.8-2. Upper Bound of Loss-of-Lock Probability, A Comparison With Four and Five Available Satellites

4. COVARIANCE ANALYSIS

Covariance analyses are used to investigate systems involving random variables. The effect of the random variables and the propagation of randomness through the system can be determined using covariance analyses. A covariance analysis is a linear analysis technique that is ideally suited for determining error sensitivity coefficients of linear systems. Monte Carlo analyses could also be used to determine the propagation of random errors through a system; however, they are more applicable to the study of nonlinear systems and are generally more expensive. During the SAATMS study, covariance analyses were performed on the satellite tracking, surveillance, and navigation subsystems. This section presents a general discussion of the covariance analysis techniques and models prior to a discussion of the individual subsystem models.

4.1 Analysis Techniques

4.1.1 SAMUS Program

The basic program used for the covariance analysis is the State Space Analysis of Multisensor Systems (SAMUS) program. This existing program was modified from its original intended purpose to serve the dicta of this program. Since the basic elements of this program were developed on company funding, only a brief outline of its main functions will be described.

The SAMUS program is a specific set of algorithms which allows the effects of under modeling a system to be analyzed. The basic program allows the propagation of a fully modeled system model and a suboptimal filter state model. This dual state vector approach allows a short solution time with respect to the more usual Monte Carlo techniques whose only advantage is the ability to handle non-linear models.

The essence of the problem solving process utilized by SAMUS is depicted in Figure 4.1-1.

The propagation of the dual state vector is based on a linear differential equation of the term

$$\begin{bmatrix} \dot{\underline{X}}_S \\ \dot{\underline{X}}_E \end{bmatrix} = \left[\begin{array}{c:c} F_S & 0 \\ \hdashline 0 & F_F \end{array}\right] \begin{bmatrix} \underline{X}_S \\ \underline{X}_E \end{bmatrix} + \begin{bmatrix} G_S \\ 0 \end{bmatrix} \begin{bmatrix} \underline{U}_S \end{bmatrix} \qquad (1)$$

where $\underline{X}$ = state vector
$\underline{F}$ = state description matrix
G = driving function matrix
$\underline{U}$ = unity Power Spectral Density (PSD) noise driving function vector

with subscript S for the system model, subscript F for the filter, and subscript E for the filter estimate model. For non-unity driving functions, the appropriate terms in G are scaled by the driving noise PSD so that $\underline{U}$ remains unity,

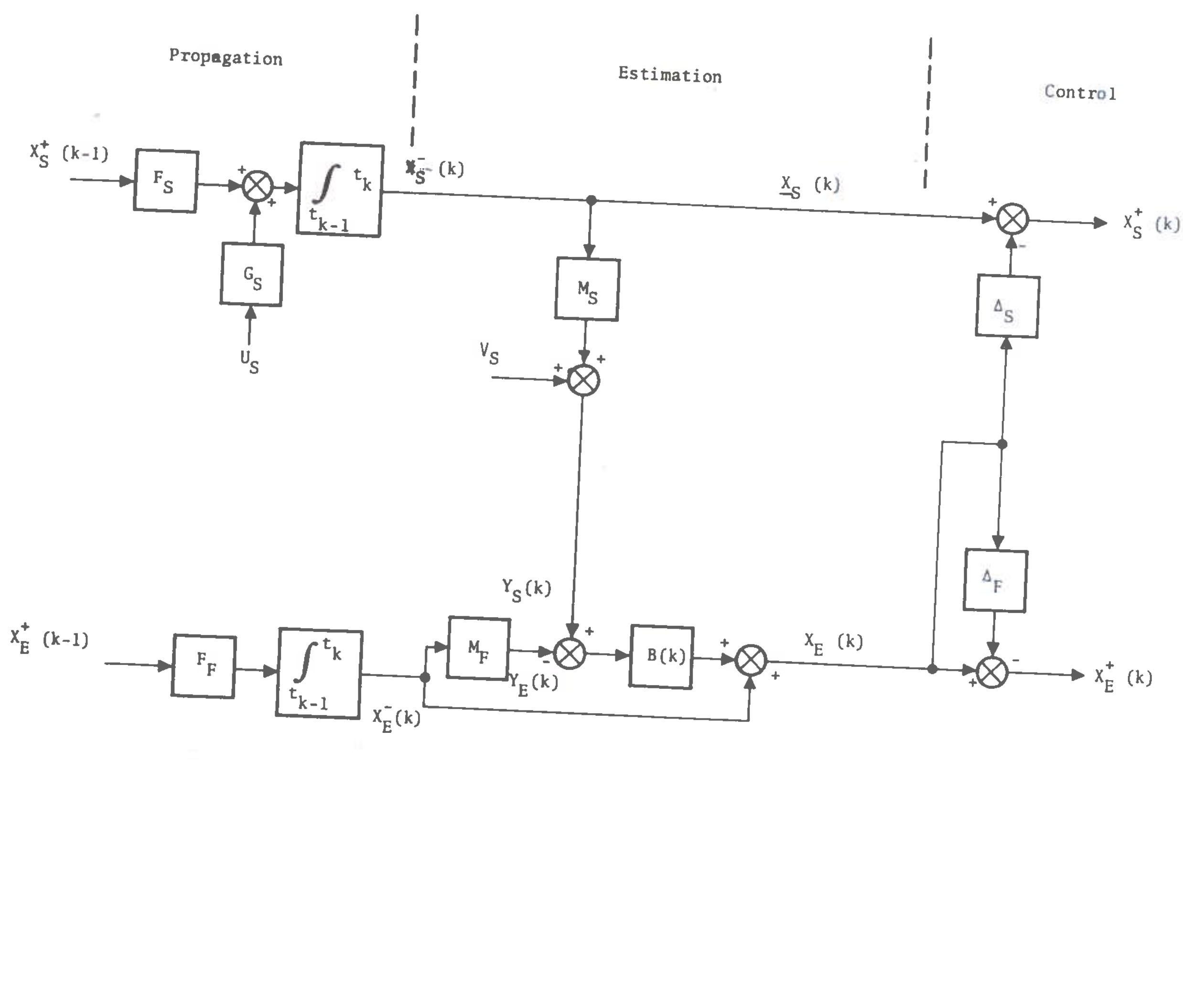

Figure 4.1-1. Problem Solving Process

The measurement equations are

$$\begin{bmatrix} \underline{Y}_S \\ \underline{Y}_E \end{bmatrix} = \begin{bmatrix} M_S & 0 \\ 0 & M_E \end{bmatrix} \begin{bmatrix} \underline{X}_S \\ \underline{X}_E \end{bmatrix} + \begin{bmatrix} \underline{V}_S \\ 0 \end{bmatrix} \tag{2}$$

where Y = observable vector
M = measurement matrix
V = observation noise

Let

$$Q_S = E\left\{ \underline{X}_S \, \underline{X}_S^T \right\} = \text{system covariance matrix}$$

$$\underline{Q}_E = E\left\{ \underline{X}_E \, \underline{X}_E^T \right\} = \text{filter estimate covariance matrix}$$

$$\underline{Q}_{SE} = E\left\{ \underline{X}_S \, \underline{X}_E^T \right\} = \text{system/filter cross covariance matrix} \tag{3}$$

The filter state equations and measurement matrix are

$$\dot{\underline{X}}_F = F_F \underline{X}_F + G_F \underline{U}_F \tag{4}$$

$$\underline{Y}_F = M_F \underline{X}_F + \underline{V}_F \tag{5}$$

and

$$Q_F = E\left\{ \underline{X}_F \, \underline{X}_F^T \right\} \tag{6}$$

When the filter covariances are to be propagated either the Matrix Ricatti equation

$$\dot{Q}_F = F_F Q_F + Q_F F_F^T + G_F G_F^T \tag{7}$$

is integrated or if the state equations are time invariant, then

$$Q_F(t + \Delta t) = \emptyset_F(\Delta t) \; Q_F(t) \; \emptyset_F^T(\Delta t) + N_F \tag{8}$$

where $\emptyset_F(\Delta t) = \exp(F_F \Delta t)$

$$N_F = \int_0^{\Delta t} \int_0^{\Delta t} \left[\emptyset_F(\Delta t - \tau_1) G_F E\left\{ \underline{U}_F(\tau_1) \underline{U}_F(\tau_2)^T \right\} G_F^T \emptyset_F^T(\Delta t - \tau_2) \right] d\tau_1 d\tau_2$$

The filter covariance is propagated to the time of an observation at which point the covariance is called $Q_F^-(k)$. The filter weighting coefficient is then

$$B(k) = Q_F^-(k)\, M_F^T \left[M_F Q_F^-(k)\, M_F^T + R_F(k) \right]^{-1} \tag{9}$$

where $R_F(k) = E\left\{ \underline{V}_F \underline{V}_F^T \right\}$

The filter covariance is updated using

$$Q_F^+(k) = \left[I - B(k)\, M_F \right] \underline{Q}_F^-(k) \tag{10}$$

The system covariances are propagated as

$$\dot{Q}_S = F_S Q_S + Q_S F_S^T + G_S G_S^T \tag{11}$$

$$\dot{Q}_E = F_F Q_E + Q_E F_F^T \tag{12}$$

$$\dot{Q}_{SE} = F_S Q_{SE} + Q_{SE} F_F^T \tag{13}$$

The above equations are propagated ahead until time for a filter estimation. Prior to estimation, the system state is given as $\underline{X}_S^-(k)$ and the filter estimate state as $\underline{X}_E^-(k)$. The system's best estimate of its own state is of course

$$\underline{X}_S(k) = \underline{X}_S^-(k) \tag{14}$$

The filter estimate of the system state is a linear combination of the filter estimate state and a weighted difference in the state and filter estimate measurements, or

$$\begin{aligned} \underline{X}_E^-(k) &= \underline{X}_E^-(k) + B(k) \left[\underline{V}_S(k) - \underline{Y}_E(k) \right] \\ &= \underline{X}_E^-(k) + B(k) \left[M_S \underline{X}_S^-(k) + \underline{V}_S - M_F \underline{X}_E^-(k) \right] \\ &= B(k) M_S \underline{X}_S^- + \left[I - B(k)\, M_F \right] \underline{X}_E^-(k) + B(k) \underline{V}_S \end{aligned} \tag{15}$$

Thus

$$\begin{bmatrix} \underline{X}_S(k) \\ \underline{X}_E(k) \end{bmatrix} = \begin{bmatrix} I & 0 \\ B(k)M_S & I-B(k)M_F \end{bmatrix} \begin{bmatrix} \underline{X}_S^-(k) \\ \underline{X}_E^-(k) \end{bmatrix} + \begin{bmatrix} 0 \\ B_k \end{bmatrix} \underline{V}_S \tag{16}$$

The covariance matrices for the state estimates are

$$\begin{aligned}
Q_S(k) &= Q_S^-(k) \\
Q_E(k) &= \left[B(k)M_S\right] Q_S^-(k) \left[B(k)M_S\right]^T + B(k)R_S B^T(k) \\
&\quad + \left[I-B(k)M_F\right] Q_E^-(k) \left[I-B(k)M_F\right]^T \\
&\quad + \left[B(k)M_S\right] Q_{\overline{SE}}(k) \left[I-B(k)M_F\right]^T \\
&\quad + \left\{\left[B(k)M_S\right] Q_{\overline{SE}}(k) \left[I-B(k)M_F\right]^T\right\}^T \\
Q_{SE}(k) &= Q_S^-(k) \left[B(k)M_S\right]^T + Q_{\overline{SE}}(k) \left[I-B(k)M_F\right]^T
\end{aligned} \tag{17}$$

where $R_S = E\left\{\underline{V}_S \underline{V}_S^T\right\}$

Control is applied to the system using

$$\begin{bmatrix} \underline{X}_S^+(k) \\ \underline{X}_E^+(k) \end{bmatrix} = \begin{bmatrix} I & -\Delta S \\ & I-\Delta F \end{bmatrix} \begin{bmatrix} \underline{X}_S(k) \\ \underline{X}_E(k) \end{bmatrix} \tag{18}$$

The system covariance matrices after control is applied are

$$\begin{aligned}
Q_S^+(k) &= Q_S(k) + \Delta S Q_E(k)\,\Delta S^T - \left[Q_{SE}(k)\,\Delta S^T\right] \\
&\quad - \left[Q_{SE}(k)\,\Delta S^T\right]^T
\end{aligned} \tag{19}$$

$$Q_E^+(k) = \left[I-\Delta F\right] Q_E(k) \left[I-\Delta F\right]^T \tag{20}$$

$$Q_{SE}^+(k) = \left[Q_{SE}(k) - \Delta S Q_E(k)\right] \left[I-\Delta F\right]^T \tag{21}$$

The SAMUS program contains all of the elements necessary to solve general covariance analysis problems. It is particularly suited to the solution of sub-optimal filter problems where the filter model contains fewer states than the system model.

4.1.2 Error Models

There are a number of error sources in the satellite tracking, surveillance and navigation subsystems which are common. Rather than considering these error sources in a number of different sections, a single discussion of the effects will be presented in the following paragraphs, and then applied without further discussion as appropriate.

4.1.2.1 General SAMUS Modeling. The following paragraphs will describe the general models to be used with the SAMUS program. The models to be considered are a bias, a random walk and an exponentially correlated model. The general form of the models are:

$$\dot{\underline{x}} = F\,\underline{x} + G\,\underline{u} \tag{22}$$

The bias or constant level deterministic error source is modeled as

$$\dot{x} = 0$$
$$x(0) = \sigma_i \tag{23}$$

Thus

$$R(\tau) = E\left\{x(t)\;x(t+\tau)\right\} = x^2(0) = \sigma_i^2 \tag{24}$$

A random walk error source is modeled as

$$\dot{x} = \sigma_r\,u$$
$$x(0) = \sigma_i \tag{25}$$

Thus $$x(t) = x(0) + \int_0^t \sigma_r U(\xi)d\xi \tag{26}$$

The autocorrelation function become

$$R(t,\ t+\tau) = E\{x(t)\ \ x(t+\tau)\}$$

$$= E\{x^2(0)\} + \sigma_r\ E\{x(0)\int_0^{t+\tau} u(\xi)d\xi\}$$

$$+ \sigma_r\ E\{x(0)\int_0^{t} u(\xi)d\xi\}$$

$$+ \sigma_r^2\ E\{\int_0^{t} u(\xi)d\xi\int_0^{t+\tau} u(\xi)d\xi\}$$

$$= \sigma_i^2 + \sigma_r^2 t \tag{27}$$

An exponentially correlated error source autocorrelation function is

$$R(\tau) = \sigma^2\ e^{-B|\tau|} \tag{28}$$

The shaping filter required to form this autocorrelation function has a PSD output given by

$$S(\omega) = \int_{-\infty}^{\infty} R(\tau)\cos(\omega\tau)d\tau$$

$$= \int_{-\infty}^{\infty}\sigma^2\ e^{-B|\tau|}\ \ \cos(\omega\tau)d\tau$$

$$= \int_{-\infty}\sigma^2\ e^{-B\tau}\ \cos(\omega\tau)d\tau\ \ + \int_0^{\infty}\sigma^2\ e^{-B\tau}\ \cos(\omega\tau)d\tau$$

$$= 2\int_0^{\infty}\sigma^2\ e^{-B\tau}\ \cos(\omega\tau)d\tau$$

$$= \sigma^2\ \frac{2B}{B^2+\omega^2} \tag{29}$$

Since the PSD of the input is related to the output by

$$S_o(\omega) = G(J\omega)\ G(-J\omega)\ S_I(\omega) \tag{30}$$

and since $S_I(\omega) = \sigma^2$ for a unity PSD input then

$$S_o(\omega) = \left(\frac{\sqrt{2B}}{B+J\omega}\right)\left(\frac{\sqrt{2B}}{B-J\omega}\right)\sigma^2 \tag{31}$$

The required transfer function for a shaping filter driven by a unity PSD white noise to have an exponentially correlated output is given by

$$G(J\omega) = \frac{\sigma\sqrt{2B}}{B+J\omega} \tag{32}$$

Therefore

$$\dot{x} = Bx + \sigma_i\sqrt{2B}\,u$$

$$x(0) = \sigma_i \tag{33}$$

This filter can also be used to approximate the effect of a white noise error source. This can be accomplished by selecting B to be small with respect to the system eigenvalues and scaling the PSD as appropriate.

4.1.2.2 Clock Error Models. There are several different clocks that are of importance in the subsystem analysis. For satellite tracking, the on-board satellite clock and the master clock are used. For surveillance, the master clock is used. For navigation, the user's clock is employed. All of these clocks were modeled using a four state model.

All clocks may be approximated as having four different types of errors; an initial offset, a frequency error, a random walk error and a 1/f or flicker noise error.

The clock initial offset error or synchronization error is a deterministic error. The error is modeled as a bias with only an initial condition specified. For the high accuracy master clock, the satellite clock and the user's clock the error was assumed to have a variance of 1 usec. These terms are quite systematic and are readily estimated, thus the apriori statistics are not critical.

The frequency error in clocks lead to a drift rate in time. This is modeled as a constant error source with the time dependence in the measurement matrix or

$$\dot{x} = 0$$
$$x(0) = \sigma_i$$
$$\underline{y} = t\underline{x} \tag{34}$$

The variance for the satellite and master clock was selected as 10^{-9} sec and the user's clock was selected at 10^{-6} sec. These are very conservative values, but, since they are easily estimated, the apriori statistics are relatively unimportant.

The random walk phenomena is an attempt to model one component of emperically observed random clock fluctuations. This type of model stems from a white noise frequency error. The high quality satellite and master clocks were assumed to have variances of 10^{-10} t while the user's clock was assumed to have a variance of 4×10^{-10} t. These lead to rms time errors of 6 nsec and 24 nsec in one hour which are typical values for high quality and good quality crystal oscillators, respectively.

Over a considerable period of time experimentation with crystal oscillators has revealed that the power spectrum of frequency deviations from nominal has a component which drops off inversely with the first power of frequency (this latter frequency refers to the Fourier transform frequency domain whereas the frequency deviations mentioned are deviations of the real variable oscillator frequency). This random effect has been called flicker or 1/f noise.

It is well known that if f(t) and g(t) are related by the following equation

$$f(t) = \frac{dg(t)}{dt} \tag{35}$$

and if the power spectrum of f(t) is $S_f(\omega)$, then the power spectrum of g(t) is given by

$$Sg(\omega) = \frac{S_f(\omega)}{\omega^2} \tag{36}$$

In words, an integration in the time domain corresponds to division by ω^2 in the frequency domain. Now suppose that f and g are not constrained by the relation (35) but have some other relationship. Further, suppose that the power spectrum of f(t), $S_f(\omega)$ is just a constant. That is

$$S_f(\omega) = R$$

which implies that f(t) is white noise (g correlated). If g(t) is the "1/2 fold" integral of f(t) then the power spectrum of g(t) is

$$Sg(\omega) = \frac{k}{\omega} \tag{37}$$

which is the desired spectrum for the emperically observed flicker noise.

Fractional order integration has been developed (Reference 22) and may be applied to determine a model for g(t). However, it is noted that g(t) here represents a component of the random frequency deviation. The actual quantity of interest is phase error $\emptyset(t)$ which is directly related to time error. Thus the "3/2 fold" integral of a white noise process $\dot{u}(t)$ is needed. Formally this integral is

$$\emptyset(t) = \frac{1}{\Gamma(\frac{3}{2})} \int_0^t \sqrt{t-\alpha}\ \dot{u}(\alpha)d\alpha \tag{38}$$

As an end result elements of the transition matrix for the state vector containing all modeled error sources is sought. For this $E\left[\emptyset(t+T) \mid \emptyset(t)\right]$ is required. Calculation of this quantity (Reference 23) leads to

$$E\left[\emptyset(t+T) \mid \emptyset(t)\right] = \frac{t^2 + T^2 - |t-T|^2}{2T^2} E\left[\emptyset^2(T)\right] \tag{39}$$

Another required expression gives the variance of this error.

$$E\left[\emptyset^2(t)\right] = \int_0^t (t-\alpha)d\alpha \tag{40}$$

With these it is possible to develop a model for this error source which can be incorporated into the state vector representation of system error dynamics.

Statistics for actual crystal oscillators describing flicker noise behavior are given in reports of experimental studies (Reference 24). These have been used in the simulation and error analysis of the navigation subsystem. Flicker noise is a small error source and it has not been necessary to include it in the navigation subsystem filter.

4.1.2.3 Atmospheric Errors. Ionospheric errors are due to an apparent increase in the transit time of a signal propagating through the ionospheric layer. For range measurements R_1 and R_2 made at different times and places, the space-time covariance of the time of arrival error, $\delta\epsilon$, is

$$E \left| \delta t_1 \quad \delta t_2 \right| = 1/C^2 \, E \left| \delta R_1 \quad \delta R_2 \right|$$

$$= A \, e^{-|T|/T_1} + B \, e^{-T/T_2} \qquad (41)$$

where $A = 0.45 \, \sigma_i \, \sigma_j / C^2$

$B = 0.55 \, \sigma_i \, \sigma_j / C^2$

C = speed of light

$T_1 = 1/2.5$ hr. $+ \dot{R}_{350_1}/2500$ km

$T_2 = 1/28$ hr. $+ \dot{R}_{350_2}/2500$ km

$\dot{R}_{350_i}$ = horizontal component of a point on the i^{th} ray path at 350 km altitude

$$i = \begin{cases} 8.3 \csc\sqrt{E_i^2 + (18^o)^2} \text{ ft. at L Band} \\ 0.8 \csc\sqrt{E_i^2 + (18^o)^2} \text{ ft. at C Band} \end{cases}$$

E_i = elevation angle of the i^{th} ray path

Define the state vector with an auxiliary variable, such that

$$\begin{bmatrix} \dot{\delta t} \\ \dot{\alpha} \end{bmatrix} = \begin{bmatrix} -1/T_2 & C/T_2 - D/T_1T_2 \\ 0 & -1/T_1 \end{bmatrix} \begin{bmatrix} \delta t \\ \alpha \end{bmatrix} + \begin{bmatrix} \sqrt{2}/T_1 \\ D\sqrt{2}/T_1T_2 \end{bmatrix} \underline{u} \qquad (42)$$

where $\underline{u}$ = unity PSD white noise

$C = \sqrt{AT_1 + BT_2}$

$D = \sqrt{AT_1T_2^2 + B\,T_2T_1^2}$

This model accounts for the residual ionospheric errors.

An additional delay term arises from propagation delays in the troposphere. This term is treated as a constant error with a time error of

$$\Delta t = -(8.8 \text{ ft}/C) \csc E_i \tag{43}$$

4.1.2.4 <u>Speed of Light Uncertainty</u>. A speed of light uncertainty of 1/3 ppm is included in the satellite tracking model. Since this error is almost totally correlated for any location close to the tracking sites, no provision for inclusion of this error in surveillance and navigation models were made.

4.1.2.5 <u>Satellite Covariance Models</u>. Both the surveillance and navigation subsystem performance analysis require that satellite position errors be computed as a function of time. The covariance of the satellite position and velocity errors are computed by the models for the satellite tracking analysis. The results of the satellite tracking analysis are used to determine an initial set of covariances. These covariances are then extrapolated forward in time for each satellite in the constellation.

Let the initial state and covariance of each satellite be defined of

$$\bar{S}_o = \left[x \; y \; z \; \dot{x} \; \dot{y} \; \dot{z} \right]^T \tag{44}$$

and

$$P_o = E\left\{ \underline{S}_o \underline{S}_o^T \right\} \tag{45}$$

The state of the satellite time can be computed at any future time if two-body dynamics are assumed. A general method of extrapolation (Reference 25) the two-body problem, assuming a central force field u, was used to compute the state transition matrix, $\emptyset(\Delta t)$, such that

$$\underline{S}_{\Delta t} = \emptyset(\Delta t) \underline{S}_o \tag{46}$$

Clearly then

$$P_{\Delta t} = \emptyset(\Delta t) P_o \emptyset(\Delta t)^T \tag{47}$$

The covariance for each satellite was used to initiate the value of P_o. This quantity and the estimated state then allowed the computation of the satellite position covariance at each measurement time. The position co-variance elements then lead to timing error covariances as follows:

Therefore

$$\delta_{tp} = \left[\left(\frac{1}{c}\right) \frac{\partial \bar{I}_R}{\partial x} \quad \left(\frac{1}{c}\right) \frac{\partial \bar{I}_R}{\partial y} \quad \left(\frac{1}{c}\right) \frac{\partial \bar{I}_R}{\partial z} \quad 0 \quad 0 \quad 0 \right]_{\Delta t} S(\Delta t) \tag{48}$$

where the partial derivatives are evaluated at time Δt and $\bar{1}_R$ is the unit vector from the user to satellite or satellite to RCC. Note that in the surveillance case the uplink and downlink timing errors due to satellite position errors are highly correlated.

4.2 Satellite Tracking Models

4.2.1 Development of System Description Matrix

The equation of motion in the Earth's gravity field, Φ, with a perturbative potential function $\tilde{R}$ is

$$\ddot{\bar{r}} + \bar{\nabla}\Phi(\bar{r}) = -\bar{\nabla}\tilde{R}(\bar{r}) \tag{1}$$

where $\bar{r}$ is the position vector, and $\tilde{R}$ is due to errors in the Earth's gravity constant, errors in the spherical harmonic coefficients, and any other external forces such as solar radiation, drag, etc. Neglecting these other external forces for the moment, we have (to a first order):

$$\tilde{R} = \frac{\partial\Phi}{\partial\mu}\Delta\mu + \frac{\partial\Phi}{\partial J_2}\Delta J_2 + \frac{\partial\Phi}{\partial J_3} J_3 + \dots \tag{2}$$

$$= \Phi\frac{\Delta\mu}{\mu} - \frac{\mu a_e^2}{2r^3}(3\sin^2\phi - 1)\Delta J_2 - \frac{\mu a_e^3}{2r^4}(5\sin^3\phi - 3\sin\phi)\Delta J_3$$

$$+ \dots$$

where ϕ is geocentric latitude, a_e is mean equatorial Earth radius, r is the magnitude of $\bar{r}$, μ is the Earth's gravity constant, and J_i are the spherical harmonic coefficients in the expansion of the gravity potential, Φ.

For the case $\tilde{R}=0$, the solution of Equation (1) at some time t can be defined by a vector of six orbital elements $\bar{\epsilon}$, and their derivatives with respect to time. This solution will be defined as the nominal or reference solution about which Equation (1) will be expanded.

The equations defining the required derivatives of $\bar{\epsilon}$, known as Lagrange's Planetary equations, are of the form

$$\dot{\bar{\epsilon}} = \left[A\right]\bar{U}_{\bar{\epsilon}} \tag{3}$$

where the elements A_{ij} of the 6 x 6 matrix $\left| A \right|$ are expressed in terms of the orbital elements $\bar{\epsilon}$, and

$$\bar{U}_{\bar{\epsilon}} = \left(\frac{\partial U}{\partial \epsilon_1}, \frac{\partial U}{\partial \epsilon_2}, \ldots, \frac{\partial U}{\partial \epsilon_6} \right)^T \tag{4}$$

where: $U = \tilde{R} + \Phi - \frac{\mu}{r}$

Taking derivatives

$$\bar{U}_{\bar{\epsilon}} = \bar{\tilde{R}}_{\bar{\epsilon}} + \bar{\Phi}_{\bar{\epsilon}} - \overline{\left(\frac{\mu}{r}\right)}_{\bar{\epsilon}} \tag{5}$$

Since the actual trajectory differs from the reference solution only due to the perturbative function $\tilde{R}$ (assuming known initial conditions) we can use the linearity of (3) and (5) to define the perturbative rates as

$$\dot{\overline{\Delta \epsilon}} = \left[A \right] \bar{\tilde{R}}_{\bar{\epsilon}} \tag{6}$$

Now define the vector of gravity model errors

$$2 = \begin{bmatrix} \Delta \mu \\ \Delta J_2 \\ \Delta J_3 \\ \vdots \end{bmatrix} \tag{7}$$

and note that Equation (2) can be written as the vector dot product

$$\tilde{R} = \bar{\Phi}_2 \cdot 2 \tag{8}$$

Taking the derivative of (8)

$$\bar{\bar{R}}_{\bar{\epsilon}} = \left[\frac{\partial \bar{\Phi}_2}{\partial \bar{\epsilon}} \right] 2 \tag{9}$$

Define the matrix $\left| Q \right|$ according to (9) such that (6) may be written

$$\dot{\overline{\Delta \epsilon}} = \left| A \right| \left| Q \right| \; 2 \tag{10}$$

Now define the vector of orbital element errors

$$\bar{x}_1 = \Delta\epsilon = \begin{bmatrix} \Delta a \\ \Delta e \\ \Delta i \\ \Delta \Omega \\ \Delta \omega \\ \Delta E \end{bmatrix}$$

Since the set of elements selected includes the eccentric anomaly E, which is not constant for a Keplerian orbit, Equation (3) must be modified by adding the term

$$\dot{E}_k = \frac{n}{1-e\cos E} \quad \text{to the sixth element of } \dot{\epsilon}$$

where n is the mean motion.

We can now rewrite Equation (10) to include this effect as

$$\dot{\bar{x}} = \left[F\right] \bar{x} \tag{11}$$

where

$$\bar{x} = \left[\begin{array}{c} 1 \\ \hdashline 2 \end{array}\right]$$

$$\left[F\right] = \left[\begin{array}{c:c} \left[F_{11}\right] & \left[F_{12}\right] \\ \hdashline \left[0\right] & \left[F_{22}\right] \end{array}\right]$$

and $\left[F_{11}\right]$ is a 6 x 6 matrix with only the following 3 non-zero elements:

$$F_{11_{6,1}} = \frac{\partial \dot{E}_k}{\partial \epsilon_1} = -\frac{3}{2}\,\frac{n}{a(1 - e\cos E)}$$

$$F_{11_{6,2}} = \frac{\partial \dot{E}_k}{\partial \epsilon_2} = \frac{n\cos E}{(1 - e\cos E)^2}$$

$$F_{11_{6,6}} = \frac{\partial \dot{E}_k}{\partial \epsilon_6} = -\frac{ne\sin E}{(1 - e\cos E)^2}$$

Equation (11) is the desired system description equation, for the case of no white noise driving functions.

Given Keplers equation:

$$E - e \sin E = n(t-T) \tag{12}$$

the eccentrix anomaly rate can be computed as

$$\dot{E}_k = \frac{n}{1-e \cos E} = \sqrt{u/a^3}\Big/(1-e \cos E) \tag{13}$$

From which the partial derivatives necessary for the non-zero terms of the $[F_{11}]$ matrix were obtained.

Define $$\left[F_{12}\right] = \left[A\right] \quad \left[Q\right] \tag{14}$$

The 6 x 6 matrix $\left[A\right]$ is defined by Lagranges Planetary Equations in the form

$$\dot{\bar{\epsilon}} = \left[A\right] \quad \bar{U}_{\bar{\epsilon}} \tag{15}$$

Where $\dot{\bar{\epsilon}}$ is the vector of orbital element rates $\dot{a}$, $\dot{e}$, $\dot{i}$, $\dot{\Omega}$, $\dot{\omega}$, and $\dot{E}'$, where the last element is only the perturbative rate of E (i.e., $\dot{E}=\dot{E}'+\dot{E}_k$). And $\bar{U}_\epsilon$ is the 6 x 1 vector of partial derivatives of the perturbative potential function U with respect to the orbital elements. With these definitions, the matrix $\left[A\right]$ is defined as:

$$\left[A\right]_{6x6} = (A_{i,j}) \tag{16}$$

where $$A_{1,1} = A_{1,2} = A_{1,3} = A_{1,4} = A_{1,5} = A_{2,2} = A_{2,3} = A_{2,4}$$

$$= A_{3,3} = A_{3,6} = A_{4,4} = A_{4,5} = A_{4,6} = A_{5,5} = A_{6,6} = 0$$

$$A_{1,6} = \frac{2}{nr}$$

$$A_{2,6} = \frac{1-e^2}{nrae}$$

$$A_{2,5} = -\frac{\sqrt{1-e^2}}{na^2 e}$$

$$A_{3,4} = -\frac{1}{na^2\sqrt{1-e^2}\,\sin i}$$

$$A_{3,5} = \frac{\cos i}{na^2\sqrt{1-e^2}\,\sin i}$$

$$A_{5,6} = \frac{\sqrt{1-e^2}\,\sin E}{nrae}$$

and $\left[A\right]$ is skew symmetric, such that

$$A_{i,j} = -A_{j,i}$$

Also, note that $r = a(1-e\cos E)$

To compute the $\left[Q\right]$ matrix, define:

$$\Phi = \Phi\,(\mu,\ J_2,\ J_3, \ldots) \tag{17}$$

is the best estimate of the earth's gravity field;

$$\bar{x}_2 = \begin{bmatrix} \Delta u \\ \Delta J_2 \\ \vdots \\ \Delta J_{N-1} \end{bmatrix}$$ is the Nx1 vector of

gravity model coefficient errors to be estimated;

$$\bar{\Phi}_J^T = \left[\frac{\partial \Phi}{\partial \mu}, \quad \frac{\partial \Phi}{\partial J_2}, \ \ldots \ \frac{\partial \Phi}{\partial J_N} \right] \tag{18}$$

is a Nx1 vector of partial derivatives.

Then the 6xN $\left[Q \right]$ matrix is made up of the partial derivative

$$Q_{i,j} = \frac{\partial \Phi \bar{x}_{2_j}}{\partial \epsilon_i} \qquad , \ j=1, \ 2, \ldots, \ N \tag{19}$$

For purposes of evaluating the $Q_{i,j}$ write $\Phi(r, \emptyset, \lambda)$ in the form

$$\Phi = \frac{\mu}{r} + \sum_{j=2}^{N} u_j(r, \emptyset, \lambda) J_j \tag{20}$$

Then $$\Phi_{J_1} \equiv \frac{\partial \Phi}{\partial \mu} = \frac{\partial \Phi}{\partial \mu} \tag{21}$$

and $$\Phi_{J_j} \equiv \frac{\partial \Phi}{\partial J_j} = u_j \quad , \quad j=2, \ldots, N \tag{22}$$

Using the chain rule:

$$\frac{\partial \Phi_{Jj}}{\partial \varepsilon_i} = \frac{\partial \Phi_{Jj}}{\partial r} \frac{\partial r}{\partial \varepsilon_i} + \frac{\partial \Phi_{Jj}}{\partial \phi} \frac{\partial \phi}{\partial \varepsilon_i} + \frac{\partial \Phi_{Jj}}{\partial \lambda} \frac{\partial \lambda}{\partial \varepsilon_i} \tag{23}$$

and defining

$$\alpha_j = \frac{\partial u_j}{\partial r}, \ B_j = \frac{1}{r} \frac{\partial u_j}{\partial \phi}, \ \gamma_j = \frac{1}{r \cos \phi} \frac{\partial u_j}{\partial \lambda} \tag{24}$$

we obtain

$$\frac{\partial \Phi_{Jj}}{\partial \varepsilon_i} = \frac{g_r}{\mu} \frac{\partial r}{\partial \varepsilon_i} + \frac{r g_\phi}{\mu} \frac{\partial \phi}{\partial \varepsilon_i} + \frac{r \cos \phi g \lambda}{\mu} \frac{\partial \lambda}{\partial \varepsilon_i}$$

and $$\frac{\partial \Phi_{Jj}}{\partial \varepsilon_i} = \alpha_j \frac{\partial r}{\partial \varepsilon_i} + r B_j \frac{\partial \phi}{\partial \varepsilon_i} + r \cos \phi \ \gamma_j \frac{\partial \lambda}{\partial \varepsilon_i}, \ j = 2, \ \ldots, \ N \tag{25}$$

The expressions g_r, g_ϕ, $g\lambda$ are the components of gravity acceleration in the directions of increasing r, ϕ, and λ (radial distance, latitude, longitude).

4.2.2 Gravity Coefficient Models

The submatrix $\left[F_{22}\right]$ of the system description matrix defines the systematic (non-random) variation in the vector $\bar{x}_2$ of gravity coefficient errors. Three types of models can easily be considered for this variation. First, if $\bar{x}_2$ is modeled as a vector of constants, $\left[F_{22}\right] = \left[0\right]$, and no further terms are required. Second, if the gravity model error coefficients are modeled as random walk stochastic processes, $\left[F_{22}\right] = \left[0\right]$, and an additional term is required in Eq. (11) as follows:

$$\dot{\bar{x}} = \left[F\right] \bar{x} + \left[G\right] \bar{v} \tag{26}$$

where $\left[G\right]$ and $\bar{v}$ are partitioned consistent with $\bar{x}$, and

$$\left[G\right] = \left[\begin{array}{c|c} G_1 & 0 \\ \hline G_2 & I \end{array}\right]$$

$$\bar{v} = \left[\begin{array}{c} \bar{v}_1 \\ \hline \bar{v}_2 \end{array}\right] = \left[\begin{array}{c} \bar{0} \\ \hline \bar{v}_2 \end{array}\right]$$

and $\bar{v}_2$ is a vector of independent mean zero white Gaussian noise random processes, with $E\left\{v^2(t)\right\} = \sigma_v^2$

The solution of Eq. (26) for $\bar{x}_2$, in this case, is

$$\bar{x}_2(t_n) = \bar{x}_2(t_{n-1}) + \int_{t_{n-1}}^{t_n} \bar{v}_2(t)dt, \tag{27}$$

and the covariance of the system response to this white noise driving function is

$$R_{jj} = \sigma^2_{v_{2j}} (t_n - t_{n-1}) \tag{28}$$

Define $\sigma^2_{\Delta x_{2j}}$ as the mean square change in the j^{th} element of $\bar{x}_2$ per unit distance. Then at each point in time we can compute

$$\sigma^2_{v_{2j}} = \dot{r}^2 \sigma^2_{\Delta x_{2j}} \tag{29}$$

where $\dot{r}$ is the current speed of the sub-satellite point relative to the earth.

The third and last model considered for the variation in gravity coefficients is an exponentially correlated random process. In this case we have, for the j^{th} element,

$$\dot{x}_{2j}(t) = -\beta \; x_{2j}(t) + \sigma \beta \, v_j(t) \tag{30}$$

where $v_j(t)$ is a zero mean unit variance white noise random process, and

$$x_{2j_0} = x_{2j}(t=0) \sim N\left(0, \frac{\sigma^2 \beta}{2}\right) \tag{31}$$

For this model the solution to Eq. (26) is

$$x_{2j}(t) = x_{2j_0} \; e^{-\beta t} + \sigma\beta \int_0^t e^{-\beta(t-s)} \; v_j(s) ds \tag{32}$$

Clearly we can see that $\left[F_{22}\right]$ and $\left[G_2\right]$ are diagonal matrices with

$$F_{22_{jj}} = -\beta, \quad G_{2_{jj}} = \sigma\beta$$

and it can be shown that the diagonal terms of the system response covariance matrix are given by

$$R_{jj}(t_n) = \frac{\sigma^2 \beta}{2} \left[1 - e^{-2\beta(t_n - t_{n-1})}\right] \tag{33}$$

Assume that the exponential parameter of the model is a "distance" constant ρ_d. Then

$$\beta = \dot{r}/\rho_d \tag{34}$$

and from (31) $\sigma^2 = 2\sigma^2_{x_{2j}} / \beta$ (35)

where $\sigma^2_{x_{2j}}$ is the apriori error variance of x_{2j}.

Of the three models considered, the exponential model is recommended as being more realistic. However, as good estimates of the parameter ρ_d are not available, the other two models were used.

4.2.3 Observations and Measurement Errors

Observations for this problem will be in the form of times of receiving periodic signals at points fixed to the earth's surface. These measurements will be corrupted by errors, including (but not limited to) the following contributors:

1. Random variations in ionospheric and tropospheric delay.
2. Random and systematic clock errors at both the satellite and the tracker.
3. Tracker site location error (constant)
4. Resolution of signal time of arrival measurement at tracker (measurement noise)

The observable in this problem will be a scalar time-of-arrival measurement, T, for each ground tracker. This measurement will be related to the state vector $\bar{x}$ by

$$T = \left[M \right] \bar{x} \tag{36}$$

where $\bar{x} = \begin{bmatrix} \bar{x}_1 \\ \bar{x}_2 \\ \bar{x}_3 \\ \bar{x}_4 \\ \bar{x}_5 \end{bmatrix}$ $\qquad \bar{x}_1 = \begin{bmatrix} \Delta a \\ \Delta e \\ \Delta i \\ \Delta \Omega \\ \Delta \omega \\ \Delta E \end{bmatrix}_{6x1}$ is a vector of delta orbital elements

$$\bar{x}_2 = \begin{bmatrix} \Delta\mu \\ \Delta J_2 \\ \vdots \\ \Delta J_N \end{bmatrix}_{N\times 1}$$ is a vector of delta gravity model coefficients

$\bar{x}_3$ is a 3xl vector of tracker site location errors

$\bar{x}_4$ is a 4xl vector of transmission time error parameters

$\bar{x}_5$ is a 3xl vector of atmospheric delay error parameter

Assume that the satellite transmits a pulse at intervals of size δt, ideally a constant. The n^{th} pulse will be transmitted at time t_n where

$$t_n = n(\Delta t) + \delta t_n \tag{37}$$

where δt_n is the error in t_n, and the time-of-arrival T_n is

$$T_n = \frac{R_n}{c} + n(\Delta t) + \delta t_n + e_n + w_n \tag{38}$$

where R_n is the distance traveled

c is the speed of light

δt_n is the satellite clock error

e_n is the atmospheric delay

w_n is measurement noise due to quantization

An approximate linear expression for small errors in T_n is

$$\delta T_n = 1/c \quad \delta R_n - R_n/c \quad \delta c/c + \delta t_n + \delta e_n + w_n \tag{39}$$

The term R_n in Eq. (38) is the magnitude of the difference of the tracker and satellite position vectors:

$$R_n = \left| \left[T_{S,T}\right] \bar{P}_{S_n} - \bar{P}_T \right| \tag{40}$$

where $\left[T_{S,T}\right]$ is a satellite-coordinate to tracker-coordinate transformation. Expanding Eq. (40) to first order we obtain

$$\delta R_n = \sum_{i=1}^{3} \frac{\partial R_n}{\partial P_{s_i}} \delta P_{s_i} + \sum_{j=1}^{3} \frac{\partial R_n}{\partial P_{T_j}} \delta P_{T_j} \tag{41}$$

But, note that $\overline{P}_s$ is expressible in terms of the six orbital elements e_k. Then to first order

$$\delta P_{s_i} = \sum_{k=1}^{6} \frac{\partial P_{s_i}}{\partial e_k} \delta e_k \tag{42}$$

Substituting (42) into (41) gives

$$\delta R_n = \sum_{i=1}^{3} \sum_{k=1}^{6} \frac{\partial R_n}{\partial P_{s_i}} \frac{\partial P_{s_i}}{\partial e_k} \delta e_k + \sum_{j=1}^{3} \frac{\partial R_n}{\partial P_{T_j}} \delta P_{T_j} \tag{43}$$

Writing (43) in matrix form and noting that $\delta T_n = 1/c \ \delta R_n$

$$\delta T_n = \left[M_1\right]_n \bar{x}_{1_n} + \left[M_3\right]_n \bar{x}_3 \tag{44}$$

where $\bar{x}_3$ is a constant vector of site location errors, and $\bar{x}_1$ is a 6x1 vector of orbital element differences. There will be one $\left[M_3\right] \bar{x}_3$ term for each tracker.

The terms in Eq. (44) are defined below.

$$\bar{x}_{1_n} = \begin{bmatrix} \Delta a_n \\ \Delta e_n \\ \Delta i_n \\ \Delta \Omega_n \\ \Delta \omega_n \\ \Delta E_n \end{bmatrix}, \qquad \bar{x}_3 = \begin{bmatrix} \delta P_{T_1} \\ \delta P_{T_2} \\ \delta P_{T_3} \end{bmatrix}$$

$$\left[M_3\right]_n = 1/c \begin{bmatrix} -\frac{x_n}{R_n} & -\frac{y_n}{R_n} & -\frac{z_n}{R_n} \end{bmatrix} \tag{45}$$

where $R_n = \left|\bar{R}_n\right|$, $\qquad \bar{R}_n = \begin{bmatrix} x_n \\ y_n \\ z_n \end{bmatrix}$

and the x, y, z tracker coordinate system is a local earth fixed North, West, Up orthogonal set. The $\left[M_1\right]$ matrix is defined as

$$\left[M_1\right]_{n_{1x6}} = 1/c \left[M_3\right]_{n_{1x3}} \left[T_{E,T}\right]_{n_{3x3}} \left[\frac{\partial P_{ECI}}{\partial \bar{e}}\right]_{3x6} \tag{46}$$

where $\left[T_{E,T}\right]_n$ is a transformation of earth-centered inertial coordinates to tracker coordinates (a function of time and tracker latitude and longitude), and the 3x6 matrix of partial derivatives $\partial P_{ECI_i}/\partial e_j$ is evaluated as a function of current values of the orbital elements e_j on the reference orbit.

4.3 Surveillance Covariance Model

The surveillance covariance model consists of a system model and a suboptimal filter model. These models are substantially different.

The surveillance system model consists of the following states

$$\underline{x}_s \triangleq \begin{vmatrix} \underline{S}_1 \\ \vdots \\ \underline{S}_{15} \\ \underline{T} \\ \underline{A} \\ \underline{P}_s \end{vmatrix} \begin{array}{l} \left.\begin{array}{l} \\ \\ \\ \end{array}\right\} \text{3 position error and 3 velocity error states for each of 15 satellites for a total of 90 states} \\ \text{4 clock error state} \\ \text{6 atmospheric error states} \\ \text{6 user dynamic states} \end{array}$$

All of the models have been discussed except the user dynamic models.

The user dynamic model employed consists of a simple representation of an aircraft in straight and level flight. Position and velocity states along track, cross track and vertically are modeled as

$$\begin{vmatrix} P_{AT} \\ P_{CT} \\ P_V \\ \dot{P}_{AT} \\ \dot{P}_{CT} \\ \dot{P}_V \end{vmatrix}_{t_{k+1}} = \left|\begin{array}{c|c} I & I(t_{k+1}-t_k) \\ \hline 0 & I \end{array}\right| \bar{P}_{t_k} + \left|\begin{array}{c|c} 0 & 0 \\ \hline 0 & 0 \end{array}\right| \underline{u} \tag{1}$$

where $$c = \begin{bmatrix} \sigma_{AT}\, t & 0 & 0 \\ 0 & \sigma_{CT}\, t & 0 \\ 0 & 0 & \sigma_V\, t \end{bmatrix}$$

The model consists of a random walk velocity driving state which couples into a position error. The initial covariance in position was selected as $(40m)^2$ and in velocity as $(1m/sec)^2$. The velocity noise was selected as

$$\begin{aligned} \sigma^2_{AT} &= \sigma^2_V = (0.22)^2\ m^2/sec \\ \sigma^2_{CT} &= (0.9)^2\ m^2/sec \end{aligned} \tag{2}$$

The system and filter measurement matrices were chosen to yield a sequence of time observations $\left| \delta t_k \right|$ at each measurement time with only those satellites that are visible leading to a time sequence entry. Visibility was determined using the GDOP program criteria. The time sequence was used to form a delta time sequence of observables where

$$\Delta t_j = \delta t_j - \delta t_{j-1} \qquad j=2, k \tag{3}$$

The filter model for the surveillance system consists of

$$\underline{x}_F = \left| \underline{P}_F \right| \qquad \text{6 user dynamic states}$$

The state model is similar to Eq. (1) except the initial state covariances and driving noise differed from the state model. The initial covariances were selected as $(100\ m)^2$ in position and $(2m/s)^2$ in velocity. The velocity noise was

$$\begin{aligned} \sigma^2_{AT} &= \sigma^2_V = (0.45)^2\ m^2/s \\ \sigma^2_{CT} &= (1.8)\ m^2/s \end{aligned} \tag{4}$$

Note that both the system model and the filter model assume larger uncertainties in cross track than in the other directions. This accounts for larger heading uncertainties as well as keeping the filter gains high in order to respond to aircraft maneuver.

4.4 Navigation Covariance Models

The navigation covariance model consists of a system model and a filter model, both similar to the surveillance models.

The navigation system model consists of the following states

$$\underline{x}_N = \begin{vmatrix} \underline{S}_1 \\ \vdots \\ \underline{S}_{15} \\ \underline{A} \\ \underline{T} \\ \underline{P}_N \end{vmatrix} \begin{array}{l} \left.\begin{array}{l} \\ \\ \\ \end{array}\right\} \text{3 position error and 3 velocity error states for each of 15 satellites} \\ \text{3 atmospheric error states} \\ \text{4 user clock error states} \\ \text{6 user dynamic states} \end{array} \qquad (1)$$

Note that only 3 atmospheric error states and no satellite error states are employed. The former reflects the single L-band downlink. The latter results from the fact that the satellite clock errors are fully correlated with the satellite ephemeris errors.

The user dynamic model is exactly as previously employed for the surveillance model.

The filter model for the navigation analysis is

$$\begin{vmatrix} P_{AT} \\ P_{CT} \\ P_V \\ \dot{P}_{AT} \\ \dot{P}_{CT} \\ \dot{P}_V \\ B \\ D \end{vmatrix}_{t_{k+1}} = \left|\begin{array}{c|c|c} I & I(t_{k+1}-t_k) & 0 \\ \hline 0 & I & 0 \\ \hline 0 & 0 & I \end{array}\right| \left|\frac{P}{T}\right|_{tk} + \left|\begin{array}{c|c|c} 0 & 0 & 0 \\ \hline 0 & c & 0 \\ \hline 0 & 0 & d \end{array}\right| \underline{u} \qquad (2)$$

where $$c = \begin{vmatrix} \sigma_T \sqrt{t} & 0 & 0 \\ 0 & \sigma_{cT} \sqrt{t} & 0 \\ 0 & 0 & \sigma_v \sqrt{t} \end{vmatrix}$$

$$d = \begin{vmatrix} \sigma_B \sqrt{t} & 0 \\ 0 & \sigma_D \sqrt{t} \end{vmatrix}$$

The values for all quantities are the same as for the surveillance with the addition of the clock bias and drift models.

The clock model consists of an initial offset and a frequency drift state. Both models consists of a deterministic error plus a random walk driving noise. The initial offset statistics consist of a $(1\ \mu sec)^2$ deterministic error plus a $(2.2 \times 10^{-10})^2$ sec random walk. The frequency drift state consists of a $(10^{-9}\ ppm)^2$ deterministic error plus a $(10^{-11})^2\ sec^{-1}$ random walk.

The system and filter measurement matrices were chosen to yield a time of arrival error at each time a visible satellite transmission was received. Satellite visibility was determined using the GDOP program criteria.

5. SATELLITE CONSTELLATION ANALYSIS

The satellite constellation analysis was conducted using a Geometric Dilution of Precision (GDOP) Analysis Program. This program is a computer program which includes the physical parameters required to fully analyze a general, hyberbolic, multilateration surveillance system employing satellites.

5.1 Geometric Dilution of Precision

To firmly establish the form of the GDOP performance index, a complete derviation of GDOP will be presented. This development is similar to that contained in Reference 26 with some additional comments and clarifications.

Consider a surveillance system composed of N satellites each of which receives a coded time marker transmitted by an aircraft. The satellites receive the time marker and retransmit the incoming signal to an earth fixed station where the time of arrival (TOA) of the signal is to be measured. Let the N satellites, the aircraft, and the receiving station position vectors in a Euclidian 3 space be denoted by the vectors $\underline{s}_1$, $\underline{s}_2$, ..., $\underline{s}_n$. $\underline{p}$, and $\underline{r}$, respectively.

The time at which the ground station will receive the N time marks may be represented by the N-vector $\underline{t}$ where

$$\underline{t} = (1/c)\ \underline{F}\ (\underline{s}_i,\ \underline{p},\ \underline{r},\ N)\ +\ t_0\ \underline{1}\ +\ \underline{\varepsilon}_1 \qquad (1)$$

where

c = the speed of light

t_0 = time of aircraft pulse transmission

$\underline{1}$ = the N-vector $(1\ 1 \ldots 1)^T$

$$\underline{F}\,(\underline{s}_i, \underline{p}, \underline{r}, N) = \begin{vmatrix} \|\underline{p} - \underline{s}_1\| + \|\underline{s}_1 - \underline{r}\| \\ \vdots \\ \|\underline{p} - \underline{s}_N\| + \|\underline{s}_N - \underline{r}\| \end{vmatrix}$$

$\|\underline{x}\|$ = Euclidian norm of the vector $\underline{x}$

$\underline{\varepsilon}_1$ = A random time vector which accounts for atmospheric delay effects in the up link and down link

The times of arrival of the pulses are measured with an error denoted by the N-vector $\underline{\varepsilon}_2$. The estimated time of arrivals is an N-vector $\hat{\underline{t}}$, where

$$\hat{\underline{t}} = \underline{t} + \underline{\varepsilon}_2 \tag{2}$$

or

$$\hat{t} = (1/c)\, F\,(\underline{s}_i, \underline{p}, \underline{r}, N) + t_0\,\underline{1} + \underline{\varepsilon}_1 + \underline{\varepsilon}_2 \tag{3}$$

The exact locations of the satellites are not known but an estimate of the satellite position is the 3-vector $\hat{\underline{s}}_i$ which is derived from satellite tracking. Since $(\hat{\underline{s}}_i - \underline{s}_i)$ is small compared to $(\underline{p} - \underline{s}_i)$ and $(\underline{s}_i - \underline{r})$, to good approximations

$$\|\underline{p} - \underline{s}_i\| = \|\underline{p} - \hat{\underline{s}}_i\| - \underline{u}_i^T (\hat{\underline{s}}_i - \underline{s}_i) \tag{4}$$

$$\|\underline{s}_i - \underline{r}\| = \|\hat{\underline{s}}_i - \underline{r}\| - \underline{v}_i^T (\hat{\underline{s}}_i - \underline{s}_i \tag{5}$$

where

$$\underline{u}_i = (\underline{s}_i - \underline{p}) / \|\underline{p} - \underline{s}_i\| \tag{6}$$

$$\underline{v}_i = (\underline{s}_i - \underline{r}) / \|\underline{s}_i - \underline{r}\| \tag{7}$$

See Figure 5.1-1 for a graphic description of this vector approximation.

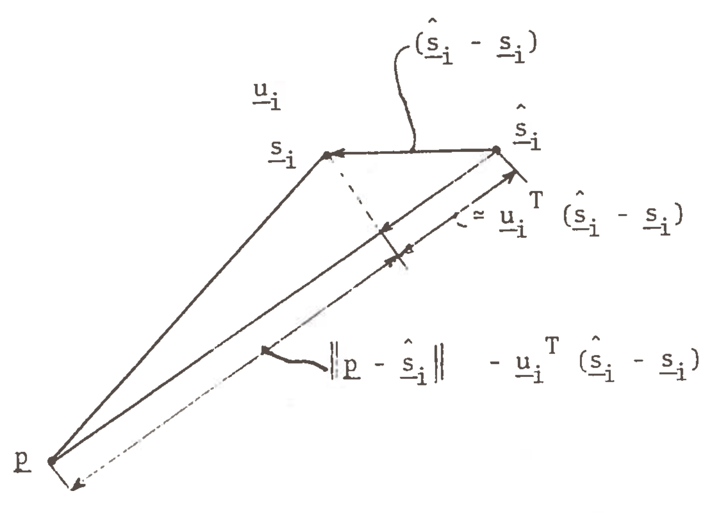

Figure 5.1-1. Vector Approximation

Thus the vector $\underline{t}$ may be expressed as

$$\hat{\underline{t}} = (1/c)\ F\ (\hat{\underline{s}}_i,\ \underline{p},\ \underline{r},\ N) + t_0\ \underline{1} + \underline{\varepsilon}_1 + \underline{\varepsilon}_2 - (1/c)\ \underline{\varepsilon}_3 \qquad (8)$$

where

$$\underline{\varepsilon}_3 = \begin{vmatrix} \underline{u}_1^T\ (\hat{\underline{s}}_1 - \underline{s}_1) + \underline{v}_1^T\ (\hat{\underline{s}}_1 - \underline{s}_1) \\ \vdots \\ \underline{u}_N^T\ (\hat{\underline{s}}_N - \underline{s}_N) + \underline{v}_N^T\ (\hat{\underline{s}}_N - \underline{s}_N) \end{vmatrix} \qquad (9)^*$$

The error sources $\underline{\varepsilon}_1$, $\underline{\varepsilon}_2$, and (1/c) $\underline{\varepsilon}_3$ can be separated into deterministic and uncorrelated, zero mean random vectors. The deterministic vector arises from such phenomenon as a portion of the refractive effect of the atmosphere, certain satellite tracking errors, and correlated timing errors over the measurement period. Thus

$$t = (1/c)\ F\ (\hat{\underline{s}}_i,\ \underline{p},\ \underline{r},\ N) + t_0\ \underline{1} + \underline{\varepsilon}_D + \underline{\varepsilon}_u \qquad (10)$$

Since it is assumed that t_0 is a completely unknown quantity, it must be removed from Eq. (10). This may be accomplished by using time differences as the observable, rather than time, for estimation of aircraft position. The time differences may be generated by operating on Eq. (10) by an operator $\mathbb{H}$ such that

$$\mathbb{H}\ \underline{1} = \underline{0} \qquad (11)$$

$$\text{rank}\ (\mathbb{H}) = N-1 \qquad (12)$$

to obtain a time difference vector $\hat{\underline{d}}$.

$$\hat{\underline{d}} = \mathbb{H}\ \hat{\underline{t}} = (1/c)\ \mathbb{H}\ F\ (\hat{\underline{s}}_i,\ \underline{p},\ \underline{r},\ N) + \mathbb{H}\ \underline{\varepsilon}_d + \mathbb{H}\ \underline{\varepsilon}_u \qquad (13)$$

An example for $\mathbb{H}$ is given by

$$\mathbb{H} = \left| \begin{array}{c|c} -1 & \\ -1 & \\ \vdots & I_{N-1\ X\ N-1} \\ -1 & \end{array} \right| \qquad (14)$$

---

*This assumes that error in $\underline{r}$ is small compared to the error in $\underline{s}_i$

yielding $$\hat{d}_1 = \hat{t}_2 - \hat{t}_1$$
$$\hat{d}_2 = \hat{t}_3 - \hat{t}_1$$
$$\vdots$$
$$\hat{d}_{N-1} = \hat{t}_N - \hat{t}_1 \tag{15}$$

It should be noted that the information content of d with regard to aircraft location is independent of $\mathbb{H}$, as long as Eq. (11) and (12) are satisfied.

Equation (13) is non-linear in $\underline{p}$. An expression for estimating the aircraft position may be derived by linearizing Eq. (13) about a predicted aircraft position vector, $\underline{p}^*$.

$$\hat{d} = (1/c)\ \mathbb{H}\ F\ (\hat{\underline{s}}_i,\ \underline{p}^*,\ \underline{r},\ N) + (1/c)\ \mathbb{H}\ \underline{f}\ \Delta\underline{p}$$
$$+ \mathbb{H}\ \underline{\varepsilon}_D + \mathbb{H}\ \underline{\varepsilon}_u \tag{16}$$

$$\Delta\underline{p} = \underline{p} - \underline{p}^* \tag{17}$$

$$\underline{f} = \partial F/\partial\underline{p}\Big|_{\underline{p} = \underline{p}^*} \tag{18}$$

Now if the position error $\Delta\underline{p}$ is small, then to a good approximation

$$\underline{f} = \begin{vmatrix} \underline{u}_1^T \\ \vdots \\ \underline{u}_N^T \end{vmatrix} \tag{19}$$

It is readily apparent that Eq. (16) has a deterministic part, α, where

$$\underline{\alpha} = (1/c)\ \mathbb{H}\ F\ (\hat{\underline{s}}_i,\ \underline{p}^*,\ \underline{r},\ N) + \mathbb{H}\ \underline{\varepsilon}_D \tag{20}$$

Here it should be noted that the deterministic error $\mathbb{H}\ \underline{\varepsilon}_D$ is included in $\underline{\alpha}$ and that $\underline{\alpha}$ is assumed to be a known quantity.

Equation (16) can now be written in the form

$$\underline{\hat{d}} = \underline{\alpha} + (1/c)\ \mathbb{H}\ \underline{f}\ \Delta\underline{p} + \mathbb{H}\ \underline{\varepsilon}_u \tag{21}$$

There are a number of assumptions that can be made with regard to a solution of this equation. One method is to assume the $\underline{\Delta p}$ is a non-random but unknown quantity and to find the estimated aircraft position, $\underline{\hat{p}}$, which is consistent with the smallest measurement error, $\underline{\varepsilon}_u$. The problem is to find min. $\| \underline{\varepsilon}_D \|^2$ subject to the constraint

$$\mathbb{H}\ \underline{\hat{\varepsilon}}_u = \underline{\hat{d}} - \underline{\alpha} - (1/c)\ \mathbb{H}\ \underline{f}\ \underline{\Delta\hat{p}} \tag{22}$$

Now since $\mathbb{H}$ has rank N-1 while $\underline{\varepsilon}_u$ is an N vector, only a minimum norm vector solution of Eq. (22) is unique. Clearly then

$$\underline{\hat{\varepsilon}}_u = \mathbb{H}^T (\mathbb{H}\ \mathbb{H}^T)^{-1} \{\underline{\hat{d}} - \underline{\alpha} - (1/c)\ \mathbb{H}\ \underline{f}\ \underline{\Delta\hat{p}}\} \tag{23}$$

and

$$\| \underline{\hat{\varepsilon}} \|^2 = \{\underline{\hat{d}} - \underline{\alpha} - (1/c)\ \mathbb{H}\ \underline{f}\ \underline{\Delta\hat{p}}\}^T (\mathbb{H}\ \mathbb{H}^T)^{-1} \{\underline{\hat{d}} - \underline{\alpha} - (1/c)\ \mathbb{H}\ \underline{f}\ \underline{\Delta\hat{p}}\} \tag{24}$$

The vector $\underline{\Delta\hat{p}}$ which minimized $\| \underline{\varepsilon}_u \|^2$ is

$$\underline{\Delta\hat{p}} = [\underline{f}^T\ \mathbb{H}^T (\mathbb{H}\ \mathbb{H}^T)^{-1}\ \mathbb{H}\ \underline{f}]^{-1}\ \underline{f}^T\ \mathbb{H}^T (\mathbb{H}\ \mathbb{H}^T)^{-1}\ c\ \{\underline{\hat{d}} - \underline{\alpha}\} \tag{25}$$

or

$$\underline{\Delta\hat{p}} = K\ (\underline{\hat{d}} - \underline{\alpha}) \tag{26}$$

where

$$K = [f^T \; \mathbb{H}^T \; (\mathbb{H} \;\; \mathbb{H}^T)^{-1} \;\; \mathbb{H} \; \underline{f}^T \; \mathbb{H}^T \; (\mathbb{H} \;\; \mathbb{H}^T)^{-1} \tag{27}$$

From Eq. (17), since $\underline{p}^*$ is a known quantity

$$\hat{\underline{p}} = \underline{p}^* + K \; (\hat{d} - \underline{\alpha}) \quad . \tag{28}$$

Using Eq. (21), then

$$\hat{\underline{p}} = \underline{p}^* + K \; \{(1/c) \;\; \mathbb{H} \; \underline{f} \; (\underline{p} - \underline{p}^*) + \mathbb{H} \; \underline{\varepsilon}_u\} \tag{29}$$

or

$$\hat{\underline{p}} - \underline{p} = K \;\; \mathbb{H} \; \underline{\varepsilon}_u \tag{30}$$

The position error

$$\underline{\delta} = \hat{\underline{p}} - p \tag{31}$$

is thus independent of $\underline{p}^*$ assuming that $\underline{\Delta p}$ is small, i.e., the approximation of Eq. (19) is valid.

The covariance of the position error is thus

$$\begin{aligned} P_{\underline{\delta}} &= E \; \{\underline{\delta} \; \underline{\delta}^T\} = K \;\; \mathbb{H} \; E \; \{\underline{\varepsilon}_u \; \underline{\varepsilon}_u{}^T\} \;\; \mathbb{H}^T \; K^T \\ &= K \;\; \mathbb{H} \; P_{\underline{\varepsilon}_u} \;\; \mathbb{H}^T \; K^T \end{aligned} \tag{32}$$

where it must be remembered that the original assumption was a zero mean for $\underline{\varepsilon}_u$. If the components of $\underline{\varepsilon}_u$ are assumed to be uncorrelated and of equal variance then

$$P_{\underline{\varepsilon}_u} = \sigma^2 \; I \tag{33}$$

$$P_{\underline{\delta}} = (\sigma \; c)^2 \; [\; \underline{f}^T \;\; \mathbb{H}^T \; (\mathbb{H} \;\; \mathbb{H}^T)^{-1} \;\; \mathbb{H} \; \underline{f}]^{-1} \tag{34}$$

The mean squared position error is now

$$E\{\|\delta\|^2\} = \text{Trace } P_{\underline{\delta}}$$
$$= (\sigma c)^2 \text{ Trace } \{[f^T \mathbb{H}^T (\mathbb{H} \mathbb{H}^T)^{-1} \mathbb{H} f]^{-1}\} \qquad (35)$$

The ratio of the rms position error to the rms error in each of the components of (c) $\underline{t}$ is defined to be GDOP or

$$K \triangleq \frac{\|\delta\|_{rms}}{\sigma c} = \sqrt{\text{Trace } \{[f^T \mathbb{H}^T (\mathbb{H} \mathbb{H}^T)^{-1} \mathbb{H} f]^{-1}\}} \qquad (36)$$

Several comments are in order about this derivation. GDOP as defined is the ratio of the rms position error in the aircraft to the equivalent rms position error of the satellite as determined by a single set of observations of the TOA signals. It is a static quantity. The assumption that $\underline{\varepsilon}_D$ is a known quantity is somewhat fallacious and will yield a position error that is smaller than can actually be achieved in terms of absolute position determination. The assumption that the components of $\underline{\varepsilon}_u$ are uncorrelated and of equal variance is not reasonable for most situations. As is shown in Reference (6) for any assumption of the covariance of $\underline{\varepsilon}_u$

$$\|\delta\|_{rms} \leq K \quad \|\varepsilon\|_{rms} \qquad (37)$$

Thus K is in general, an optimistic estimate of the true geometric dilution.

The crux of the situation now rests in the applicability of the GDOP criterion to the problem at hand. There are several arguments for the use of this criteria. The basic argument is simply that it will show the relative value of one set of satellites versus another set. The preceeding objections were basically directed toward the relationship between GDOP and actual accuracy of the surveillance. In point of fact, a GDOP of 5 will yield better surveillance capability than a GDOP of 10 although the surveillance accuracy may not be different by a factor of 2. Additionally, since the rms position error is used, it is impossible to tell which component of the error is most affected by different GDOPs.

A simplified form of GDOP for use in computation may be developed from Eq. (26). Since K is invarient with respect to the form of $\mathbb{H}$ as long as Eq. (11) and (12) are met, choose $\mathbb{H}$ as follows:

$$H = \left| \begin{array}{c|c} I_{N-1 \times N-1} & \begin{matrix} -1 \\ \vdots \\ -1 \end{matrix} \end{array} \right|_{N-1 \times N} \qquad N \geq 4 \tag{38}$$

If $\underline{u}_i \ \varepsilon \ E_3$ then N must be greater or equal to four. Thus

$$\mathbb{H} \ \mathbb{H}^T = I + U \qquad (N-1 \times N-1)$$

$$U \triangleq \text{matrix of all 1's} \tag{39}$$

Therefore

$$(\mathbb{H} \ \mathbb{H}^T)^{-1} = I - (\tfrac{1}{N}) \ U \tag{40}$$

and

$$\mathbb{H}^T (\mathbb{H} \ \mathbb{H}^T)^{-1} \ \mathbb{H} = \mathbb{H} \ \mathbb{H}^T - (1/N) \ \mathbb{H}^T U \ \mathbb{H} \tag{41}$$

But

$$\mathbb{H}^T U \mathbb{H} = \left[\begin{array}{ccc:c} & U & & -(N-1) \\ & & & \vdots \\ & & & -(N-1) \\ \hdashline -(N-1) & \cdots & -(N-1) & (N-1)^2 \end{array}\right] \tag{42}$$

and

$$\mathbb{H}^T \mathbb{H} = \left[\begin{array}{ccc:c} & I_{n-1 \times n-1} & & -1 \\ & & & \vdots \\ & & & -1 \\ \hdashline -1 & \cdots & -1 & (N-1) \end{array}\right]$$

$$= I - \frac{1}{N} \left[\begin{array}{ccc:c} & 0 & & N \\ & & & \vdots \\ & & & N \\ \hdashline N & \cdots & N & -N(N-2) \end{array}\right] \tag{43}$$

therefore $\mathbb{H}^T \mathbb{H} - (1/N)\ \mathbb{H}^T U \mathbb{H} = I - (1/N)\ U$ (44)

Now from Eq. (19), (36) and (41) through (44)

$$\underline{f}^T \mathbb{H}^T (\mathbb{H} \mathbb{H}^T)^{-1} \mathbb{H} \underline{f} = \underline{f}^T \underline{f} - (1/N)\ \underline{f}^T U \underline{f}$$

$$= \sum_{i=1}^{N} \underline{u}_i \underline{u}_i^T - (1/N) \left(\sum_{i=1}^{N} \underline{u}_i\right) \left(\sum_{i=1}^{N} \underline{u}_i^T\right) \tag{45}$$

Thus

$$K = \sqrt{\text{Trace}\ \{[\sum u_i u_i^T - (1/N)\ (\sum \underline{u}_i)(\sum u_i)^T]^{-1}\}} \tag{46}$$

This is the form used in computing GDOP.

5.2 GDOP Analysis Program Description

There are a number of simplifying assumption which were used in developing the GDOP analysis program. The assumptions are not very restrictive but yield simplified mathematics.

In all of the satellite position computations, pure Keplerian orbit equations about a spherical earth are used. This simplification is not realistic with regard to actual satellite motion but is adequate for the nominal orbit positions required for GDOP calculations.

All time values used are based on sidereal time rather than solar time. The difference between these times is small, but the use of sidereal time preserves the basic periodicity between the earth and the orbits.

In computing GDOP, all visible satellites, i.e., those satisfying the RF path loss criterion are included in the GDOP computation. This is opposed to the more normal procedure of using those four visible satellites which yield the best GDOP. The rationale for this is based on three factors. The problem of selecting which satellite to employ during actual surveillance operation is probably as complex as mechanizing an overdetermined solution using all visible satellites. The navigation mechanization will undoubtedly use an overdetermined set including all visible satellites. Since the navigation mechanization will undoubtedly be a recursive estimator, the selected GDOP formula is somewhat optimistic for bounding surveillance performance but pessimistic for navigation performance. Finally, prior experience has shown a good correlation between the GDOP computations for the best four and for all visible satellites with the latter yielding slightly smaller values.

All inclined orbit satellites are assumed to have antenna pointing control to direct the beam center to the sub-satellite point. This type of control scheme is less expensive to implement than one that points the antenna toward an earth fixed location. Further, better coverage is achieved beyond the edges of CONUS. Equatorial satellites are assumed to point their antenna at an arbitrary latitude on their longitude location line.

The above factors allow a somewhat simpler form of GDOP analysis program to be developed than could otherwise be achieved.

5.2.1 General Program Description

The general GDOP program is designed to compute GDOP on an arbitrary, earth fixed grid with equal spaced increments of latitude and longitude. Both size and spacing of the grid is arbitrary. GDOP is computed for each grid intersection point at arbitrarily equal spaced time intervals beginning at time zero.

Satellite locations are specified at time zero by a set of orbit descriptors. Up to 20 inclined orbits and 8 equatorial locations may be entered. Sub-satellite point coordinates for each satellite are provided for each specified time.

A general GDOP program flow is shown in Figure 5.2-1.

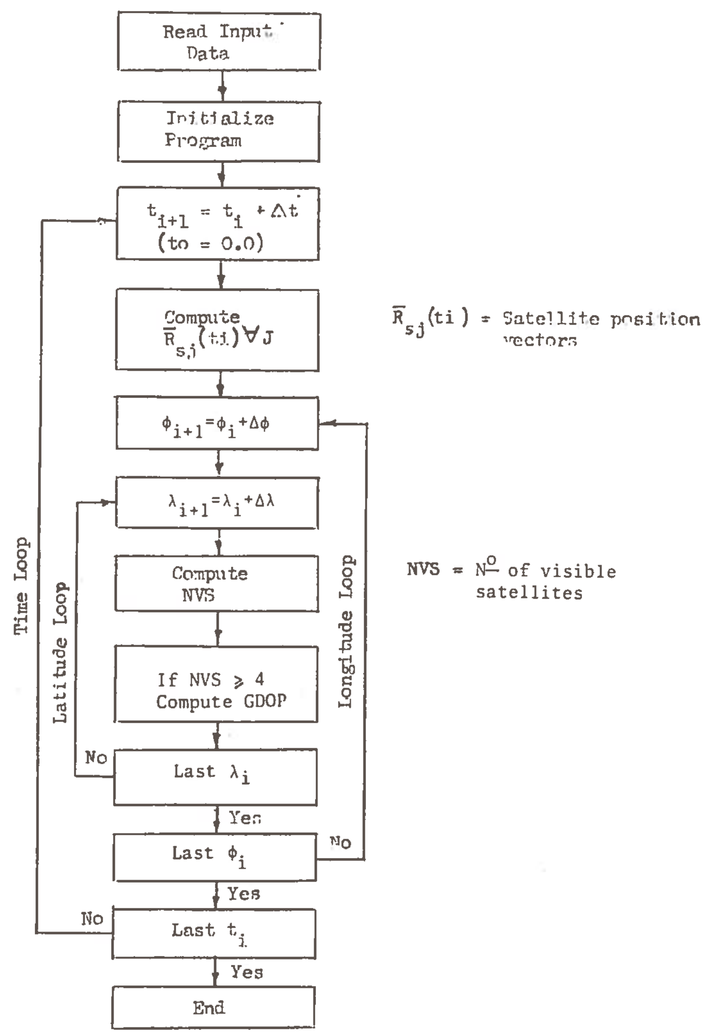

Figure 5.2-1. GDOP Program Flow

All computations are referenced to an earth fixed latitude-longitude frame, i.e., the normal geodetic coordinates, with the origin at the Greenwich meridian.

5.2.2 Satellite Equations

The input descriptors for the satellites are required as follows:

Orbit Type	Parameter
Inclined	i = Inclination of the orbit plane with respect to the earth's equatorial plane
	tp = Time of perigee where $0 < tp < 24$ sidereal hours
	λp_1 = Longitude at the perigee point
	e = Orbit eccentricity
Equatorial	λp_2 = Longitude location

For the assumed satellite orbit restrictions, these parameters are sufficient to completely specify the temporal behavior of the satellites.

The characteristic of geosynchronous satellites that is common, regardless of inclination or eccentricity, is that the semi-major axis value is fixed. The value of the semi-major axis for earth satellites is computed as

$$a = (K_e{}^2/\Omega^2)^{1/3} \cdot 10^{-2}$$

where

a = Semi-major axis length in meters

$K_e{}^2 = 3.9853 \times 10^{20}\ Cm^3/sec^2$, the earth's geocentric gravitational constant

$\Omega = 2\Pi/P_e$ rad/sec, the earth's inertial rate where P_e equals 86164.0917 sec, the length of a sidereal day

Location of the inclined satellites is initially determined in a satellite orbit frame and then transformed into an inertially fixed frame and finally into an earth fixed frame. All of these are right handed orthogonal coordinate frames. The relationships among these frames is depicted in Figure 5.2-2.

The satellite locations are determined in the orbit plane by solving Kepler's equations, as follows, for each satellite

$$t_j = t_{j-1} + \Delta t \qquad t_o = -\Delta t \tag{1}$$

$$M = (tp + t_j)\ K \tag{2}$$

$$E - e \sin E = M \tag{3}$$

$$r_{sx} = a\ (\cos E - e) \tag{4}$$

$$r_{sy} = a\sqrt{1 - e^2} \quad \sin E \tag{5}$$

where

$$K = 86164.0917/86400 \tag{6}$$

Here K corrects for sidereal time.

The solution for E in Eq. (3) is derived using Newton's approximation formula by iteration as follows:

$$E_i = E_{i-1} + \Delta E_i \qquad E_o = M,\ \Delta E_o = 0 \tag{7}$$

$$\Delta E_i = (M-E_i + e \sin E_i)/(1-e \cos E_i) \tag{8}$$

$$E = E_i \text{ when } \left\{ \begin{array}{l} i = 20 \\ \Delta E_i < 10^{-8} \text{ rad} \end{array} \right. \tag{9}$$

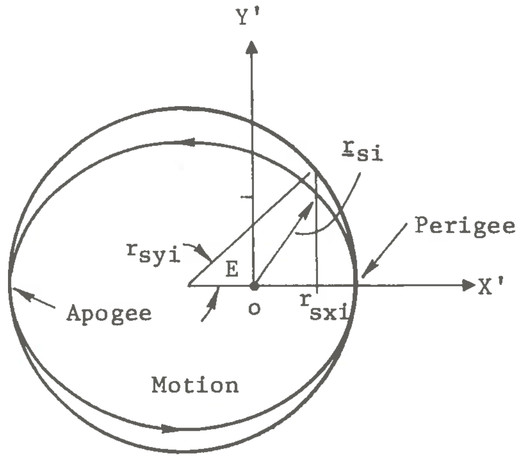

a. Orbit Frame

X_i', Y_i', Z_i' = Satellite orbit frame centered on the earth with X' - Y' the orbit plane and X' through the perigee point

$\underline{r}_{si}$ = Satellite range vector for the i^{th} satellite

a = Semimajor axis

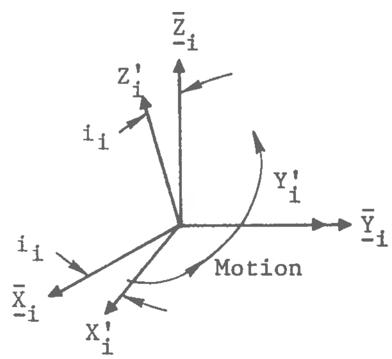

b. Inertial Frame

$\bar{X}_i, \bar{Y}_i, \bar{Z}_i$ = Inertial frame for the i^{th} satellite with Z_i along the earth's spin vector and the $\bar{X}_i - \bar{Y}_i$ plane in the earth's equatorial plane. $\bar{Y}_i$ and y_i are coincident

i_i = Inclination angle of the i^{th} satellite

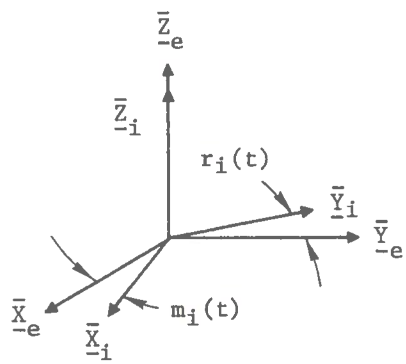

c. Earth Fixed Frame

$\bar{X}_e, \bar{Y}_e, \bar{Z}_e$ = Earth fixed frame with Z_e along the earth's spin axis and $\bar{X}_e$ cutting the earth's surface at the Greenwich meridian

$m_i(t)$ = Angle between the i^{th} satellite frame and the earth's frame measured about Z_e

Figure 5.2-2. Coordinate Frames

Extremely fast convergence is achieved with typically 4 to 5 passes being required.

Transformation of the orbit plane components of the satellite ranges into earth fixed values is computed as .

$$R_{sxi} = r_{sx}1 \cos (i_i) \cos (m_i) - r_{sy}1 \sin (m_i)$$
$$R_{syi} = r_{sx}1 \cos (i_i) \sin (m_i) + r_{sy}1 \cos (m_i)$$
$$R_{syi} = r_{sx}1 \sin (i_i) \qquad (10)$$

where

$$m_i = \lambda p1_i - \Omega (tp + t_j) K \qquad (11)$$

for inclined orbit satellites. Equatorial satellite ranges are given by

$$R_{sxi} = a \cos (\lambda p2_i)$$
$$R_{syi} - a \sin (\lambda p2_i)$$
$$R_{szi} = 0 \qquad (12)$$

5.2.3 Earth Grid Equations

The earth grid equations are based on the entry of geodetic coordinates and conversion of these equantities to geocentric values.
The geocentric latitude and radius of the oblate spheroidal earth approximation of Figure 5.2-3 is given by

$$R_B = R (\phi_i)$$
$$= r_e (0.99832 + 0.001683 \cos (2\phi_i) \qquad (13)$$
$$\phi_i' = \Phi (\phi_i)$$
$$= \phi_i + 0.003374 \cos (2\phi_i) \text{ rad} \qquad (14)$$

where

r_e = 6378388 m, the earth's equatorial radius.

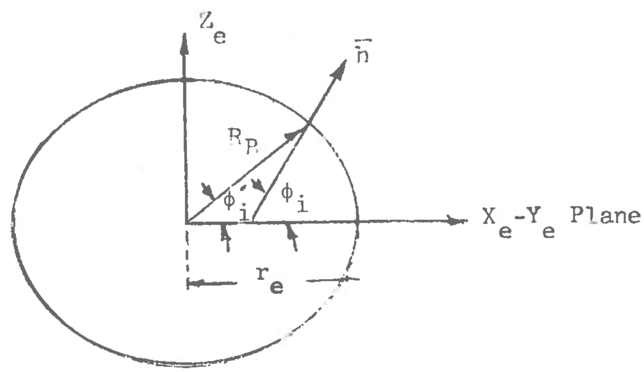

Figure 5.2-3. Earth Approximation

The aircraft is assumed to be located h kilofeet above the earth's surface. Since the earth is symmetric with respect to the Z_e axis for the assumed model, computational efficiency dictates that the grid be traversed along lines of constant latitude. The initial input required is as follows

ϕ_o = Initial geodetic latitude

λ_o = Initial geodetic longitude

$\Delta\phi$ = Grid latitude separation

$\Delta\lambda$ = Grid longitude separation

NP = Number of grid latitude lines

NG = Number of grid longitude lines

The outer or latitude loop equations are

$$\phi_i = \phi_{i-1} + \Delta\phi \qquad \phi_o = -\Delta\phi \tag{15}$$

$$R_{BZ} = R\ (\phi_i)\ \sin\ (\Phi(\phi_i)) \tag{16}$$

$$R_{BL} = R\ (\phi_i)\ \cos\ (\Phi(\phi_i)) \tag{17}$$

$$H_Z = 304.8\ h\ \sin\ (\phi_i) \tag{18}$$

$$HL = 304.8\ h\ \cos\ (\phi_i) \tag{19}$$

Where 304.8 is the conversion from h in kilofeet to meters.

The inner or longitude loop is computed from

$$\lambda_i = \lambda_{i-1} + \Delta\lambda \qquad \lambda_o = -\Delta\lambda \tag{20}$$

$$R_{BX} = R_{BL} \cos (\lambda_i) \tag{21}$$

$$R_{BY} = R_{BL} \sin (\lambda_i) \tag{22}$$

$$H_X = HL \cos (\lambda_i) \tag{23}$$

$$H_Y = HL \sin (\lambda_i) \tag{24}$$

The range to the aircraft in earth fixed coordinates may now be computed.

5.2.4. Satellite Visibility Criterion - Satellite visibility criterion is based on the amount of radiated energy received by the satellite receiver. This visibility criterion is the only valid basis for determining the usability of a particular satellite in solving the surveillance problem. The received energy is based on the amount of transmitted energy, the transmitting and receiving antenna gains, the free space loss, and a generic loss to cover unspecified miscellaneous losses. The formula used is

$$E_R = E_T + G_T (\alpha_A) + G_R (\alpha_B) - L_{FS} - L_M \tag{25}$$

where

E_T = Transmitted energy

$G_T(\alpha_A)$ = Transmitting antenna gain

α_A = Angle between aircraft antenna pointing vector and the aircraft to satellite vector

$G_R(\alpha_B)$ = Receiving antenna gain

α_B = Angle between the satellite antenna pointing vector and the aircraft to satellite vector

L_{FS} = Free space loss

L_M = Miscellaneous losses

If E_R exceeds a reference level, the satellite is assumed to be visible.

The transmitted energy is computed by

$$E_T = 10 \log (P_T) + 10 \log (\tau p) \tag{26}$$

where

E_T = Transmitted energy in db joules

P_T = Aircraft transmitter power in watts

τp = Transmitted pulse width in sec.

The free space loss is computed by

$$L_{FS} = 92.45 + 20 \log (f) + 20 \log (d) \tag{27}$$

where

L_{FS} = Free space loss in db

f = Transmitted frequency in GHz

d = Satellite to aircraft distance in meters

The miscellaneous loss is a data variable.

The antenna gains on the antenna center lines are a function of the half power beam widths of the antennas. The gain off the center axis is assumed to decay as $(\sin x)/x$ with the function normalized to yield a 3 db loss over the center gain, at an angle equal to half the half power beam width.

The formula used to compute the G_T and G_R

$$G = 10 \log \left(\frac{2}{1-\cos\,(\alpha_{HP}/2)}\right) + 10 \log \left(\frac{\sin K\alpha}{K\alpha}\right) \qquad (28)$$

where

α_{HP} = Half power beam width of the antenna

K = $3.81092/\alpha_{HP}$

α = Center line to receive energy angle

The value 3.81092 is selected since sin(x)/x equals 0.5 with x at a value of 1.90546.

The quantities required from the program to implement these above formulas are d, α_A and α_B. These values may be computed by considering Figure 5.2-4.

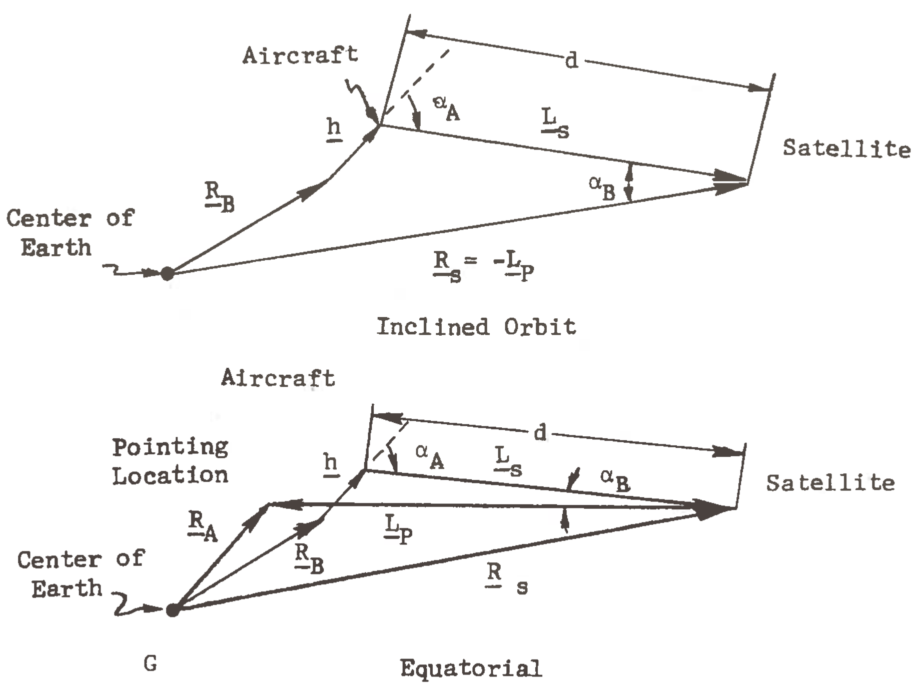

Figure 5.2-4. Aircraft-Satellite Geometry

In the case of the equatorial satellite, the antenna pointing vector is determined in earth fixed coordinates by

$$R_{AZ} = R\ (\phi p)\ \sin\ (\rho(\phi p) \tag{29}$$

$$R_{AL} = R\ (\phi p)\ \cos\ (\rho(\phi p) \tag{30}$$

$$R_{AX} = (RAL - a)\ \cos\ (\lambda p2) \tag{31}$$

$$R_{AY} = (RAL - a)\ \sin\ (\lambda p2) \tag{32}$$

where

ϕp = Satellite geodetic pointing latitude

$\lambda p2$ = Satellite location longitude

The line of sight vectors are given by

$$L_{SJ} = R_{SJ} - R_{BJ} - H_J \qquad J = X, Y, Z \tag{33}$$

The values α_A and α_B are then

$$\alpha_A = \cos^{-1}\ (\overline{1}_H \cdot \overline{1}_{LS}) \tag{34}$$

$$\alpha_B = \cos^{-1}\ (\overline{1}_{LS} \cdot -\overline{1}_{LP}) \tag{35}$$

if α_A and α_B are less than 90 deg. and in the main beam of the antenna, i.e., if

$$\alpha \leq 2\Pi/\alpha_{HP} \tag{36}$$

As an additional feature, the value of α_A may be decreased by an arbitrary constant which is entered as data.

If a satellite is visible, then the vector

$$\underline{u} = \underline{L}_S / \left\| \underline{L}_S \right\| \tag{37}$$

is saved for GDOP computation.

5.3 GDOP Analysis Program

The GDOP analysis program is a Fortran V computer program which implements the equations of Section 5.2. The program consists of the following:

MAIN	
GDØP GLØP GRPLOT	Subroutines
DØTP UNIT	Functions

Subroutine GDØP computes the value of GDOP as given in Equation (46), Section 5.1, and outputs the results if four or more satellites are visible.

Subroutine GLØP is the default output routine if less than four satellites are visible.

Subroutine GRPLOT is a graphic output routine for plotting the GDOP results.

Function DØTP computes a vector dot product.

Function UNIT computes a unit vector and a vector magnitude and includes a variable restorage integer.

MAIN includes all of the remaining coding.

A listing of the routines follow.

```
C     SATELLITE CONSTELLATION TRADEOFF PROGRAM
      IMPLICIT REAL*8 (A-H,O-Z), INTEGER (I-N)
      COMMON /OUTPUT/OUT
      LOGICAL OUT
      REAL*4 GRID(10,15),LBL(20)
      DIMENSION ECC(20),TNC(20),TP1(20),GP1(20),GP2(8),PPA(8),RSAT(3,28)
     1,RAN(3,8),RB(3),H(3),DS(3),DP(3),NOSAT(28),U(3,28)
      RAD(A)=ERAD*(0.99832+0.001683*DCOS(2.*A))
      ANG(A)=A+0.003374*DCOS(2.*A)
      GAIN(A,B,C)=10.*(DLOG10(2./(1.-DCOS(A)))+DLOG10(DSIN(B*C)/(B*C)))
      HGA(A)=10.*DLOG10(2./(1.-DCOS(A)))
C     READ ALL INPUT DATA
    5 FORMAT(6I6)
   10 FORMAT(5E12.4)
 1    READ(5,851,END=2) LBL
      READ(5,5) NT,N1,N2,NG,NP,LOUT
      OUT=LOUT.GE.2
      READ(5,10) GAMO,PHIO,DGAM,DPHI,DELT
      READ(5,10) ANG1,ANG2,ANGA,HGT,BANK
      READ(5,10) PTR,TAUP,FREQ,PMISC,PREF
      DO 15 J=1,N1
   15 READ(5,10) ECC(J),TNC(J),TP1(J),GP1(J)
      IF(N2) 21,21,16
   16 DO 20 J=1,N2
   20 READ(5,10) GP2(J),PPA(J)
C     INITIALIZE PROGRAM CONSTANTS
   21 PI=3.1415926D+0
      EKSQ=3.9853D+20
      PER=86164.0917D+0
      ERAD=6378388.D+0
      OMEGA=(2.*PI/PER)
      ASAT=((EKSQ/(OMEGA**2.))**(1./3.))*(1.D-2)
      DTR=PI/180.
      HTS=3600.D+0
      TFAC=PER/86400.
      HGT=HGT*304.8
      PLOS=10.*(DLOG10(PTR)+DLOG10(TAUP))-PMISC-92.45-20.*DLOG10(FREQ)
      XV=1.90546
      VAT=ANGA*DTR
      V1T=ANG1*DTR
      V2T=ANG2*DTR
      BANK=BANK*DTR
      FRA=XV/VAT
      FR1=XV/V1T
```

```
      FR2=XV/V2T
      TLA=PI/FRA
      TL1=PI/FR1
      TL2=PI/FR2
C     INITIALIZE TIME LOOP
      TP=-DELT
      NT=NT+1
      DO 610 JT=1,NT
      TP=TP+DELT
      TRUN=TP/60.
      WRITE(6,800) TRUN
      WRITE(6,802)
  800 FORMAT(1H1,20X,'TIME =',1F8.2,2X,'MIN.'/)
  801 FORMAT(/6X,'LAT.',5X,'LONG.',7X,'GDOP',6X,'VISIBLE SATELLITES'/)
  802 FORMAT(10X,'SUBSATELLITE POINTS'//10X,'NO.',5X,'LAT.',5X,
     1'LONG.',5X,'REF. POWER'/)
  803 FORMAT(1I12,3F10.1)
C     COMPUTE ALL SATELLITE LOCATIONS
      DO 415 J=1,N1
      ANOM=OMEGA*(TP1(J)*HTS+TP)*TFAC
      EI=ANOM
      DO 405 K=1,20
      DEI=(ANOM-EI+ECC(J)*DSIN(EI))/(1.D+0-ECC(J)*DCOS(EI))
      EI=EI+DEI
      IF(DABS(DEI)-1.D-8) 410,405,405
  405 CONTINUE
  410 RX=ASAT*(DCOS(EI)-ECC(J))
      RY=ASAT*DSIN(EI)*((1.D+0-ECC(J)**2)**0.5)
      CI=DCOS(TNC(J)*DTR)
      SI=DSIN(TNC(J)*DTR)
      GT=GP1(J)*DTR-OMEGA*(TP1(J)*HTS+TP)*TFAC
      CM=DCOS(GT)
      SM=DSIN(GT)
      RSAT(1,J)=RX*CI*CM-RY*SM
      RSAT(2,J)=RX*CI*SM+RY*CM
  415 RSAT(3,J)=-RX*SI
      IF(N2) 220,220,416
  416 DO 420 J=1,N2
      K=N1+J
      RSAT(1,K)=ASAT*DCOS(GP2(J)*DTR)
      RSAT(2,K)=ASAT*DSIN(GP2(J)*DTR)
  420 RSAT(3,K)=0.D+0
  220 N3=N1+N2
      DO 429 J=1,N3
```

```
      DO 421 K=1,3
  421 H(K)=RSAT(K,J)
      CALL UNIT(H,U,1,DIST)
      IF(J.GT.N1) GO TO 413
      FANG=ANG1*DTR
      AT1=DARSIN(U(3,1))
      DIST=DIST-RAD(AT1)
      GO TO 414
  413 FANG=ANG2*DTR
      AT1=PPA(J-N1)*DTR
      AT2=RAD(AT1)
      DIST=DSQRT(DIST*DIST+AT2*AT2-2.*DIST*AT2*DCOS(AT1))
  414 FING=ANGA*DTR
      REFP=PLOS+HGA(FING)+HGA(FANG)-20.*DLOG10(DIST*1.D-3)
      UL=DSQRT(U(1,1)**2+U(2,1)**2)
      TEST=DABS(U(1,1))-(1.D-8)
      IF(TEST) 424,424,423
  423 UL1=U(2,1)/U(1,1)
      UL1=DATAN(UL1)/DTR
      IF(U(1,1)) 422,427,427
  422 IF(U(2,1)) 411,412,412
  411 UL1=UL1-180.
      GO TO 427
  412 UL1=UL1+180.
      GO TO 427
  424 IF(U(2,1)) 425,425,426
  425 UL1=-180.
      GO TO 427
  426 UL1=0.
  427 UL2=U(3,1)/UL
      UL2=DATAN(UL2)/DTR
  429 WRITE(6,803) J,UL2,UL1,REFP
      IF(OUT) WRITE(6,801)
      IF(N2) 451,451,435
  435 DO 450 J=1,N2
      RP=RAD(PPA(J)*DTR)
      AP=ANG(PPA(J)*DTR)
      RAN(3,J)=-RP*DSIN(AP)
      RPL=ASAT-RP*DCOS(AP)
      RAN(1,J)=RPL*DCOS(GP2(J)*DTR)
  450 RAN(2,J)=RPL*DSIN(GP2(J)*DTR)
C     SET UP GRID LOOP FOR LATITUDE
  451 PP=PHIO-DPHI
      DO 605 J=1,NP
      PP=PP+DPHI
      JP1=NP+1-J
      PR=PP*DTR
      RB(3)=RAD(PR)*DSIN(ANG(PR))
```

```
      RBL=RAD(PR)*DCOS(ANG(PR))
      H(3)=HGT*DSIN(PR)
      HL=HGT*DCOS(PR)
C     SET UP GRID LOOP FOR LONGITUDE
      GP=GAMO-DGAM
      DO 600 K=1,NG
      GP=GP+DGAM
      GR=GP*DTR
      SGP=DSIN(GR)
      CGP=DCOS(GR)
      RB(1)=RBL*CGP
      RB(2)=RBL*SGP
      H(1)=HL*CGP
      H(2)=HL*SGP
      NSAT=0
      DO 490 LL=1,28
  490 NOSAT(LL)=0
C     COMPUTE RADIUS AND LOS VECTORS FOR SATELLITE TYPE 1
      DO 515 L=1,N1
      DO 500 M=1,3
      DS(M)=RSAT(M,L)-RB(M)-H(M)
  500 DP(M)=RSAT(M,L)
      F1=DOTP(DS,H)
      F2=DOTP(DS,DP)
      IF(F1) 515,515,99
   99 IF(F2) 515,515,149
  149 CONTINUE
      BA=DABS(DARCOS(F1))+BANK
      B1=DARCOS(F2)
      TEST=TLA-BA
      IF(TEST) 515,515,501
  501 IF(BA-1.D-6) 502,502,503
  502 POP=HGA(BA)
      GO TO 504
  503 POP=GAIN(VAT,BA,FRA)
  504 TEST=TL1-B1
      IF(TEST) 515,515,505
  505 IF(B1-1.D-6) 506,506,507
  506 POP=POP+HGA(B1)
      GO TO 508
  507 POP=POP+GAIN(V1T,B1,FR1)
  508 CALL UNIT(DS,DP,1,DIST)
      PWR=PLOS+POP-20.*DLOG10(DIST*1.D-3)
      IF(PWR-PREF) 515,515,510
  510 NSAT=NSAT+1
      CALL UNIT(DS,U,NSAT,DIST)
      NOSAT(NSAT)=L
```

```
  515 CONTINUE
      IF(N2) 535,535,516
C     COMPUTE PADIUS AND LOS VECTORS FOR SATELLITE TYPE 2
  516 DO 535 L=1,N2
      NPS=N1+L
      DO 520 M=1,3
      DS(M)=RSAT(M,NPS)-RB(M)-H(M)
  520 DP(M)=RAN(M,L)
      F1=DOTP(DS,H)
      F2=DOTP(DS,DP)
      IF(F1) 535,535,98
   98 IF(F2) 535,535,148
  148 CONTINUE
      BA=DABS(DARCOS(F1))+BANK
      B2=DARCOS(F2)
      TEST=TLA-BA
      IF(TEST) 535,535,521
  521 IF(BA-1.D-6) 522,522,523
  522 POP=HGA(BA)
      GO TO 524
  523 POP=GAIN(VAT,BA,FRA)
  524 TEST=TL2-B2
      IF(TEST) 535,535,525
  525 IF(B2-1.D-6) 526,526,527
  526 POP=HGA(B2)+POP
      GO TO 528
  527 POP=POP+GAIN(V2T,B2,FR2)
  528 CALL UNIT(DS,DP,1,DIST)
      PWR=PLOS+POP-20.*DLOG10(DIST*1.D-3)
      IF(PWR-PREF) 535,530,530
  530 NSAT=NSAT+1
      CALL UNIT(DS,U,NSAT,DIST)
      NOSAT(NSAT)=NPS
  535 CONTINUE
C     MATRIX U(I,J) AND VECTOR NOSAT ARE NOW FORMED
      IF(NSAT-4)  545,540,540
  540 CALL GDOP(U,NOSAT,NSAT,GP,PP,FA)
      GRID(JP1,K)=FA
      GO TO 600
  545 CALL GLOP(NOSAT,NSAT,GP,PP)
      GRID(JP1,K)=12.
C     CLOSE LONGITUDE LOOP
  600 CONTINUE
C     CLOSE LATITUDE LOOP
```

```
 605 CONTINUE
     ALONG=GAMO+(NG-1)*DGAM
     ALAT=PHIO+(NP-1)*DPHI
     WRITE(6,850) LBL
 851 FORMAT(20A4)
 850 FORMAT(2H1 ,20A4)
     WRITE(6,855) GAMO,ALONG,PHIO,ALAT,TRUN
     CALL GRPLOT(GRID,NP,NG,10)
 855 FORMAT('       LONGITUDE FROM',F6.0,' TO',F6.0/
    X'      LATITUDE FROM',F6.0,' TO',F6.0/'       TIME IS'
    X,F6.0,' MIN.')
C    CLOSE TIME LOOP
 610 CONTINUE
     GO TO 1
 2   CONTINUE
     STOP
     END
     FUNCTION DOTP(A,B)
     REAL*8 A(1),B(1),C,D
     C=0.
     D=0.
     DO 5 J=1,3
     C=C+A(J)*A(J)
   5 D=D+B(J)*B(J)
     C=DSQRT(C)
     D=DSQRT(D)
     DOTP=(A(1)*B(1)+A(2)*B(2)+A(3)*B(3))/(C*D)
     RETURN
     END
     SUBROUTINE UNIT(A,B,N,C)
     REAL*8 A(1),B(1),C
     C=DSQRT(A(1)*A(1)+A(2)*A(2)+A(3)*A(3))
     DO 5 J=1,3
     K=(N-1)*3+J
   5 B(K)=A(J)/C
     RETURN
     END
C    COMPUTE GDOP AND PRINT RESULTS
     SUBROUTINE GDOP(U,NVS,NS,GP,PP,FA)
     COMMON /OUTPUT/OUT
     LOGICAL OUT
     REAL*8 U(1),GP,PP,US(3),GM(9),FA,FB,FC,FD
     INTEGER NVS(1),NS
     DO 5 J=1,3
```

```
      US(J)=0.
      DO 5 K=1,NS
      M=(K-1)*3+J
    5 US(J)=US(J)+U(M)
      DO 15 J=1,3
      DO 15 K=1,3
      N=(K-1)*3+J
      GM(N)=0.
      DO 10 L=1,NS
      M1=(L-1)*3+J
      M2=(L-1)*3+K
   10 GM(N)=GM(N)+U(M1)*U(M2)
   15 GM(N)=GM(N)-US(J)*US(K)/NS
      FA=GM(2)**2
      FB=GM(3)**2
      FC=GM(6)**2
      FD=GM(1)*GM(5)*GM(9)+2.*GM(2)*GM(3)*GM(6)-GM(1)*FC-GM(5)*FB-
     1GM(9)*FA
      FA=DSQRT((GM(1)*GM(5)+GM(1)*GM(9)+GM(5)*GM(9)-FA-FB-FC)/FD)
      IF(OUT) WRITE(6,810) PP,GP,FA,(NVS(I),I=1,NS)
  810 FORMAT(2F10.1,1F11.2,5X,15I3/35X,13I3)
      RETURN
      END
      SUBROUTINE GLOP(NOSAT,NS,GP,PP)
      COMMON /OUTPUT/OUT
      LOGICAL OUT
      REAL*8 GP,PP
      INTEGER NOSAT(1),NS
      IF(OUT) WRITE(6,820) PP,GP,(NOSAT(I),I=1,NS)
  820 FORMAT(2F10.1,15X,15I3/35X,13I3)
      RETURN
      END
      SUBROUTINE GRPLOT(A,I1,I2,J1)
      REAL*4 A(1),ARRAY(101,121),GRID(121),C(10)
      REAL OPEN,DASH,LINE
      COMMON /OUTPUT/OUT
      LOGICAL OUT
      DATA OPEN/' '/,DASH/'-'/,LINE/'I'/
      DATA C/'1','2','3','4','5','6','7','8','9','*'/
      I7=I1-1
      DO 1 J=1,I2
      M=(J-1)*10+1
      DO 1 I=1,I7
      N1=I+(J-1)*J1
```

```
      R=A(N1)-A(N1+1)
      DO 1 K=1,6
      L=(I-1)*5+K
      ARRAY(L,M)=A(N1)-R*(K-1)/5.
1     CONTINUE
      I3=5*I7+1
      I4=I2-1
      I5=(I2-1)*10+1
      IF(.NOT.OUT) I5=MIN0(I5,120)
      I6=(I2-1)*10
      DO 2 I=1,I3
      DO 2 J=1,I4
      M=(J-1)*10+1
      N=M+10
      R=ARRAY(I,M)-ARRAY(I,N)
      DO 2 K=2,10
      L=M+K-1
      ARRAY(I,L)=ARRAY(I,M)-R*(K-1)/10.
2     CONTINUE
      DO 5 I=1,I3
      DO 4 J=1,I5
      GRID(J)=OPEN
      M=MOD(J,10)
      IF(M.EQ.1) GRID(J)=LINE
      K=MOD(I,5)
      IF(K.EQ.1) GRID(J)=DASH
4     CONTINUE
      DO 3 K=1,I6
      K1=ARRAY(I,K)
      K2=ARRAY(I,K+1)
      IF(K1.EQ.K2)GO TO 3
      L1=K2
      IF(K1.GT.K2) L1=K1
      IF(L1.GT.10) L1=10
      GRID(K)=C(L1)
3     CONTINUE
      WRITE(6,20)(GRID(NM),NM=1,I5)
20    FORMAT(' ',121A1)
5     CONTINUE
      RETURN
      END
```

6. REFERENCES

1. C71-61/301, DOT-TSC-304-1, "Fourth Generation Air Traffic Control Study", Volume II, Autonetics, Anaheim, California.

2. DOT-TSC-OST-73-29 "Concept for a Satellite-Based Advanced Air Traffic Management System, Volume V System Performance," Autonetics, Anaheim, California.

3. Proceedings IEEE, Volume 58, No. 3, March 1970, "Separation Theory in Air Traffic Control System Design", Jim Holt and G. R. Marner.

4. "An Analytical Approach to a Separation Hazard Prediction and Resolution Model", W. Wolff, Communications and Systems Incorporated - A Subsidary of Computer Science Corporation, Paramus, New Jersey, March 1969.

5. Proceedings IEEE, Volume 58, No. 3, March 1970, "Intermittent Positive Control", K. E. Willis et. al.

6. DOT-TSC-FAA-71-27, "The Calculation of Aircraft Collision Probabilities", J. Bellantoni.

7. DOT-TSC-OST-71-4, "A Theory of Aircraft Collision Avoidance System Design and Evaluation", E. Koenke.

8. "Advanced Air Traffic Management System (AATMS) Program Preliminary Requirements Specification, Appendix K," DOT TSC Working Paper, September 20, 1972.

9. "Analysis of Long-Range Air Traffic Systems - Separation Standards I, II, III", R.A.E. Technical Report, P. G. Reich.

10. DOT-TSC-FAA-71-13, "Final Report: Oceanic Surveillance and Navigation Analysis, FY 71, R. M. Hershkowitz.

11. Proceedings IEEE, Volume 58, No. 3, March 1970, "Collision and Missed Approach Risks in High-Capacity Airport Operations", H. A. Steinberg.

12. "A Probability Model of the Aircraft Separation Problem", W. Taylor, Cmdr., USN; FAA, Bureau of Research and Development, Report, April 1960.

13. "A Three Dimensional Mathematical Model of the Air Traffic Control Separation Problem", J. F. Koetsch, Lt. Cor., USMC; FAA, Bureau of Research and Development, April 1961.

14. Proceedings IEEE, Volume 58, No. 3, March 1970, "Technical Air Traffic Flow and Collision Exposure", W. Graham, R. H Orr.

15. Report of DOT for Air Traffic Control Advisory Committee, DOT ATCAC Report, Appendix C-1, "Frequency of Airspace Conflicts in the Mixed Terminal Environment", P. D. Flanagan, K. E. Willis, December 1969.

16. Proceedings of the IEEE, Volume 58, No. 3, "Aircraft Density and Mid-Air Collision", Ben Alexander, March 1970.

17. DOT FAA Air Traffic and Flight Standards Technical Report, "Near Mid-Air Collision Report of 1968", July 1969.

18. "Probability, Random Variables, and Stochastic Processes", Papoulis, McGraw Hill, 1965.

19. Report of DOT for ATCAC, December 1969.

20. Stiglitz, I. G., et. al., Concept Formulation Studies of the Surveillance Aspects of the Fourth Generation Air Traffic Control System, Project Report ATC-7, Lincoln Laboratory, Sept. 21, 1971.

21. The Application of Satellites to Communications, Navigation, and Surveillance for Aircraft Operating over the Continental United States, Volume II - Appendices, TRW 14671-6008-R-0-00, December, 1970.

22. Courant, R., and Hilbert, D., Methods of Matematical Physics, Volume II, Interscience Publishers, 1962.

23. Mandelbrot, B. and Van Ness, J., Fractional Brownian Motions, Fractional Noises, and Applications, SIAM Review, 10, October 1968, 422-437.

24. Barnes, J.A., Atomic Timekeeping and the Statistics of Precision Signal Generators, Proc. IEEE, 54, February 1966.

25. Goodyear, W. F., Completely General Closed Form Solution for Coordinates and Partial Derivatives of the Two Body Problem, Astronomical J., No. 3, April 1965.

26. Concept Formulation Studies of the Surveillance Aspects of the Fourth Generation Air Traffic Control System. ATC-7 Project Report, Massachusetts Institute of Technology, Lincoln Laboratory, September 21, 1971.

27. "Advanced Air Traffic Management System (AATMS) Program Requirements Specification", The Mitre Corporation Version, November 17, 1972.